Schweizerische Eidgenossenschaft
Confédération suisse
Confederazione Svizzera
Confederaziun svizra

Swiss Confederation

Federal Department of Home Affairs FDHA
Federal Office of Meteorology and Climatology MeteoSwiss

MeteoSwiss

Scientific Report MeteoSwiss No. 105

Representing the Urban Heat Island Effect in Future Climates

Annkatrin Burgstall

ISSN: 1422-1381

Scientific Report MeteoSwiss No. 105

Representing the Urban Heat Island Effect in Future Climates

Annkatrin Burgstall

This report is a master thesis in Climate and Environmental Sciences from University of Augsburg and represents a collaborative project between University of Augsburg, ETH Zurich and MeteoSwiss.

Author:

Annkatrin Burgstall, Faculty of Applied Computer Science, Institute of Geography, University of Augsburg, Augsburg, Germany

Supervisors:

Prof. Dr. Elke Hertig, Faculty of Medicine, University of Augsburg, Augsburg, Germany

Dr. Sven Kotlarski, Federal Office of Meteorology and Climatology, MeteoSwiss, Zurich, Switzerland

Dr. Ana Casanueva, Department of Applied Mathematics and Computer Science, University of Cantabria, Santander, Spain

Dr. Erich Fischer, Institute for Atmospheric and Climate Science, ETH Zurich, Zurich, Switzerland

Prof. Dr. Reto Knutti, Institute for Atmospheric and Climate Science, ETH Zurich, Zurich, Switzerland

Recommended citation:

Burgstall A., 2019, Representing the Urban Heat Island Effect in Future Climates, *Scientific Report MeteoSwiss,* **105,** 92 pp

Editor:

Federal Office of Meteorology and Climatology, MeteoSwiss, © 2016

MeteoSwiss
Operation Center 1
CH-8044 Zürich-Flughafen
T +41 58 460 99 99
www.meteoschweiz.ch

Acknowledgement

The present work represents a collaborative project between the University of Augsburg, ETH Zurich and MeteoSwiss. It was strongly supported by my main supervisors Ana Casanueva (University of Cantabria) and Sven Kotlarski (MeteoSwiss), who I would like to warmly thank for their extremely valuable input and the perfect supervision throughout the whole thesis process. Further, I would like to thank Elke Hertig (University of Augsburg), Reto Knutti and Erich Fischer (both ETH Zurich) for their very useful scientific input. Beside the official supervisors, the present work was strongly supported by further persons, who I would like to thank a lot. This especially concerns the very valuable scientific input of Jan Rajczak, Regula Gehrig, Anke Duguay-Tetzlaff (all MeteoSwiss) and Sebastian Sippel (ETH Zurich). Elias Zubler (MeteoSwiss) and Marius Zumwald (ETH Zurich) additionally provided helpful information. Very useful technical support was given by Rebekka Posselt (MeteoSwiss). Data was provided by Christian Feigenwinter and Roland Vogt (both University of Basel), Dasaraden Mauree (EPFL), Kaspar Frank and Florian Imbery (both Deutscher Wetterdienst), Elke Hertig (University of Augsburg) and Regula Gehrig (MeteoSwiss). I further would like to thank the entire MeteoSwiss Climate Analysis and Forecasting group for their feedback and their suggestions in numerous project meetings and discussions. Finally, I thank my family Monika, Roger and Timo Burgstall and my partner Martin Rassl for their emotional support throughout the whole thesis process.

Abstract

An increasing fraction of people living in urban areas and the expected increase in long lasting heat waves highlight the important role of urban climates in terms of future climate change impacts especially with relation to the heat-health sector. Due to the urban heat island (UHI) effect and its (generally) increased intensity during nighttime, people living in urban areas happen to be more affected by heat-related discomfort and health risks than those in non-urban regions, mainly during the night. In the present thesis, temperatures of both rural and urban sites (station couples) in Switzerland and Southern Germany are analyzed, using (i) observed and (ii) bias-corrected and downscaled climate model data for daily minimum (tmin) and daily maximum temperature (tmax) to account for the UHI in future climates. As climate scenario data, such as those of the Swiss CH2018 climate scenarios, are often restricted to rural sites, they need to be transferred to urban sites, first. For this purpose, three approaches are tested, namely (i) the well-established quantile mapping technique (QM) in a two-step manner, (ii) simple and multiple linear regression models and (iii) a physically-based, diagnostic equation designed by Theeuwes et al. (2017). While the resulting products of the former two approaches are transient urban time series at daily resolution for tmin and tmax, the latter approach results in a time series for daily maximum UHI values, valid for days that meet certain synoptic criteria, only. The derived UHI values are then added as an increment to the rural modeled data of tmin to gain a modeled time series of urban tmin. By analyzing the temperature differences of the observed climate at rural sites and their respective urban counterparts and by assuming a stationary relation between both, we can represent the UHI in future climates, which is additionally quantified in terms of heat indices based on tmin and tmax (tropical nights, summer days, hot days).

The methods` performances are evaluated using long-term weather station data of a Zurich station couple in a comprehensive validation framework. Results reveal promising performances in the present-day climate for QM and the regression-based methods. The diagnostic equation, in turn, is considered less

suitable for generating climate scenarios, given large biases and uncertainties in the validation.

Applying the methods to the employed station couples, projections simulate distinct urban-rural temperature differences (UHI) during nighttime (considering the frequency of tropical nights based on tmin) compared to weak differences during the day (considering the frequency of summer days and hot days based on tmax). Moreover, scenarios suggest the frequency of all indices to dramatically rise at the urban site by the end of the century for a strong emission scenario (RCP8.5): compared to the rural site, the number of tropical nights almost doubles while the number of summer days reveals about 15% more days at the urban site when focusing on the station couple in Zurich and the late scenario period. The lack of nighttime relief, indicated by tmin not falling below 20°C (i.e. a tropical night), is especially problematic in terms of human health and makes the study of the urban climate in general and the UHI effect in particular indispensable.

Table of Contents

List of Figures

List of Tables

Abbreviations

Meteorological parameters

DTR	diurnal temperature range; daily maximum temperature - daily minimum temperature
HD	hot days; tmax > 30°C
hurs	daily mean relative humidity
tas	daily mean 2m temperature
tmax	daily maximum 2m temperature
tmin	daily minimum 2m temperature
pr	daily mean precipitation
pre	daily mean air pressure
rsds	daily mean solar shortwave incoming radiation
SD	summer days; tmax > 25
TN	tropical nights; tmin > 20
UHI	urban heat island effect; urban temperatures - rural temperatures
wind	daily mean 10m wind speed

Statistics

bias	mean bias; offset between predicted and observed data
ecdf	empirical cumulative distribution function
LR	simple linear regression
MR	multiple linear regression
QM	quantile mapping

Validation framework

LDA	limited data approach
SSA	split sample approach
SSA (CW)	split sample approach; training in years with colder summers (C) and testing in years with warmer summers (W)
SSA (WC)	split sample approach; training in years with warmer summers (W) and testing in years with colder summers (C)

Others

CH2018	Swiss Climate Change Scenarios 2018
DWD	German Meteorological Service
ETCCDI	Expert Team on Climate Change Detection and Indices
EURO-CORDEX	Coordinated Downscaling Experiment - European Domain
fveg	vegetation fraction (analyzed within a 500m radius around the urban station)
GCM	global climate model
JJA	summer months June, July and August
MeteoSwiss	Federal Office of Meteorology and Climatology MeteoSwiss
NCCS	National Centre for Climate Services
RCM	regional climate model
RCP	Representative Concentration Pathway; RCP2.6, RCP4.5, RCP8.5
SVF	sky view factor
VIA	vulnerability, impacts and adaptation

1 Introduction

Analyses from long-term climate records and climatological scenarios suggest an increase of mean global temperatures due to climate change, even in the most optimistic projections. A direct consequence of rising temperatures is the increase of heat waves of higher intensity and longer duration (e.g. Fischer, Schär 2010; IPCC 2013; Schär et al. 2004). Exposure to high temperatures considerably influences human health and comfort and leads to increased morbidity and mortality rates (Kjellstrom, Weaver 2009; Ragettli et al. 2017). People living in urban areas are potentially more vulnerable to heat-related health risks than those in non-urban regions, mainly during the night (Gabriel, Endlicher 2011; Kovats, Hajat 2008; Scherer et al. 2013). This is due to urban air temperatures being (generally and especially during nighttime) substantially higher than corresponding temperatures in the rural surroundings. The so-called urban heat island (UHI) effect arises from different radiative, thermal, moisture and aerodynamic properties of urban and rural areas, detailed below (Fischer et al. 2012; Oke et al. 1991; Roth 2013). Distinctly higher minimum temperatures and subsequent lack of nighttime relief makes urbanites especially predisposed to heat stress, as the human body can cope less with heat when minimum temperatures are not falling below a certain level after a hot day (Gabriel, Endlicher 2011; Grize et al. 2005; Kovats, Hajat 2008; Ragettli et al. 2017; Scherer et al. 2013). In order to find effective strategies of mitigation and adaptation, a number of studies has investigated future trends of the UHI under climate change conditions. Hoffmann et al. (2012) analyzed future changes in UHI in Hamburg for the periods 2035–2065 and 2071–2100. They used regional climate model data and a statistical downscaling approach and found significant changes in the annual cycle of the UHI towards the end of the century (strengthening in July and August, decreasing for the other months). In contrast, Lauwaet et al. (2016) found that the future magnitude of the UHI in Brussels for the period 2060-2069 will slightly decrease with global warming caused by increased incoming longwave radiation. Despite UHI trends related to changes in

meteorological variables, urban-rural temperature differences can likewise vary due to changes in the urban morphology or socio-economic changes. Using satellite data, Zhou et al. (2017) found that the surface UHI intensity increases with city size and decreases with fractality. That is, the larger and the more compact cities are, the stronger their UHI intensity. Koomen and Diogo (2015) explored the impact of urban development scenarios on the UHI for the Amsterdam region for the coming 30 years. They found that strong UHI increases are to be expected from the combination of urban development and more frequent occurrences of extreme heat events.

Given the continuously growing fraction of people exposed to the atmospheric environments of cities and thus to urban heat stress, robust projections of future climatic conditions especially in cities are needed to allow for sophisticated climate impact assessments for urban areas (Arnfield 2003; Roth 2013; Stewart, Oke 2012). "Standard" climate scenarios such as the recently launched Swiss climate scenarios CH2018 (CH2018 2018) are based on a large ensemble of simulations, considering various global and regional climate models (GCMs, RCMs, respectively) and several greenhouse gas emission scenarios. In a statistical post-processing step, these climate model data are bias-corrected toward observation-based references derived from local measurements. Due to short and (or) sparse observational time series of urban stations (only very few official weather stations are located in urban areas), the proposed climate scenarios are often restricted to rural sites where stations (mostly maintained and operationally run by national weather services) provide high-quality and long-term data series.

Due to lacking temperature projections at urban sites, UHI scenarios have often been analyzed with statistical models using GCM data as input to have an estimate for the future UHI development (Wilby 2006, Wilby 2008). Yet, results are not well enough resolved or generally valid, as climate change differs regionally and so does the UHI. Other studies have successfully modeled the UHI with sophisticated atmospheric models coupled to an urban canopy or building energy model (e.g. Chen et al. 2011; Kusaka et al. 2012; Salamanca et al. 2011). However, these models require a large amount of input variables and

initialization data that are relatively difficult to measure and obtain. In order to overcome these challenges, we present and compare three approaches, detailed below (a-c), that allow for determining the future UHI by analyzing the temperatures at both rural and urban sites. To be more precisely, the tested approaches translate rural scenarios to the urban sites, using (i) observed and (ii) climate model data for a high-end emission scenario (RCP8.5) available through CH2018 (2018), where a first-step quantile mapping (QM) approach was used to bias correct and downscale modeled data to the rural site scale. The following approaches are considered in the present thesis:

a) a **second-step QM** procedure based on climate model simulations (daily minimum and daily maximum temperature) being spatially transferred to the urban target site to gain urban climate scenarios for daily minimum (tmin) and daily maximum temperature (tmax). The approach is based on the work of Rajczak et al. (2016) and uses a quantile-dependent correction function calibrated in a common reference period (i.e. urban and rural data) to translate rural data to their urban counterpart.

b) **regression-based statistical learning methods** using one to three meteorological predictor variables at the rural site in order to model urban temperatures (tmin, tmax). The statistical learning is based on regression models calibrated in a common reference period with available urban and rural data. To find the best predictor variables for the regression models, several meteorological variables are selected based on physical relevance and tested in terms of their correlation with the urban target variable. For urban tmin and tmax, the highest correlation coefficients are given for rural tmin and tmax, respectively, radiation (rsds) and humidity (hurs).

c) a physically-based method, namely the **diagnostic equation** designed by Theeuwes et al. (2017), using basic meteorological parameters at the rural site and morphology data at the urban site in order to parametrize daily maximum UHI for days that meet certain synoptic criteria. The resulting UHI is added to rural tmin scenarios in order to generate urban scenarios

for tmin - consistent with the other two approaches. Note that the diagnostic equation is not valid for creating urban scenarios for tmax, as daily maximum UHI and tmax do not show a clear temporal correspondence.

Once climate projections for urban sites are created, it is possible to quantify the urban-rural temperature difference, i.e. the UHI, in future climates, assuming a stationary relation between both. We analyze the UHI in terms of standard climate indices such as tropical nights, summer days and hot days. Climate indices are parameters that are derived from meteorological measurement data and defined for a certain threshold level (ETCCDI 2019, MeteoSwiss 2019).

Overall, the thesis aims at representing the urban heat island effect in future climates and is structured as follows. The research questions and a detailed description of the UHI are presented in Chapters 2 and 3. Considered data and heat indices are described in Chapter 4. Chapter 5 introduces the employed methods and gives a brief description of the validation framework and the skill scores used. Results of both the evaluation of the tested approaches and their application, resulting in climate scenarios for urban sites, are presented in Chapter 6. In Chapter 7, potential limitations of the considered approaches are discussed. A short summary and concluding remarks are given in Chapter 8.

2 Research Questions

The aim of the present thesis is to investigate and finally provide answers to the following research questions:

i. How can we transfer "standard" climate scenarios such as the local CH2018 products into urban settings and thereby account, among others, for the urban heat island?

ii. How will the projected future climate in urban areas differ from the future climate in the respective rural counterparts in terms of standard climate indices (tropical nights, summer days and hot days)?

3 The Urban Heat Island Effect

In urban areas, air temperatures are often systematically higher than corresponding temperatures in the surrounding rural areas. This so-called urban heat island (UHI) effect is typically defined as the temperature difference between urban and rural landscapes. The term derives from isotherm patterns of the near-surface air temperatures resembling the height contours of an island on a topographic map (Roth 2013; Vogt, Parlow 2011). Urban-rural temperature differences are well visible in high-resolved model simulations, for instance. Figure 1 shows the distinctly higher thermal conditions within the city of Zurich compared to its rural surroundings.

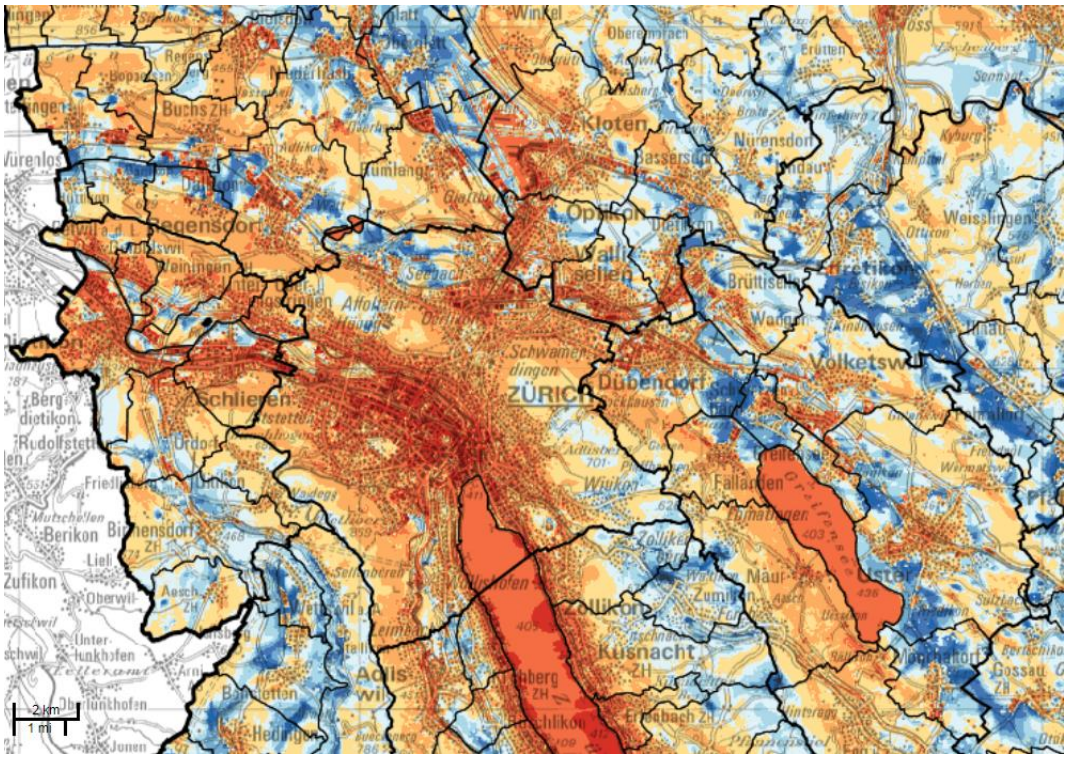

Figure 1: Thermal conditions in the city of Zurich and its adjacent areas in the Canton of Zurich, revealing higher temperatures (red colored) in urban areas and lower temperatures (blue colored) in rural surroundings, known as urban heat island (UHI) effect. The analysis is based on model simulations with FITNAH 3D and has a spatial resolution of 25m.

Source: GIS-Browser Canton of Zurich 2019.

The UHI effect arises from differing thermal, aerodynamic, radiative and moisture properties in the urban area compared to its natural surroundings and

is especially visible at nighttime and during hot summers, yet not limited to summer conditions (Fischer et al. 2012; Oke et al. 1991; Roth 2013).

Even though commonly referred to as increased temperature measured inside a settlement compared to its rural surroundings, the term *urban heat island* is used for different phenomena, giving rise to potential misunderstandings (Parlow et al. 2014). It is thus crucial to clearly state which kind of UHI is addressed (Oke 1982; Parlow et al. 2014). As heat islands can either be measured as surface or atmospheric phenomena, Voogt and Oke (2003) distinguish between *surface urban heat islands* (SUHI) and *atmospheric urban heat islands* (UHI) (Figure 2). SUHIs are observed by thermal remote sensors with satellites, estimating long-wave emission or the land surface temperature (LST), respectively. UHIs, in contrast, are primarily based on ground-based in-situ measurements of air temperature, which is often considered the most classical way for estimating UHIs. Since "air temperature does not necessarily follow the spatial pattern of surface temperatures" (Parlow et al. 2014), it is essential to draw a clear distinction between both definitions (Parlow 2011, Parlow et al. 2014). Depending on the observation height, *atmospheric urban heat islands* can be further split into two different subtypes. Air temperature measurements at street level rather relate to the *canopy layer urban heat island*, which is the most commonly assessed type of UHIs. Observations from urban flux towers, usually located on rooftops, already include properties of the urban roughness sublayer and refer to the *boundary layer urban heat island* (Figure 2; Parlow et al. 2014). In the present thesis, the focus lies on *atmospheric urban heat islands* (UHI) exclusively.

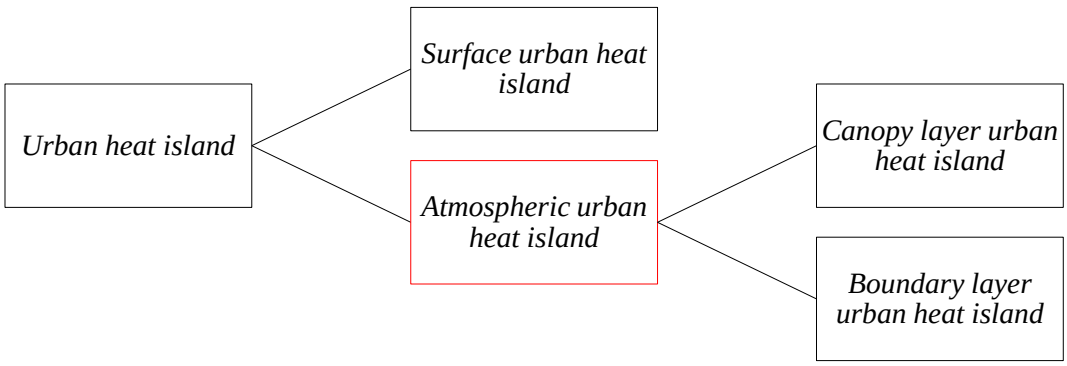

Figure 2: Classification of different urban heat islands.

Source: Own figure, modified after Parlow et al. 2014.

The fundamental factor responsible for the heat island development is the daytime heat storage, mainly ruled by heat capacity and heat conductivity, and the subsequent nighttime heat release from the ground (Fischer et al. 2012; Oke 1982; Parlow et al. 2014). Given the large admittance of urban fabrics, urban areas store more heat during the day than the rural surfaces. During nighttime, the absorbed energy is released from the ground and efficiently trapped in the urban canyons (longwave trapping) as radiative cooling is less strong in urban areas due to the smaller sky view factor (Fischer et al. 2012). With steadily decreasing incoming solar radiation in the afternoon until nighttime rural environments likewise cool down, yet much faster than the urban counterpart as their ability to store the absorbed energy is lower. As a result, UHIs reach their maxima mainly during nighttime, when air temperature differences between urban and rural environments are largest (see e.g. Figure 3; Fischer et al. 2012; Oleson et al. 2011; Parlow et al. 2014; Theeuwes et al. 2017).

Besides the influences mentioned above, several further factors determine the processes that affect and favor an UHI. Geographical latitude, topography or the distance to the open sea or lake coasts are relevant external drivers. On the local scale, albedo, imperviousness of urban surfaces, height of the buildings and thermal properties of the surface material likewise determine the UHI characteristics (Coutts et al. 2007; Parlow et al. 2014; Vogt, Parlow 2011). Extra heat release resulting from different human activities and the reduced evapotranspiration due to a low vegetation ratio compared to the rural surroundings also contribute to higher air temperatures in urban landscapes.

The UHI intensity varies not only in space with the morphology and the size of the city (Oke 1973) but also in time. As mentioned above, the UHI is mainly a nocturnal phenomenon (Oke 1982). It has a pronounced diurnal variation, meaning there are significant differences between day- and nighttime conditions. The urban-rural temperature difference is relatively small during daytime, sometimes even negative (i.e. cool island; Theeuwes et al. 2015). During the second half of the day, the heat island intensity typically starts to increase and reaches a maximum sometime between a few hours after the sun sets and before the sun rises (Fischer et al. 2012; Roth 2013). Figure 3 reveals the diurnal cycle of

the UHI intensity in Zurich over the past 24 summers, with the urban-rural air temperature difference being strongest during nighttime (about 1.0-2.3°C) and much smaller during the day (about 0.5-1.0°C). The maximum UHI is reached very early in this example, at around 9pm already.

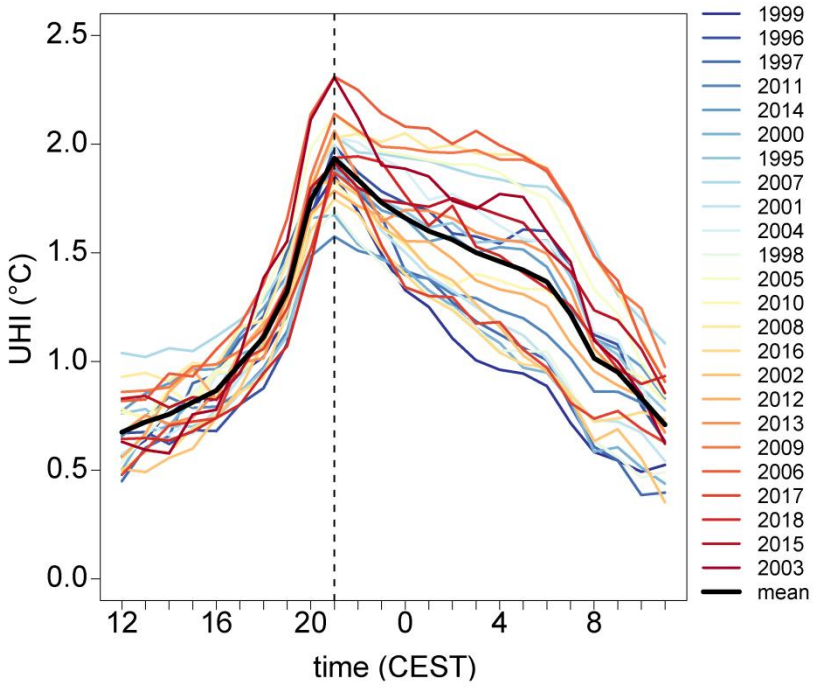

Figure 3: Mean diurnal cycles of UHI between rural station Zurich Fluntern (SMA; lapse-rate corrected data) and urban station Zurich Kaserne (NABZUE) during summer months for the period 1995-2018. Red colors refer to warmer mean summer temperatures and blue colors to colder mean summer temperatures. The solid black line marks the mean summer UHI averaged over 1995-2018. The vertical dashed black line reveals the UHI maximum.

The annual cycle of the UHI depends on the climate zone where the city is located. In moderate climates, a maximum UHI occurs during summer and a minimum UHI in winter (Arnfield 2003). During warm summers, the UHI intensity is often stronger than during colder summers (Fischer et al. 2012). Fischer et al. (2012) reveal a highly significant correlation between daily mean temperature and daily mean UHI (r = 0.64 for northern Europe, r = 0.70 for southern Europe). This indicates that the UHI amplification is greatest during hot summer days. For the analyzed station couple in Zurich (see Figure 3), this is evident for most of the cases as very warm summers (e.g. in 2003) generally offer stronger UHI values, compared to years with colder summers (e.g. in 2000).

Fischer et al. (2012) also found that the high UHI on hot days is mainly related to low cloudiness, which is associated with very warm days in the extratropics. The absence of clouds leads to more efficient rural radiative cooling at nighttime and amplifies the UHI (Steeneveld et al. 2011). This is consistent with observational studies that suggest an increasing UHI with decreasing cloud cover (e.g. Kidder, Essenwanger 1995; Morris et al. 2001).

4 Data

The employed data are introduced separately in terms of observational data (Section 4.1), modeled data (Section 4.2) and considered heat indices (Section 0).

4.1 Observations

Quantifying the UHI requires data of both urban and rural sites. We consider eight station couples, i.e. a rural station with an adjacent urban site, in Switzerland and the northern Alpine Foreland region in Germany (Figure 4 and Table 1) to develop scenarios for urban and rural settings and thereby account for the UHI effect.

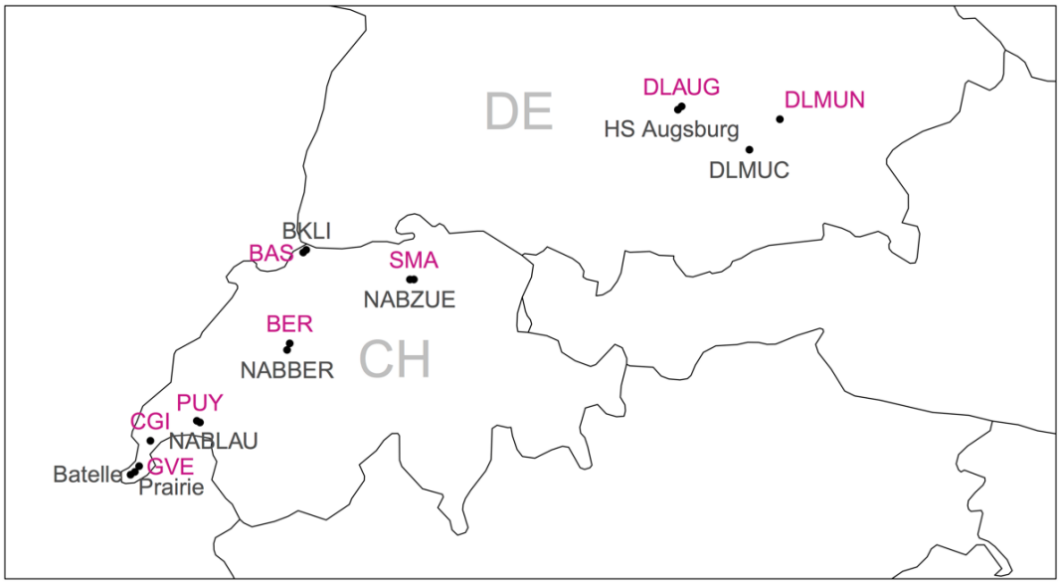

Figure 4: Proposed station couples (urban and rural site), located in Switzerland (CH) and the northern Alpine Foreland region in Germany (DE). Violet colors refer to rural stations, grey colors show urban sites. See Table 1 for full station names.

Table 1: The considered station couples (urban and rural site) with the respective abbreviation and overlapping time period of available data.

Rural station	Abbreviation	Urban station	Abbreviation	Overlapping time period
Basel Binningen	BAS	Basel Klingelberg-strasse	BKLI	2003-2018
Bern Zollikofen	BER	Bern Bollwerk	NABBER	2001-2018
Geneva Cointrin	GVE	Geneve Prairie	Prairie	2010-2016
Pully	PUY	Lausanne	NABLAU	1991-2018
Nyon Changins	CGI	Geneve Battelle	Battelle	2010-2016
Zurich Fluntern	SMA	Zurich Kaserne	NABZUE	1995-2018
Augsburg	DLAUG	Hochschule Augsburg	HS Augsburg	2004-2016
Munich Airport	DLMUN	Munich City	DLMUC	1992-2010

Eight variables with daily resolution are taken into account, namely: mean (tas), minimum (tmin) and maximum (tmax) 2m temperature for both urban and rural sites, mean precipitation (pr), mean relative humidity (hurs), mean 10m wind speed (wind), mean solar shortwave incoming radiation (rsds) and mean air pressure (pre) for rural sites. For NABZUE, the urban parameters sky view factor (SVF) and vegetation fraction (fveg) within a 500m radius around the urban station are considered additionally.

Observational data originate from various sources. The measurement data used for the rural sites in Switzerland are provided by a network of six automated stations, operated by the Swiss national weather service MeteoSwiss (SwissMetNet stations) and in accordance with World Meteorological Organization (WMO) standards. For urban sites in Switzerland, weather stations from different national, cantonal and university observational networks are considered (see Table 2).

Table 2: Partner networks for urban stations in Switzerland and Germany.

City	Abbreviation	Partner networks
Basel	BKLI	Department of Environmental Sciences, MCR-Lab, University of Basel
Bern	NABBER	National Air Pollution Monitoring Network (NABEL)
Geneva	Prairie	Service de l'air, du bruit et des rayonnements non ionisants, Canton de Genève Groupe Systèmes énergétiques Université de Genève
Lausanne	NABLAU	National Air Pollution Monitoring Network (NABEL)
Nyon	Battelle	see Lausanne
Zurich	NABZUE	National Air Pollution Monitoring Network (NABEL)
Augsburg	HS Augsburg	German Research Center for Environmental Health (Helmholtz Zentrum München)
Munich	DLMUC	German national weather service (*Deutscher Wetterdienst*, DWD)

For rural sites in Germany, observational data from weather stations operated by the German national weather service (*Deutscher Wetterdienst*, DWD) are used, which are consistent with WMO standards. For the considered urban sites in Germany, Augsburg and Munich, data are provided by the partner networks of the German Research Center for Environmental Health (*Helmholtz Zentrum München*) and the German national weather service (see Table 2).

Independent of the provider, urban stations are often subject to short and (or) sparse observational data coverage while rural stations, mostly maintained and operationally run by national weather services, offer long-term and high qualitative data sets. The overlapping time period (see Table 1, right column) for each station couple, meaning qualitative and continuous data at both urban and rural site for the same time period, is therefore mostly determined by the data availability at the urban station. For the employed station couples, the overlapping data periods range from 7 years (GVE-Prairie and CGI-Battelle) to 28 years (PUY-NABLAU). In the present thesis, the station couple SMA-NABZUE will be considered as exemplary sites for various analyses due to the long

overlapping time period of 24 years and the high-qualitative data sets at both urban and rural sites.

4.2 Regional Climate Model Data

Simulated station data at localized stations are used. The simulations are based on a multi-model combination set provided by the Swiss Climate Change Scenarios (CH2018), which are coordinated by the Swiss National Centre for Climate Services (NCCS). The climate model data originate from the Coordinated Downscaling Experiment for the European Domain (EURO-CORDEX; Jacob et al. 2014; Kotlarski et al. 2014) which provides regional climate model (RCM) simulations until the end of the 21st century at daily temporal resolution and at a spatial resolution of approximately 12km (EUR-11) and 50km (EUR-44), covering Europe and adjacent regions. RCMs are derived in a process called dynamical downscaling, i.e. a technique applied to increase the resolution of climate simulations by using a Global Climate Model (GCM) to prescribe the initial and lateral boundary conditions (typically wind components, temperature, water vapor and cloud variables, surface pressure, sea surface temperature; Giorgi 2006) for a higher-resolution RCM nested into the GCM grid (Dickinson et al. 1989; Giorgi 1990; Giorgi 2019; Giorgi, Bates 1989; McGregor 1997). Such nested GCM-RCM combinations are referred to as model chains. The RCMs thus translate the coarse global GCM projections to a finer resolution more suitable for studies of regional phenomena and the application to vulnerability, impacts and adaptation (VIA) assessments (e.g. Giorgi 2019).

The GCM-RCM simulations used in CH2018 are conditioned on scenarios of anthropogenic forcing (greenhouse gases, aerosols and land use) over the 21st century, which are referred to as Representative Concentration Pathways (RCPs). Three different RCPs are implemented in CH2018 (RCP2.6, RCP4.5, RCP8.5; Moss et al. 2010), of which we focus on the business-as-usual pathway RCP8.5 (i.e. continually increasing climate-influencing emissions and global warming) to show "worst-case" future conditions in the absence of dedicated mitigation measures. For RCP8.5, a multi-model set of 16 transient GCM-RCM climate

simulations (see Table 3, a-p) is considered, offering a broad range of possible future estimates.

Although RCM simulations from EURO-CORDEX provide information at relatively high spatial resolution, often it is still too poorly resolved for applied impact studies. Moreover, RCM simulations are subject to systematic biases. To overcome these limitations, a bias correction method and statistical downscaling to the local scale was performed to the still coarse RCM simulations by means of quantile mapping (QM; see Section 5.1.1 for further details), resulting in the CH2018 product DAILY-LOCAL, which is used in the present thesis for further analyses. Model simulations are available for the employed variables tas, tasmin, tasmax, pr, hurs, wind and rsds.

Table 3: The employed GCM-RCM climate simulations (a-p) for RCP8.5 at different spatial resolutions (EUR-11, EUR-44).

	RCM	GCM	RCP8.5	
			EUR-11	EUR-44
a	CLMcom-CCLM5-0-6	ICHEC-EC-EARTH		x
b	CLMcom-CCLM5-0-6	MIROC-MIROC5		x
c	CLMcom-CCLM5-0-6	MOHC-HadGEM2-ES		x
d	CLMcom-CCLM5-0-6	MPI-M-MPI-ESM-LR		x
e	DMI-HIRHAM5	ICHEC-EC-EARTH	x	
f	KNMI-RACMO22E	ICHEC-EC-EARTH		x
g	KNMI-RACMO22E	MOHC-HadGEM2-ES		x
h	SMHI-RCA4	CCCma-CanESM2		x
i	SMHI-RCA4	CSIRO-QCCCE-CSIRO-Mk3-6-0		x
j	SMHI-RCA4	ICHEC-EC-EARTH	x	
k	SMHI-RCA4	IPSL-IPSL-CM5A-MR	x	
l	SMHI-RCA4	MIROC-MIROC5		x
m	SMHI-RCA4	MOHC-HadGEM2-ES	x	
n	SMHI-RCA4	MPI-M-MPI-ESM-LR	x	
o	SMHI-RCA4	NCC-NorESM1-M		x
p	SMHI-RCA4	NOAA-GFDL-GFDL-ESM2M		x

4.3 Proposed Heat Indices

For quantifying the UHI in future climates, three widely-used heat indices are considered, namely the frequency of tropical nights (TN), summer days (SD) and hot days (HD) (see Table 4) for both the urban sites and their rural counterparts. Heat indices are parameters that are derived from meteorological measurement data such as temperature and defined for a certain threshold level (ETCCDI 2019, MeteoSwiss 2019). As such, they give the absolute number of days in exceedance of the respective threshold. The selection of heat indices as used in the present thesis is based on a collection of recommended indices (e.g. TN and SD) available from a WMO-initiated expert team (Expert Team on Climate Change Detection and Indices, ETCCDI; ETCCDI 2019). To be consistent with CH2018 (2018) and to account for temperature extremes, the employed selection additionally includes the heat index HD. The selected indices are based on both daily minimum temperature and daily maximum temperature (see Table 4) and thus take into account day- and nighttime conditions.

Table 4: The considered heat indices tropical nights (TN), summer days (SD) and hot days (HD) with the respective underlying meteorological variable and threshold.

Index	Meteorological variable	Threshold
Tropical nights (TN)	Tmin	> 20°C
Summer days (SD)	Tmax	> 25°C
Hot days (HD)	Tmax	> 30°C

Source: Own table, based on ETCCDI 2019.

5 Methods

Three different approaches are tested with the aim to transfer "standard" climate scenarios such as the localized CH2018 products, available for various rural sites for the period 1981-2099, into urban settings in order to gain transient climate scenarios for urban sites. We focus on generating urban scenarios for daily minimum (tmin) and daily maximum temperature (tmax), which will be referred to as *urban (climate) scenarios* in the following chapters. Once urban scenarios are set up, it enables us to analyze how the projected future climate in urban areas will differ from the future climate in the respective rural counterparts. These differences are investigated in terms of the standard heat indices TN, SD and HD, as introduced in Section 4.3. By comparing the frequency of the projected heat indices at the urban and the rural site, it is possible to account for the UHI in future climates

The simulated frequency of heat indices in future climates at both urban site and rural counterpart is (i) averaged over periods of 30 years to reveal the long-term climate change signal (temporal average). Consistent with CH2018 (2018), the frequency of TN, SD and HD is investigated with respect to the official WMO climate normal period 1981-2010 and for three scenario periods spanning the 21st century: 2020-2049, 2045-2074 and 2070-2099. These four 30-year periods will be referred to as *1995*, *2035*, *2060* and *2085*, respectively. To account for model uncertainty, we use (ii) the ensemble median frequency (multi-model median) of the obtained 30-year means and additionally consider the 5th - 95th percentile of the multi-model ensemble to account for model uncertainty range.

The order of the selected approaches, as discussed hereafter, follows certain considerations: First, those approaches will be introduced that use just one variable of the rural site to predict urban tmin or tmax (QM, simple linear regression; Sections 5.1 and 5.2). We then continue with increasing the number of parameters of the rural station considered for generating urban climate scenarios (multiple regression; Section 5.2). The third approach takes into account overall six variables, including two non-meteorological parameters of the urban site, in

order to parametrize the UHI, which is then added to the rural scenario data of tmin in order to gain urban scenarios for tmin (diagnostic equation; Section 5.3).

5.1 Two-Step Quantile Mapping

Climate model data of GCM-RCM simulations offer an attractive tool for various applications, including regional to local assessments of future climate change impacts. Yet, due to the scale gap between RCM output (about 10 to 50km) and applied impact studies and the systematic biases inherent to the RCM projections the direct use of raw model output in subsequent applications is often not possible. To overcome these challenges, empirical-statistical downscaling (ESD) approaches are promising tools to translate coarsely resolved and potentially biased climate model output to the local scale and, in turn, make it directly applicable to impact assessments. A large number of recent studies widely acknowledge the high performance of the statistical approach *quantile mapping* (QM) both for correcting systematic biases of climate model data and for downscaling the model simulations to the site scale (e.g. Gudmundsson et al. 2012; Monhart et al. 2018; Themeßl et al. 2012). Gutiérrez et al. (2018), for instance, found that QM is among the best performing methods in an intercomparison of statistical downscaling and bias correction methods over Europe. For Switzerland, Ivanov and Kotlarski (2017) and Rajczak et al. (2016) validated QM for several meteorological variables and a large number of MeteoSwiss stations, confirming its high performance and robust results.

In the framework of the present thesis, QM is applied in a two-step manner, using (i) bias-corrected scenarios of rural sites, generated on the basis of a first-step QM from model output to the site scale within CH2018 (2018) (Section 5.1.1), and (ii) spatially transfer these scenarios within the present thesis to the respective urban site on the basis of a second-step QM (Section 5.1.2). The QM technique as used in CH2018 (2018) and in this work originates from Ivanov and Kotlarski (2017) and Rajczak et al (2016) and has been implemented in an extensive R-package[1], which is applied in the present thesis for the second-step

[1] qmCH2018 v1.0.1, doi: 10.5281/zenodo.3275571, https://github.com/SvenKotlarski/qmCH2018.

QM. Even though in this work only the latter step has been carried out, both QM steps will be introduced in the following for the sake of completeness.

5.1.1 First-Step Quantile Mapping

The basic principle of the employed QM approach is to (approximately) match simulated and observed distributions by calibrating a quantile-dependent correction function (see 1. in Figure 5) in a historical reference period (in CH2018: 1981-2010) that translates simulated quantiles into their observed counterparts. The so established correction function is then used to translate a transient simulated time series into a bias-corrected series (in CH2018: 1981-2099) with a distribution representative of the observed one (see 2. in Figure 5). In doing so, QM implicitly corrects for both systematic model biases and errors related to the different scales (Rajczak et al. 2016).

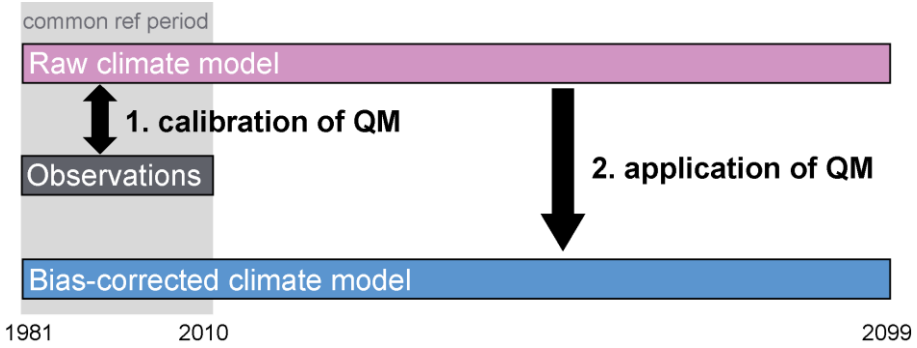

Figure 5: Methodological overview of the first-step QM.
Source: Own figure, based on CH2018 (2018).

The QM implementation used in CH2018 is based on 99 percentiles (1st to 99th percentile) of the daily time series. In between the 99 percentiles, the correction function is linearly interpolated. Values smaller than the 1st and larger than the 99th percentile are corrected according to the correction function of the 1st and 99th percentile, respectively (Themeßl et al. 2012). The QM correction function is calibrated separately for each day of the year (DOY) using a moving window of 91 days. By using a 91-day moving window, the QM calibration is done with a quasi-seasonal transfer function centered over the considered day (including 45 days before and 45 days after the respective DOY), which has the advantage of less occurring new extremes (i.e. values that lie outside the range of observed

values in the historical period 1981-2010), resulting in a reduced sampling uncertainty (Feigenwinter et al. 2018; Rajczak et al. 2016).

As shown in previous studies (Themeßl et al. 2012; Wilcke et al. 2013), QM corrects a raw climate model time series X at time (t) and location (s) to a time series Y according to

$$Y_{t,s} = ecdf_{DOY,s}^{obs,cal^{-1}}\left[ecdf_{DOY,s}^{mod,cal}\left(X_{t,s}\right)\right] \quad (1)$$

where *ecdf* is the empirical cumulative distribution function, *obs* refers to observations and *mod* to raw model output, both in the calibration period *cal* 1981-2010. Note that, in contrast to Swiss stations, the sites in Germany were calibrated in 1992-2018 due to shorter data availability. X and *mod* do not necessarily need to be model data, but can also be a time series from another station, as used for the second-step QM approach (Section 5.1.2).

The first-step QM as used within CH2018 (2018) comprises both a climate model bias correction and a downscaling component. A typical example of the first-step QM application is the mapping of climate model projections (raw RCM data) onto specific weather stations with long-term observational records (here MeteoSwiss stations at rural sites; see "first-step QM" in Figure 6). QM thus enables to generate transient scenarios for rural sites from climate model data (Feigenwinter et al. 2018; Rajczak et al. 2016). These generated scenario products referred to as DAILY-LOCAL in CH2018 (2018) are then used for a subsequent QM step, as introduced below.

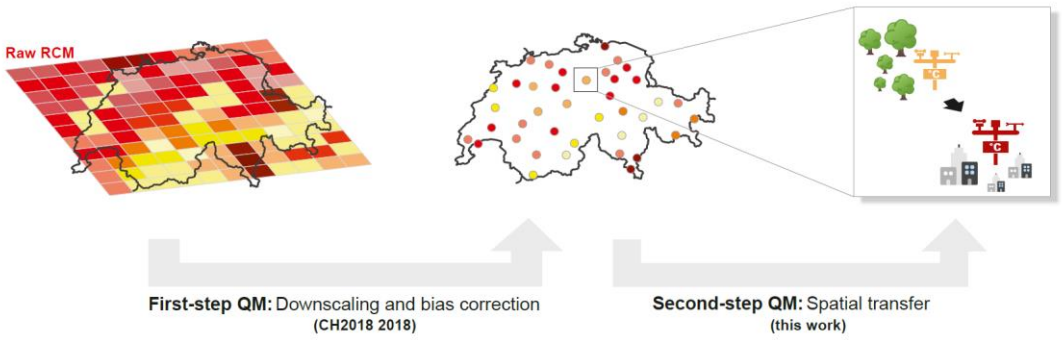

Figure 6: Two-step quantile mapping (QM) approach.

5.1.2 Second-Step Quantile Mapping

In order to generate scenarios for urban sites, the identical method as described in Section 5.1.1 is used a second time, yet this time not for downscaling and bias-correcting but for spatially transferring climate scenarios (here CH2018 scenarios of rural sites resulting from the first-step QM; CH2018 2018) to the urban target sites (second-step QM; see "second-step QM" in Figure 6). The second-step QM (in the following referred to as QM) as originated from the work of Rajczak et al. (2016) for permafrost research thus enables to generate transient climate scenarios for urban sites, despite their often short and low qualitative data series. The second-step QM is applied to all station couples introduced in Table 1. The QM correction function is based on pairwise daily observations at both urban and rural location and calibrated in an common reference period (see 1. in Figure 7 and Table 1, right column). As Figure 7 shows, the correction function is then applied to the entire time series of the rural site (see 2. in Figure 7; 1981-2099) to spatially translate it into a transient time series at the urban target site (1981-2099).

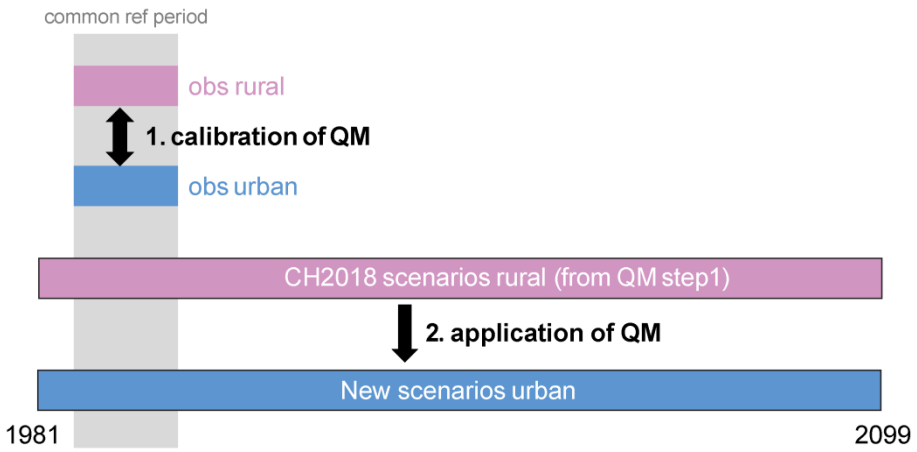

Figure 7: Methodological overview of the second-step QM.

For calibrating the correction function, Equation (1) is applied but with the urban station representing *obs* and the rural counterpart representing *mod*. By calibrating the function with observational data in a historical reference period, the statistical relationship between urban and rural site, i.e. the UHI, is assumed to hold for the period in present climate and not to change in the future climate either. Still, we are aware of the fact that this assumption might not be valid until

the end of the century for multiple reasons. Urban areas, for instance, will change in size, energy consumption, or other characteristics, affecting the local climate and thus the UHI (see further Chapter 7; Hoffmann et al 2012).

5.2 (Multiple) Linear Regression

As a second approach, a statistical learning method is applied, namely simple (LR) and multiple linear regression-based (MR) models, used for generating urban scenarios on the basis of meteorological variables of the rural site. These models are then used to investigate future urban temperatures as a function of modeled rural scenarios calculated in CH2018 (2018). Note that this approach is applied to the exemplary station couple SMA-NABZUE only. The aim is to use one (LR) or several meteorological predictor variables (MR) X of the rural site to predict the target variable or predictand Y by linearly estimating their relationship in a common reference period (here 1995-2018).

As the thesis aims at generating scenarios for the urban site, the predictand will be tmin and tmax, respectively, at NABZUE for the time period 1981-2099. In order to find appropriate predictors X for LR and MR, the correlation of the predictand and potential meteorological predictors is investigated first, using summer months (JJA) in the observational period 1995-2018. Those variables with the strongest correlation with the predictand will later serve as predictors to generate urban scenarios. Five potential predictors were chosen for the correlation analysis based on physical relevance, namely: tmin and tmax, respectively, hurs, pre, wind and rsds (of the previous day). Table 5 shows the results of the correlation analysis for the predictands urban tmin and tmax. All correlation coefficients, except for pre (for urban tmin) are statistically significant (at significance level $\alpha = 0.05$). As expected, rural tmin (tmax) offers the strongest relationship with urban tmin (tmax). Thus, (i) it is used as predictor in a simple linear regression, training in the period 1995-2018 to generate urban scenarios (LR; Equation 2 and 5 for tmin and tmax, respectively). Hurs and rsds also highly correlate with urban tmin (tmax), with rsds showing the second highest correlation for urban tmin and the third highest correlation for urban tmax, and

the other way around for hurs. In contrast, the relationship of wind and pre with urban tmin and tmax, respectively, is very low.

Table 5: Pearson correlation coefficient of daily series of urban tmin and tmax and different meteorological variables of the rural site for the summer months of 1995-2018. Asterisks mark statistically significant correlation coefficients at the significance level α = 0.05.

Rural variables	Urban tmin (°C)	Urban tmax (°C)
tmin (°C)	0.980*	-
tmax (°C)	-	0.993*
rsds (W/m²)	0.412*	0.568*
hurs (%)	-0.275*	-0.650*
wind (m/s)	-0.223*	-0.289*
pre (hPa)	0.029	0.135*

The results from the correlation coefficients show that, in addition to rural tmin (tmax), the variables rsds and hurs could be used to predict urban tmin (tmax). We thus consider for the same training period 1995-2018 (ii) rsds (hurs) and tmin (tmax) of the rural site as predictors in a multiple linear regression (MR, Equation 3 and 6 for tmin and tmax, respectively) and (iii) also use hurs (rsds) to see potential improvements in the prediction performance (MR, Equation 4 and 7 for tmin and tmax, respectively). This way six different configurations of the regression models are tested (three for urban tmin and the respective ones for urban tmax), with increasing number of predictors.

$$tmin_{urban} = a_1 * tmin + b_1 \quad (2)$$

$$tmin_{urban} = a_2 * tmin + b_2 * rsds + c_1 \quad (3)$$

$$tmin_{urban} = a_3 * tmin + b_3 * rsds + c_2 * hurs + d_1 \quad (4)$$

$$tmax_{urban} = a_4 * tmax + b_4 \quad (5)$$

$$tmax_{urban} = a_5 * tmax + b_5 * hurs + c_3 \quad (6)$$

$$tmax_{urban} = a_6 * tmax + b_6 * hurs + c_4 * rsds + d_2 \quad (7)$$

To be consistent with the QM approach and to reduce uncertainties, a time-dependent, quasi-seasonal transfer function is calibrated separately for each DOY using a 91-day moving window. We then use the generated regression

coefficients of each DOY to predict the urban tmin (tmax) values for the respective DOY. Similar to the QM technique, the statistical relationship between urban and rural site, i.e. the UHI, is assumed to be stationary over time, when calibrating the regression models with observational data in the historical reference period 1995-2018.

Regression-based methods in the climate context have already been successfully used in a number of studies. Gutiérrez et al. (2018), for instance, investigated among other approaches the performance of linear regressions as a statistical downscaling method for temperature (tmin, tmax) taking large-scale meteorological predictors. Similarly, Hessami et al. (2008) considered an automated statistical downscaling (ASD) regression-based approach to reconstruct the observed climate in eastern Canada. Sippel et al. (2019) used advanced statistical learning methods, namely so-called regularized linear models (ridge regression, lasso regression, elastic net regression), to model the relationship between circulation variability and atmospheric target variables in order to uncover the externally-forced response, which is expected to be contained in the residual component of the regression.

5.3 Diagnostic Equation for Daily Maximum UHI

The third method tested is a physically-based parametrization designed by Theeuwes et al. (2017). The diagnostic equation provides a straightforward tool to quantify the daily maximum UHI (UHI Theeuwes) at street level, valid for various urban locations in northwestern Europe. For designing the equation, Theeuwes et al. (2017) use variables they consider influencing the maximum UHI the most and that are straightforward to obtain, according to the authors. As such, the formula requires routine meteorological variables (tmin, tmax, wind, rsds) of the rural site at daily resolution and basic morphology data of the urban area, such as the sky view factor (SVF) and the surface vegetation fraction around the urban station (in a radius of 500m; fveg). The input data of urban and rural site are estimated in separate parts and then multiplied to obtain the UHI Theeuwes (see Equation 8).

$$UHI_{Theeuwes} = \left(2 - SVF - f_{veg}\right) \sqrt[4]{\frac{rsds\ DTR^3}{wind}} \quad \textbf{(8)}$$

$UHI_{Theeuwes}$	maximum urban heat island (K)
SVF	sky view factor
f_{veg}	vegetation fraction within a 500m radius of the urban weather station
rsds	incoming solar shortwave radiation at the rural site (K ms^{-1})
DTR	diurnal temperature range at the rural site (tmax-tmin) (K)
wind	10m wind speed at the rural site (ms^{-1})

The first factor of Equation 8, given by the term 2-SVF-fveg, denotes a morphological factor specific to each urban site. As such, the design of the equation considers the urban-rural temperature difference to be caused by urban characteristics such as street geometry and urban vegetation fraction only (Zhang et al. 2019). Accordingly, the morphology factor representing urban characteristics could be considered a comprehensive index that translates climatic conditions at the rural site (second factor in Equation 8) to the respective urban-rural temperature difference given at the considered station couple.

Note that the equation is derived and thus valid only for 0.2 < SVF < 0.9 and for 0 < fveg < 0.4. According to Theeuwes et al. (2017), the equation also holds true only for certain synoptic situations. Weather events like frontal systems that cause differences in the urban and rural temperatures not related to the UHI need to be excluded, first. Frontal systems are excluded by only considering days with very few rain (pr < 0.3mm) and fog (hurs < 80%). Moreover, wind speed is limited to values in exceedance of 0.5ms^{-1}. To exclude the largest anthropogenic heat fluxes, heating degree days (HDD)[2] of more than 17 (base temperature of 18°C; tbase) need to be excluded as well (Theeuwes et al. 2017).

The approach is tested for the Zurich station couple SMA-NABZUE, using a SVF for NABZUE of 0.8, which lies in the SVF range of the respective local climate

[2] HDD = $\sum_{days}(tbase - tas)$ (Büyükalaca et al. 2001).

zone (Stewart, Oke 2012), that has been identified as "open midrise"[3] (Gehrig et al. 2018). The fveg of 0.125 is derived by an optical analysis based on Google maps and consistent with Gehrig et al. (2018). It is important to mention, that SVF and fveg are assumed to stay constant during the entire reference and scenario periods. For the meteorological variables, CH2018 (2018) scenario data of the rural site are considered for the time period 1981-2099 to calculate the future maximum UHI, having left about 31% of data for the subsequent analysis after applying the exclusion criteria. We translate rsds values from the current unit W/m^2 into the desired kinematic unit K ms^{-1} (rsds_kin) with

$$\rho = \frac{pre}{(R_d * tas)} \quad \textbf{(9)}$$

and

$$rsds\_kin = \frac{rsds}{(\rho * c_p)} \quad \textbf{(10)}$$

where ρ is the air density (kg/m^3), R_d (287.07 J/(kg*K)) is the gas constant for dry air (AMS 2019) and c_p (1005 J/kg*K) is the specific heat capacity for dry air at 273K (AMS 2019). Note that pre is not provided in CH2018 (2018). Thus, the 30-year average over the WMO normal period 1981-2010 is used, justified by the IPCC (2013) results that reveal very little changes of air pressure in a climate change context.

To be consistent with the former approaches that directly result in climate scenarios of tmin for urban sites (Sections 5.1 and 5.2), the derived UHI Theeuwes is added as an increment to the rural modeled data of tmin (CH2018 2018) to gain a modeled time series of urban tmin for the period 1981-2099. Note that this technique is only valid for tmin values. As the UHI is mainly a nocturnal phenomenon (see Chapter 3) it shows temporal correspondence with tmin rather

[3] The local climate zone (LCZ) „open midrise" is characterized by midrise buildings (3-9 stories) and the abundance of pervious land cover (low plants, scattered trees). Concrete, steel, stone and glass are mainly used as construction materials (Stewart, Oke 2012).

than with tmax values. For generating urban scenarios for tmax, this approach is thus not possible to use.

5.4 Validation Framework

For evaluating the proposed methods, three independent cross-validation strategies (see Table 6) are considered and applied to daily summer data of the exemplary station pair SMA-NABZUE in the observational period 1995-2018. Choosing the station couple SMA-NABZUE as exemplary site for the evaluation is motivated by its long and qualitative overlapping data set of 24 years.

Table 6: The considered cross-validation approaches with the respective abbreviation and short definition.

Validation approach	Abbreviation	Definition
Split sample approach	SSA	the model is trained with the first half of data and tested on the remaining half, and vice versa
Split sample approach (warm/cold) and (cold/warm)	SSA(WC), SSA(CW)	same as SSA, but splitting the data set in terms of years with warmer summers used for training the model and years with colder summers used for testing (WC) the model, and vice versa (CW)
Limited data approach	LDA	the data set is split into thirds with the first two-thirds used for training the model and the remaining for testing the model. Within the training set, different calibration period lengths are tested, starting with 1 year and steadily increasing with an increment of 1; years are randomly combined (no repetition, no permutation)

Note that for the different approaches (QM, regression-based methods, diagnostic equation), not all three validation strategies are considered for every approach. For the first-step QM, a large number of existing literature has already demonstrated its ability and skill in correcting climate model biases at the local scale (e.g. Gudmundsson et al. 2012; Gutiérrez et al. 2018; Ivanov, Kotlarski 2017; Rajczak et al 2016; Themeßl et al. 2012). A brief description of the employed

validation techniques followed by a short introduction of the used skill measures is provided in the following. Note that regardless of the validation technique, the calibration is always done for each DOY with a 91-day moving window (for QM and the regression methods).

5.4.1 Validation Techniques

The **split sample approach (SSA)** splits the overlapping time period of the urban and the rural site 1995-2018 (24 years) into two chronological data sets of 12 full years each, namely from 1995-2006 and from 2007-2018 (Figure 8). First, the first half is taken for calibrating the model and the second half for validating it. Second, the second half serves as calibration period and the first half as validation period. The cross-validation exercise thus guarantees independent calibration and validation periods. The predicted results are merged, so that one skill measure can be calculated for the independent evaluations for the whole period 1995-2018. The SSA is applied to the second-step QM technique.

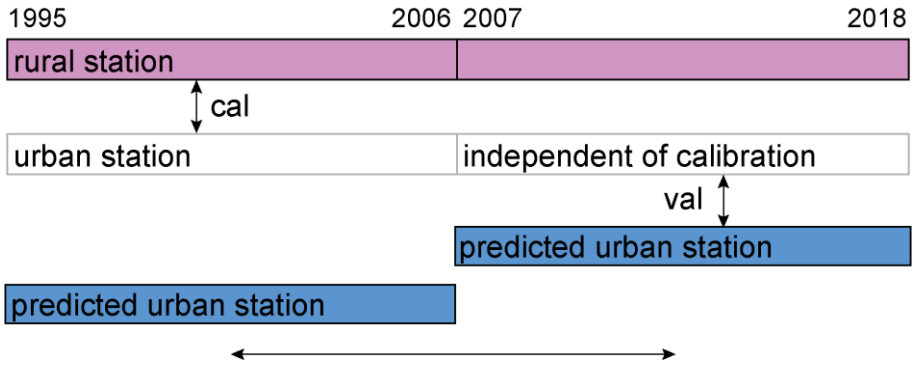

Figure 8: Split sample approach (SSA) for the overlapping time period of urban (white, blue) and rural site (violet) from 1995-2018 (24 years).

Similar to the SSA, the warm/cold -**SSA(WC)**- and cold/warm -**SSA(CW)**- approaches split the overlapping time period 1995-2018 into two data sets of 12 full years each. The splitting, however, is not done chronologically, but takes as divisive criterion the 12 warmer and the 12 colder summers, based on summer mean temperature within the 24-years period of the rural site (Figure 9). On the basis of this principle, the 24-years period of the urban site is divided accordingly. First, the 12 years with the warmer summers are used for calibration and the remaining 12 years with the colder summers for validation. Second, the

12 years with the colder summers are taken for calibration and the remaining 12 years with the warmer summers for validation. This approach additionally evaluates the methods' performance in a climate change context with observed trends in temperature inducing a warmer testing than training period. The approach results in two independent skills, one for the SSA(WC) setting and one for the SSA(CW) setting. Due to the relevant information on the methods' performance in a climate change context, this validation technique is applied to all employed approaches (see Sections 5.1-5.3). However, note that for the diagnostic equation (Theeuwes et al. 2017), the validation technique cannot be applied the same way as for QM and the regression models, since there is no model to be trained. To nevertheless evaluate the equation, the respective performance during warm summers (warm) and cold summers (cold) is analyzed.

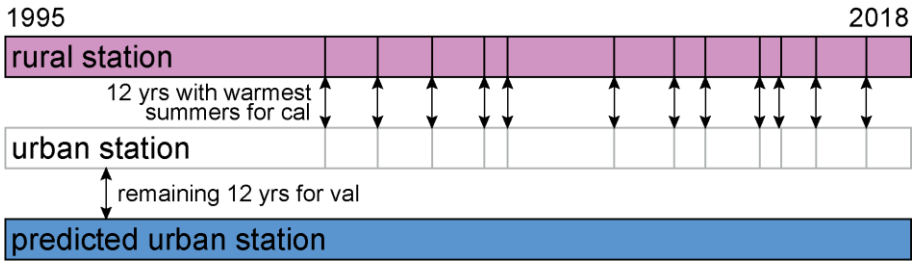

Figure 9: Split sample approach warm/cold -SSA(WC)- and cold/warm -SSA (CW)- for the overlapping time period of urban (white, blue) and rural site (violet) from 1995-2018 (24 years).

The **limited data approach (LDA)** splits the series into the periods 1995-2010 (16 years) and 2011-2018 (8 years), with the calibration based on the first period and the validation based on the remaining second period. Within the period 1995-2010, different calibration period lengths are used, starting with 1 year and steadily increasing to 15 years with an increment of 1 (Figure 10). By random combination of years, 16 different calibration samples for each length are validated against observations for the period 2011-2018. For instance, if the length is 3, one realization could consist of the years 1995, 1998 and 2004. During randomization, no year is taken twice within one calibration sample (no repetition). The order within one sample does not matter (no permutation),

meaning for length 2, for instance, the exemplary combination of 1995 and 2003 counts the same as 2003 and 1995. The aim of this approach is both to quantify uncertainties by using random combinations of calibration years and to simulate a lack of data availability by using various sample sizes (Rajczak et al. 2016). Accordingly, the LDA helps to identify the minimum length of overlapping data of urban and rural sites in order to still gain robust results, i.e. the bias is distinctly smaller compared to shorter calibration lengths. Note that this approach is applied to the second-step QM technique.

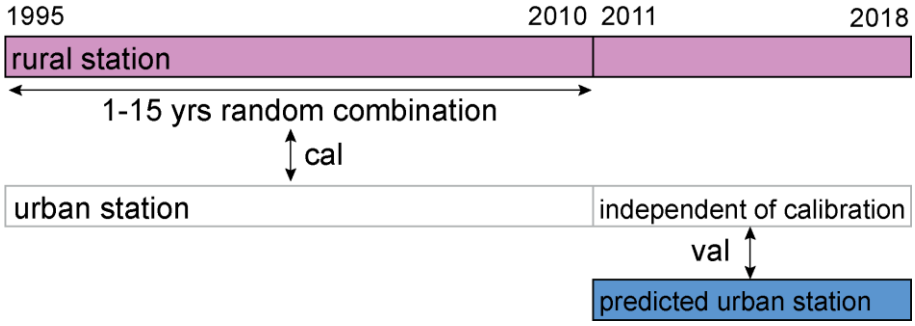

Figure 10: Limited data approach (LDA) for the overlapping time period of urban (white, blue) and rural site (violet) from 1995-2018 (24 years).

5.4.2 Skill Scores

The validation focuses on the mean bias (bias), which is considered the most relevant score within a climatological context. The bias describes the simple offset between predicted (X_{pred}) and observed data (X_{obs}), defined as

$$Bias = \overline{X}_{pred} - \overline{X}_{obs} \quad \textbf{(11)}$$

where $\overline{X}$ is the mean value over the validation period. The bias is used to evaluate several parameters, namely: tmin, tmax, UHI and the frequency of heat indices (TN, SD, HD).

It is true that sharp thresholds, as valid for the proposed heat indices, may cause substantial biases in the absolute numbers of heat indices, even though the differences in tmin (tmax) are small. This might happen if one time series offers values slightly above the threshold while values of the verifying time series lie slightly below the threshold. Therefore, to account for the performance in the

upper tail of the distribution, the bias of a percentile-based threshold (95^{th} percentile) for tmin and tmax is considered additionally.

Further, Pearson correlation coefficients (cor) are taken into account to assess the temporal correspondence between predicted and observed values at daily resolution and to validate the relation between input and target variables. The R-squared is additionally considered as a measure of goodness of fit for the comparison of the regression models.

6 Results

In the following, we provide an overview on the results of the three considered approaches used to transfer climate scenarios of rural sites into urban settings in order to account for the UHI in future climates. We first present evaluation results for each employed approach separately (Section 6.1-6.3) and, in a second step, discuss respective performances in a comparative framework (Section 6.4). Third, we will provide and analyze the final results of climate scenarios for urban sites, and discuss how the projected future climate in urban areas will differ from the future climate in the respective rural counterparts in terms of the standard heat indices TN, SD and HD (Section 6.5).

6.1 Evaluation of QM

We present a summary of the biases of the second-step QM application used for spatially transferring bias-corrected climate scenarios of the rural site to specific urban target sites. The evaluation is done for the variables tmin, tmax and the employed heat indices TN, SD and HD for the exemplary station couple SMA-NABZUE and the observational period 1995-2018 (JJA). Evaluation results are derived by using the three validation techniques introduced in Section 5.4.1. Figure 11 summarizes the results for tmin (a) and tmax (b).

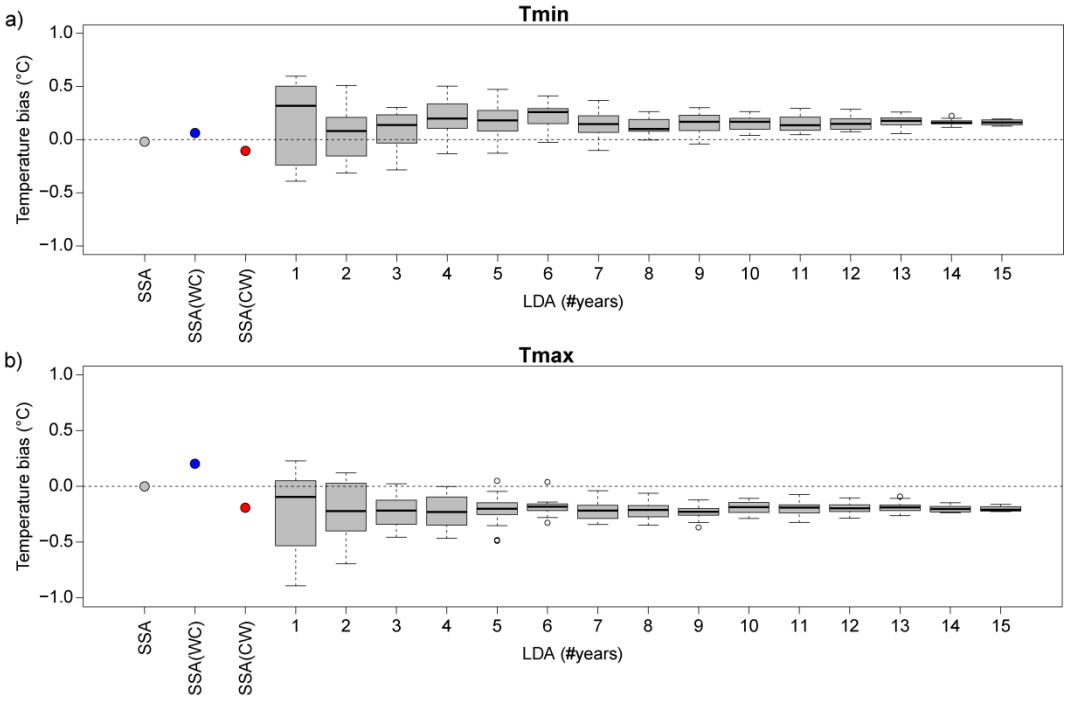

Figure 11: Validation results for urban daily minimum temperature (tmin; a) and urban daily maximum temperature (tmax; b) predicted by the two-step QM for the station couple SMA-NABZUE. The x-axis denotes different validation techniques (Section 5.4.1): SSA (split sample approach), SSA(WC) (SSA warm/cold), SSA(CW) (SSA cold/warm), LDA (limited data approach) with the number of considered years for calibration (#years) increasing from left (one) to right (15). The y-axis shows the temperature bias (Section 5.4.2). The boxplots for the LDA mark in grey the range between the 1st quartile (Q1, lower border) and the 3rd quartile (Q3, upper border), referred to as interquartile range (IQR). The bold black line centered within the IQR indicates the median. The lower whisker refers to Q1-1.5*IQR and the upper whisker to Q3+1.5*IQR. Dots below/above the whiskers reveal outliers. For the three SSA techniques, the calibration and validation periods are 12 years, respectively. For the LDA, the calibration period is 1995-2010 and the validation period is 2011-2018.

The independent cross-validation exercise SSA with contiguous training and testing periods of 12 years, respectively, reveals the highest skill of almost zero bias for both tmin (Figure 11a) and tmax (Figure 11b). It needs to be mentioned, however, that for SSA, as defined in Section 5.4.1, modeled results of both periods (12 years each) are merged before comparing it to the whole observational time series (24 years, 1995-2018). By doing so, slightly positive and negative biases of the respective results are compensated.

Considering not a single bias for the whole time series but for 12 years, the SSA(WC) and SSA(CW) reveal for both tmin and tmax slightly positive (WC) and negative (CW) biases, respectively (Figure 11). We assume, these differences result from the correction functions being calculated in different calibration periods, namely (i) in years with warmer summers, as for SSA(WC), and (ii) in years with colder summers, as for SSA(CW). We focus on the observed UHI to see if the urban-rural temperature difference varies depending on the cold/warm nature of the years considered for training and testing. Figure 12 shows the course of the UHI for tmin (a) and tmax (b).

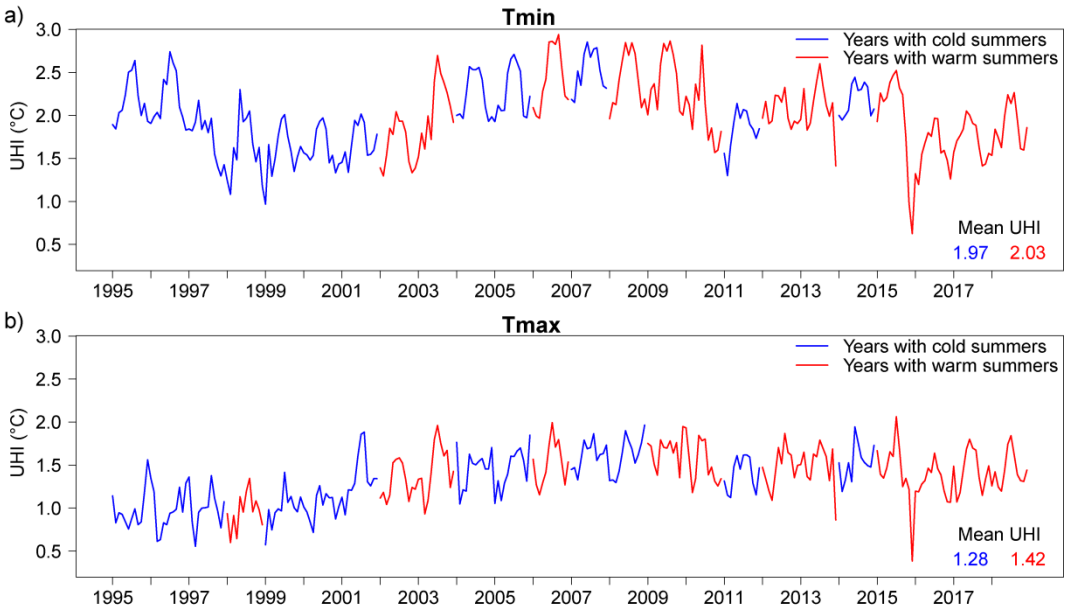

Figure 12: Monthly mean course of the UHI based on urban and rural observations of daily minimum temperatures (tmin; a) and daily maximum temperatures (tmax; b) of the exemplary station couple SMA-NABZUE over the period 1995-2018.The blue-colored fractions refer to the 12 years with colder summers, the red-colored fractions refer to the 12 years with warmer summers, defined on the basis of the summer mean temperature at the rural site SMA. The 12-year average of UHI is 1.97°C (1.28°C) for years with colder summers and 2.03°C (1.42°C) for those with warmer summers.

For tmin (tmax), we find that the calibration in years with colder summers is based on a monthly mean UHI of 1.97°C (1.28°C), whereas in years with warmer summers the monthly average is slightly higher, namely 2.03°C (1.42°C) (Figure 12). Applying the so established correction function to the remaining 12 years of

rural tmin (tmax) results in slightly overestimated urban temperatures when calibrated for years with colder summers and slightly underestimated urban temperatures when calibrated for years with warmer summers, as shown in Figure 11 (blue and red dots). The over/underestimation is more pronounced for tmax (Figure 11b) than for tmin (Figure 11a). The larger monthly mean UHI difference based on tmax between the calibration and validation period (0.14°C for tmax vs 0.06°C for tmin) is assumed to be responsible for the larger bias.

The LDA (Figure 11) indicates a systematic overestimation of the observed tmin and a systematic underestimation of the observed tmax. Interestingly, for tmin, the respective median biases approach the bias of SSA(WC) the more years are considered for calibration. This is due to the fact that in the calibration period 1995-2010, where years are randomly selected, the monthly mean UHI is slightly higher (2.04°C; not shown) than for the validation period 2011-2018 (1.92°C; not shown), as are monthly mean UHIs for SSA(WC). For tmax, biases behave similar to the results of SSA(CW); especially when increasing the number of years used for calibration. As expected, the monthly mean UHI is lower for the training period (1.31°C; not shown) than for the testing period (1.44°C; not shown). Moreover, the validation exercise reveals the performance's dependency on the number of considered years for calibration, which increases with the length of calibration (#years in Figure 11). However, already three years of calibration offer reasonable results with a bias close to zero, even though large uncertainties, i.e. extended whiskers due to different combinations of years, remain.

Throughout all validation techniques, it is obvious that the highest skills with very few uncertainty ranges are achieved for long calibration periods (> 12 years). However, based on the results of the LDA, a minimum calibration length of seven (median bias of 0.15 for tmin, -0.22 for tmax) to eight years (median bias of 0.10 for tmin, -0.21 for tmax) is suggested to still gain robust results, i.e. the bias is distinctly smaller compared to shorter calibration lengths.

As the thesis aims at quantifying the UHI effect in future climates on the basis of heat indices, it makes sense to evaluate the performance specifically for the frequency of TN, SD and HD. We evaluate the QM performance for the different

heat indices on the basis of the employed validation techniques SSA, SSA(WC), SSA(CW) and LDA (see Section 5.4.1).

Considering the biases in the frequency of TN (Figure 13a), we can detect a very similar pattern compared to the biases for tmin (Figure 11a).

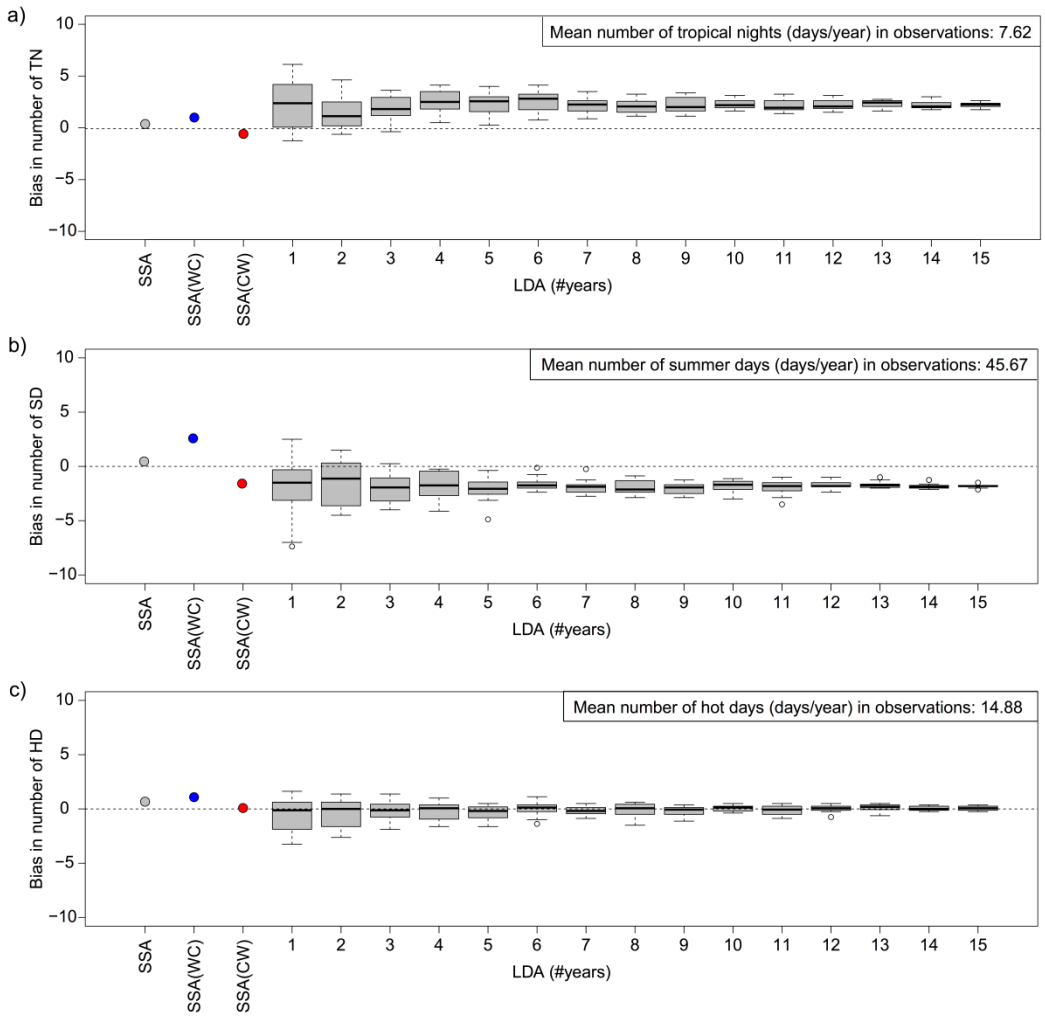

Figure 13: Same as Figure 11 but for the frequency of the employed heat indices tropical nights (TN; a), summer days (SD; b) and hot days (HD; c), respectively. Averaged over the observational period 1995-2018, there are 7.62 TN, 45.67 SD and 14.88 HD per year at the urban site.

The SSA reveals the highest skill with a bias of almost zero, whereas its variants WC and CW offer slightly positive and negative biases of +1 and –0.5 TN (Figure 13a). For the LDA, the performance (especially in terms of the uncertainty range) strongly depends on the number of considered years for calibration. As for tmin, the skill is sharpened when considering seven (median bias 2.25) or more years

for the model calibration. However, a systematic overestimation of about two TN per year remains, even when using an extended calibration length of 15 years. The differing UHI intensities during training and testing periods are assumed to be responsible for the systematic positive biases, i.e. modeled values are overestimated, as the calibrated correction function for the LDA is based on a larger urban-rural temperature gradient (2.04°C for 1995-2010; not shown) as it prevails in the testing period (1.92°C for 2011-2018; not shown). Note that by having on average about 8 TN per year at the urban site during the summers of 1995-2018, QM overestimates the number of TN by more than 26%, when using 15 years for calibration.

Besides varying UHI intensities in the training and testing set, we generally assume the absolute TN threshold of tmin>20°C to contribute to the considerable biases. Figure 14a reveals the overall good performance of QM for most of the analyzed summers of 1995-2018, cross-validated by the SSA. Even in years with no TN at the rural site (SMA), QM manages to (approximately) model the number of TN at the urban site (see e.g. 1995, 2005, 2010). Still, there are years with large biases, for instance in 2017, where the frequency of TN is highly overestimated. Bear in mind that for the SSA, the predicted time series of 12 years respectively (1995-2006 and 2007-2018) are merged before calculating the bias for the whole period (1995-2018; see Section 5.4.1). This explains the still low bias for the SSA in Figure 13a, despite strong biases for specific years. For an exemplary analysis, we focus on the tmin daily time series during summer 2017 to better explain the varying results of QM and the observations (Figure 14b).

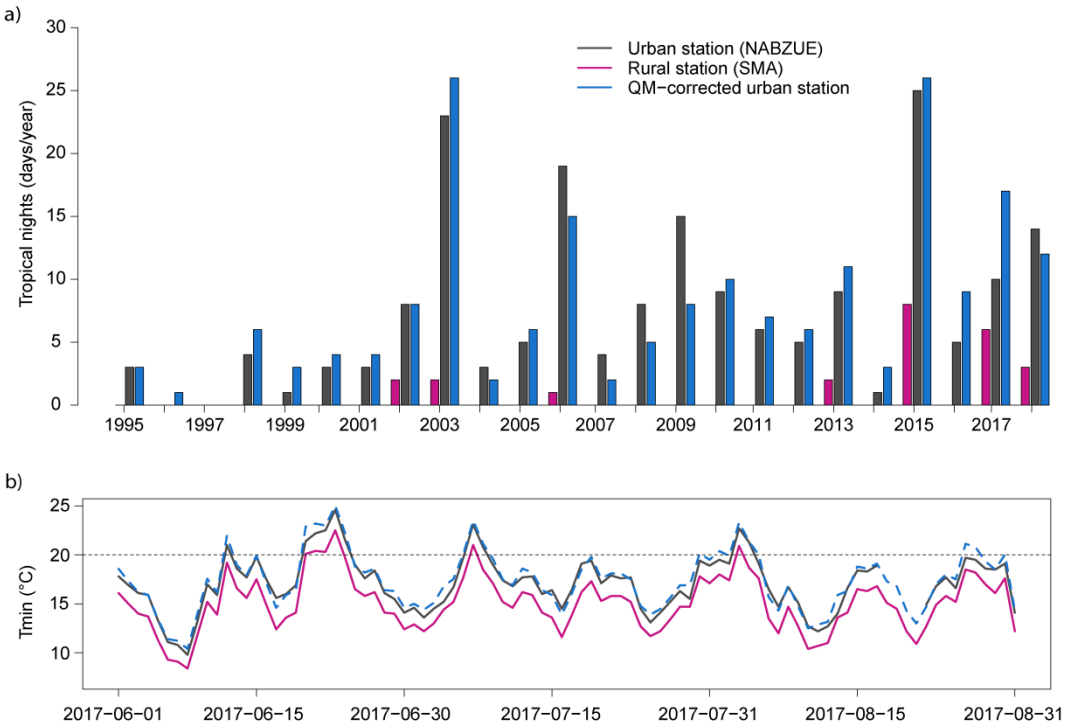

Figure 14: Bar plot with the frequency of tropical nights (TN; days/year) for the urban (NABZUE; grey), rural (SMA; violet) and QM-corrected urban station (blue) based on SSA for the summers of 1995-2018 (a). The line plot reveals the daily evolution of minimum temperatures (tmin) for the urban (grey), rural (violet) and QM-corrected urban time series (dashed and blue) in summer 2017, where the bias in the number of TN (QM vs observations) is especially large (b). The dotted horizontal line refers to the TN threshold of 20°C.

The strong positive bias in 2017, shown in Figure 14a, can be explained when focusing, for instance, on the first and the last week of August in Figure 14b, where urban observations happen to be slightly below 20°C frequently. The quantile-mapped time series, however, translates these instances to temperatures slightly above the 20°C-threshold, leading to more TN during these two periods. As a result, QM appears to strongly overestimate the number of TN during the considered periods, even though the bias of tmin is as small as in other years. We thus assume the absolute threshold of TN to play an important role in terms of biases. Accordingly, we additionally consider the bias in the 95th percentile in Section 6.4 to account for the performance in the upper tail of the tmin distribution, for the comparison with the other approaches.

Figure 13b shows the evaluation of SD, offering similar results compared to tmax (see Figure 11b). Considering the LDA, biases indicate a systematic

underestimation, which can be sharpened when using six (-1.75 SD) or more years for calibration. Still, differences of at least -1.68 SD (#10 years) remain. Overall, QM underestimates SD approximately 4%, when comparing the median LDA bias of a 15 year-calibration and the mean number of SD per year, averaged over 24 summers (1995-2018).

The numbers of HD, which occur far less than SD, are generally captured very well (Figure 13c). All validation techniques offer robust results with low biases. When focusing on six or more years for calibration, the remaining differences to the observational reference lie between -0.18 and +0.18 HD, taking the median numbers of HD for each calibration length. For 15 years of calibration, the bias is even closer to zero (0.06 HD).

6.2 Evaluation of (Multiple) Linear Regression

In the following, we analyze the performance of the (multiple) linear regression models used for generating climate scenarios of urban sites on the basis of meteorological variables of rural sites. We consider three regression analyses for the predictand variables urban tmin and tmax, respectively, based on different rural predictor variables (see Section 5.2). The evaluation exercise has been performed for the exemplary station couple SMA-NABZUE and the observational period 1995-2018 (JJA), considering the correlation of predicted versus observed values (Section 5.4.2). The validation techniques SSA(WC) and SSA(CW), as introduced in Section 5.4.1, are used to likewise validate the regression performance in a climate change context. For further evaluation results on the respective biases see Section 6.4, where the performances of all employed methods (Sections 5.1-5.3) are compared.

Figure 15 summarizes the evaluation results between observed and predicted urban tmin, obtained from different regression models. As the prediction of urban tmax indicates very similar evaluation results, we focus on tmin only and kindly refer the reader to Appendix 1 for results of tmax. Independent of the number of predictors used, all regression techniques reveal high performances when comparing the predicted urban tmin values with the observations. They are strongly positively correlated both for SSA(WC) and SSA(CW).

While only using rural tmin as predictor already indicates very high correlations (0.979 for both SSA(WC) and SSA(CW); Figure 15a,b) and R-squared values (approximately 0.958 for both validation techniques) additionally considering rural rsds of the previous day slightly improves the correlation coefficient (0.980 for SSA(CW); Figure 15d) and the goodness of fit (R-squared approximately 0.960). The largest correlation exists when tmin, rsds and hurs are taken as predictors to model urban tmin (0.980 for both SSA(WC) and SSA(CW); Figure 15e,f; R-squared values of approximately 0.961 for both validation techniques). Independent of the number of predictors used, correlations based on the SSA(CW) technique are slightly stronger than for the SSA(WC) approach (comparing Figure 15a,c,e with b,d,f). When focusing on the green crosses in the respective scatter plots which indicate the TN threshold of tmin>20°C, the frequency of TN appears to be well captured by the statistical regression models as well. Detailed evaluation results of the employed heat indices TN, SD and HD will be discussed in Section 6.4.

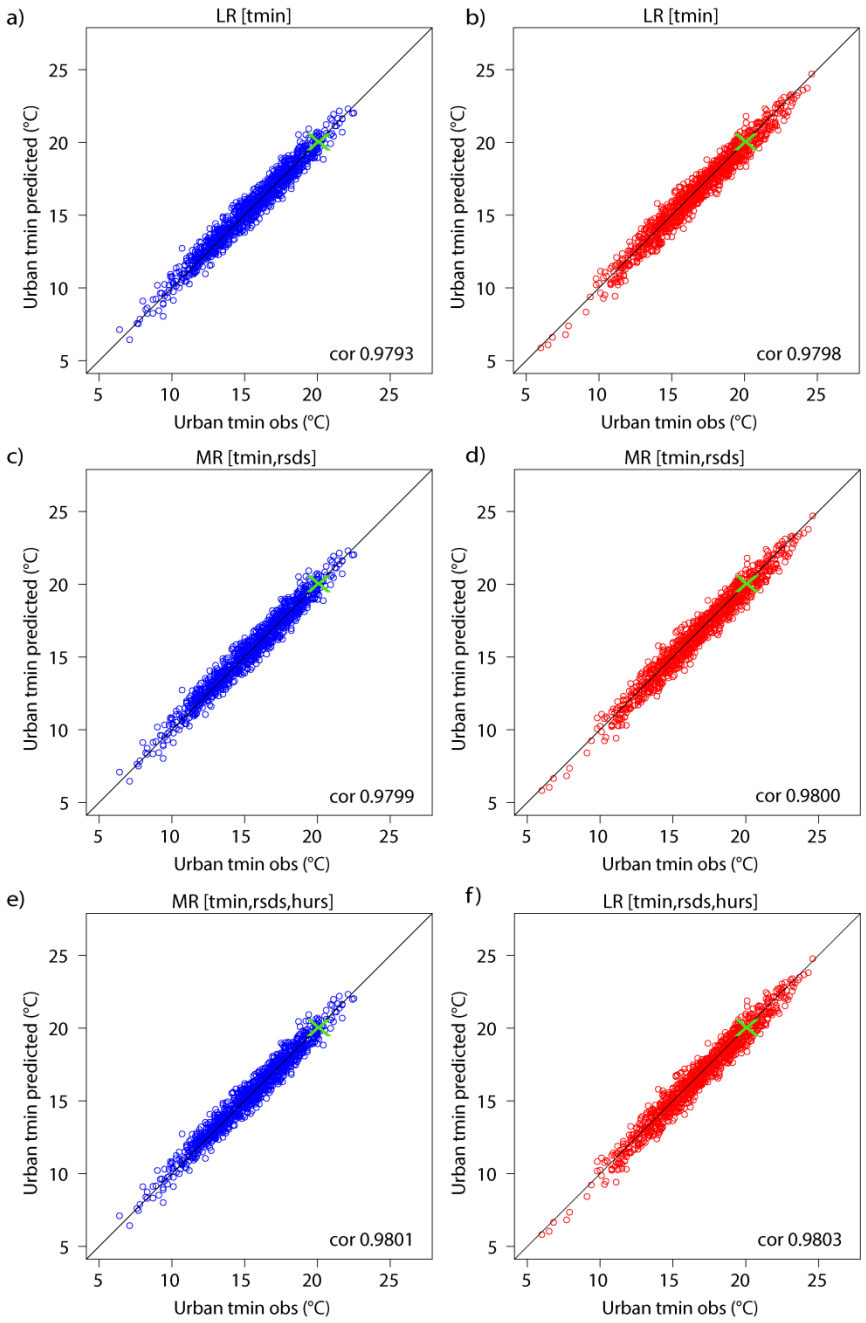

Figure 15: Scatter plots with predicted daily minimum temperature (urban tmin predicted) on the y-axes and observed daily minimum temperature on the x-axes (urban tmin obs) both at the urban site NABZUE for the validation techniques SSA(WC) in blue (a,c,e) and SSA(CW) in red (b,d,f) for the summer months of 1995-2018, based on different numbers of predictors: simple linear regression (LR) using daily minimum temperature (tmin) at the rural site SMA (LR[tmin]; a,b), multiple linear regression (MR) using tmin and radiation (rsds) at SMA (MR[tmin,rsds]; c,d) and MR using tmin, rsds and humidity (hurs) at SMA (MR[tmin,rsds,hurs]; e,f). The green cross refers to the TN threshold of tmin>20°C. The black line shows a correlation of 1, the numbers at the respective bottom-right corner indicate the measured correlation of predicted and observed urban tmin (cor).

6.3 Evaluation of Diagnostic Equation for Daily Maximum UHI

Below we present the evaluation results of the diagnostic equation used to calculate the daily maximum UHI (UHI Theeuwes; Section 5.3) in future climates, which has been added to rural tmin scenarios in order to generate scenarios for urban tmin. The evaluation has been carried out for the UHI and tmin for the exemplary station couple SMA-NABZUE and the observational period 1995-2018, considering the equation`s performance during cold summers (cold JJA) and warm summers (warm JJA) (see Section 5.4.1).

The scatter plot analysis (Figure 16) of the observed daily maximum UHI (UHIobs)[4] and the modeled daily maximum UHI based on Theeuwes (UHI Theeuwes) indicates a strong overestimation of urban-rural temperature differences both during cold summers (Figure 16a) and warm summers (Figure 16b). Correlation coefficients of 0.50 for cold summers and 0.49 for warm summers reveal a moderate correlation between modeled and observed UHI values. In their study, Theeuwes et al. (2017) reveal higher performances of the equation (correlation coefficient of approximately 0.80), considering 11 cities of different size across northwestern Europe.

[4] The observed daily maximum UHI is calculated on the basis of urban-rural differences of hourly tmin, tmax and tas values aggregated to daily maxima, respectively. Out of the resulting three maxima for one day, always the maximum value is taken for the analysis.

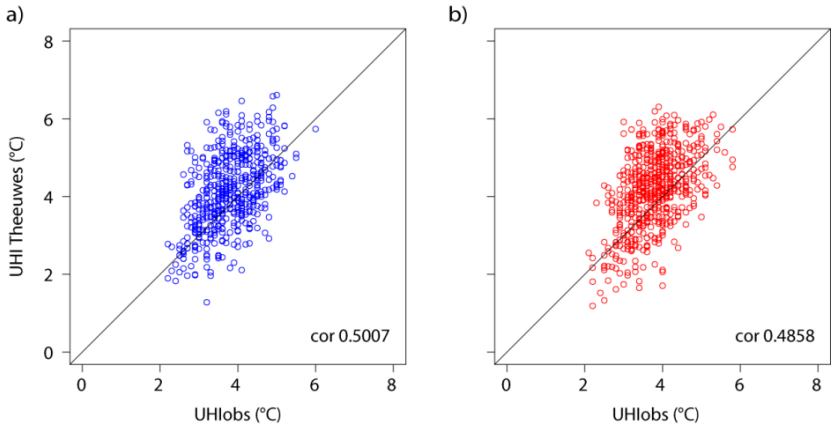

Figure 16: Scatter plots with predicted daily maximum UHI (UHI Theeuwes) on the y-axes and observed daily maximum UHI (UHIobs) on the x-axes for cold summers in blue (a) and warm summers in red (b) for the period 1995-2018. The black line shows a correlation of 1, the numbers at the respective bottom-right corner indicate the measured correlation of predicted and observed maximum UHI (cor).

For predicted and observed urban tmin values, in contrast, Figure 17a,b indicates a strong correlation both in cold (0.938) and warm summers (0.944). Still, urban tmin values are strongly overestimated throughout the whole period considered, as already suggested by the overestimation of UHIobs (Figure 16). For values exceeding the TN threshold, marked by the green cross in Figure 17a,b, the overestimation is even more intense, indicated by the steeper slope of values exceeding 20°C. The evolution of observed and predicted urban tmin values, shown in Figure 17c,d, confirms the strong overestimation. This becomes especially relevant when considering indices with absolute threshold levels like TN, where already a slight overestimation of tmin can cause large biases in the number of TN. This might happen if predicted values are slightly above the threshold while observed values lie slightly below, which results in a much larger number of modeled TN compared to observations. Focusing on the example in Figure 17c,d, this seems to be true for several days. For detailed evaluation results on the respective biases we refer to Section 6.4.

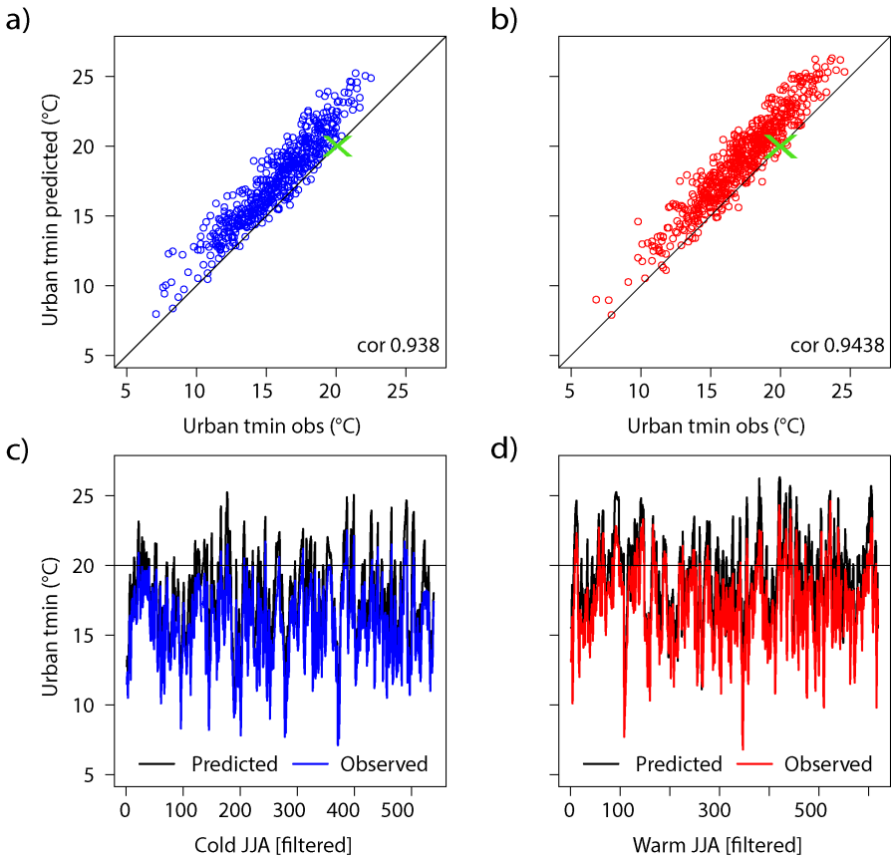

Figure 17: Scatter plot with predicted daily minimum temperature (urban tmin predicted) on the y-axes and observed daily minimum temperature on the x-axes (urban tmin obs) both at the urban site for cold summers (cold JJA) in blue (a) and warm summers (warm JJA) in red (b) for the period 1995-2018, based on the diagnostic equation of Theeuwes et al. (2017). Both time series are filtered considering the validity criteria for which the Theeuwes equation holds (see Section 5.3). The green cross refers to the TN threshold of tmin>20°C. The black line shows a correlation of 1, the numbers at the respective bottom-right corner indicate the measured correlation of predicted and observed urban tmin (cor). The plots below (c,d) contain the same data but show predicted (black line) and observed data (blue line in c and red line in d) as line plots on the y-axis, and the number of data on the x-axis. The horizontal black line indicates the TN threshold of tmin>20°C.

6.4 Intercomparison of the Employed Approaches

So far, we have mainly focused on the correlation of modeled and observed values, which gives a good estimate on the strength of the relation. Moreover, scatter plot analyzes could reveal potential over- and underestimations of modeled data. In the following, the focus lies on the approaches' performances in terms of the mean bias (bias), as introduced in Section 5.4.2. The bias gives more

detailed information on the skill of the respective methods and will be discussed in terms of tmin and tmax, the derived indices and the respective 95th percentile of tmin and tmax in a comparative framework considering all tested approaches together. Figure 18 summarizes the biases for tmin (a), UHI (b), the frequency of TN (c) and the 95th percentile of tmin (d), using the SSA(WC) and SSA(CW) cross-validation techniques for QM and the (multiple) linear regressions, and the bias during cold summers (cold) and warm summers (warm) for the diagnostic equation of Theeuwes et al. (2017).

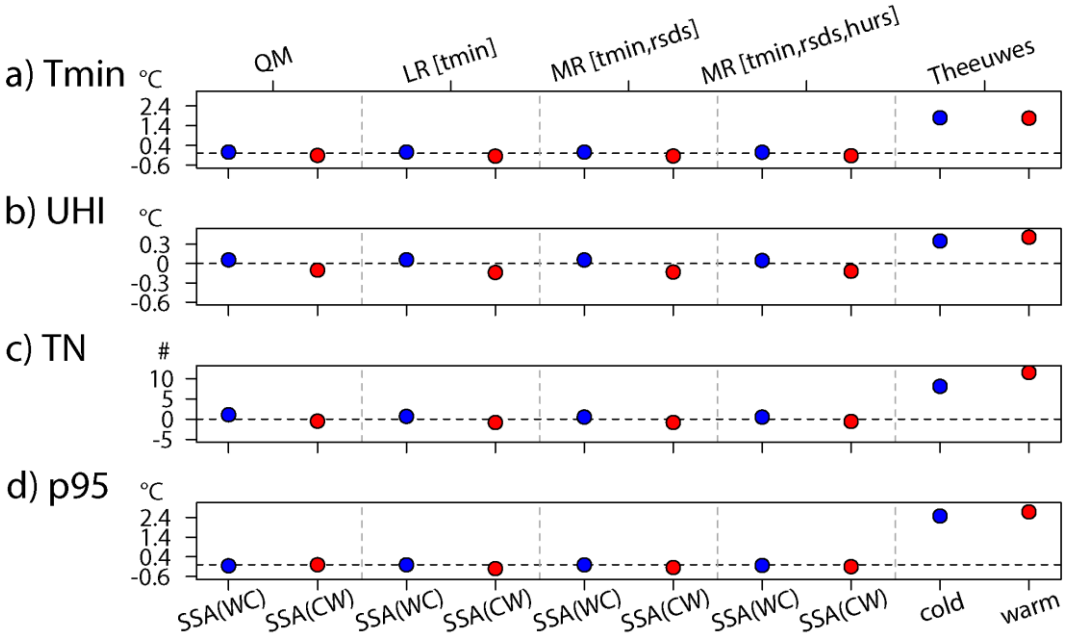

Figure 18: Mean bias for urban daily minimum temperature (tmin) predicted by the different tested approaches shown on the upper x-axis. The evaluation is done for tmin (a), urban heat island (UHI; b), number (#) of tropical nights (TN; c) and the 95th percentile of tmin (p95; d) shown on the y-axis at the exemplary station couple SMA-NABZUE for the period 1995-2018 (JJA). The bias has been calculated based on the split sample approach warm-cold -SSA(WC)- (blue dot) and cold-warm -SSA(CW)- (red dot) for the first four approaches and for cold (cold; blue dot) and warm summers (warm; red dot) for the diagnostic equation of Theeuwes et al. (2017), shown on the lower x-axis. The horizontal dashed line indicates a bias of zero; the vertical dashed lines split the results of the different approaches.

Considering the biases for tmin, UHI, TN and p95 of tmin, Figure 18 reveals very similar results for QM and the (multiple) linear regressions (first four methods in Figure 18). These approaches show an overall good performance with relatively

low biases over all analyzed parameters: except a larger positive bias in the number of TN (Figure 18c), the SSA(WC) validation technique indicates positive biases close to zero for all parameters tested. When trained in colder summers and tested in warmer - SSA(CW) - predicted values are slightly underestimated. We refer to Section 6.1, where we discuss the influence of varying correction functions as reasons for the slightly positive or negative biases. A negative bias in the SSA(CW) validation, which evaluates the approaches' performance in a climate change context, implies that urban scenarios based on QM and the (multiple) linear regressions are conservative estimations and the urban predicted number of TN might be even larger. For QM, the number of TN is underestimated by 6.5% (compared to the mean number of TN per year in the observational period 1995-2018) when trained in colder summers and tested in warmer, but overestimated by more than 14% if training and testing periods are turned around. The regression-based models show almost the same results. The biases in the 95th percentile of tmin, in turn, reveal very robust results compared to the biases in the number of TN both for QM and the regression-based models and for both cross-validation techniques SSA(WC) and SSA(CW). Thus, we assume the absolute threshold of TN (tmin>20°C) to be mainly responsible for the large difference between predicted and observed values, as already discussed for the example of summer 2017 in Section 6.1 (Figure 14b).

These overall robust results of QM and the (multiple) linear regressions stand in stark contrast to results based on the diagnostic equation (rightmost method in Figure 18; Theeuwes et al. 2017), with the greatest complexity in terms of number of variables to model the maximum UHI. Biases for all considered validation criteria indicate substantial differences between modeled and observed values. More precisely, predicted values are strongly overestimated with about 1.8°C for tmin (a), 0.4°C for UHI (b), 8-11.5 TN (c) and 2.6°C for p95 (d), as already indicated in the scatter analyses in Figure 17a,b. For those metrics that relate to the upper tail of the tmin distribution (TN, p95; Figure 18c,d) biases are systematically higher during warm summers (warm in Figure 18) than during cold summers (cold in Figure 18). For tmin and UHI (Figure 18a,b), where averaged values are compared, biases are approximately equal. See further

Chapter 7, where we discuss potential limitations of the approach and propose possible explanations for the large biases and the highly differing results of the equation compared to QM and the regression-based models.

Figure 19 provides an overview on the biases of tmax (a) and further parameters based on maximum temperature, namely UHI (b), SD (c), HD (d) and p95 (e), and the ability of QM and the simple linear (LR) and multiple linear regressions (MR) to model these parameters.

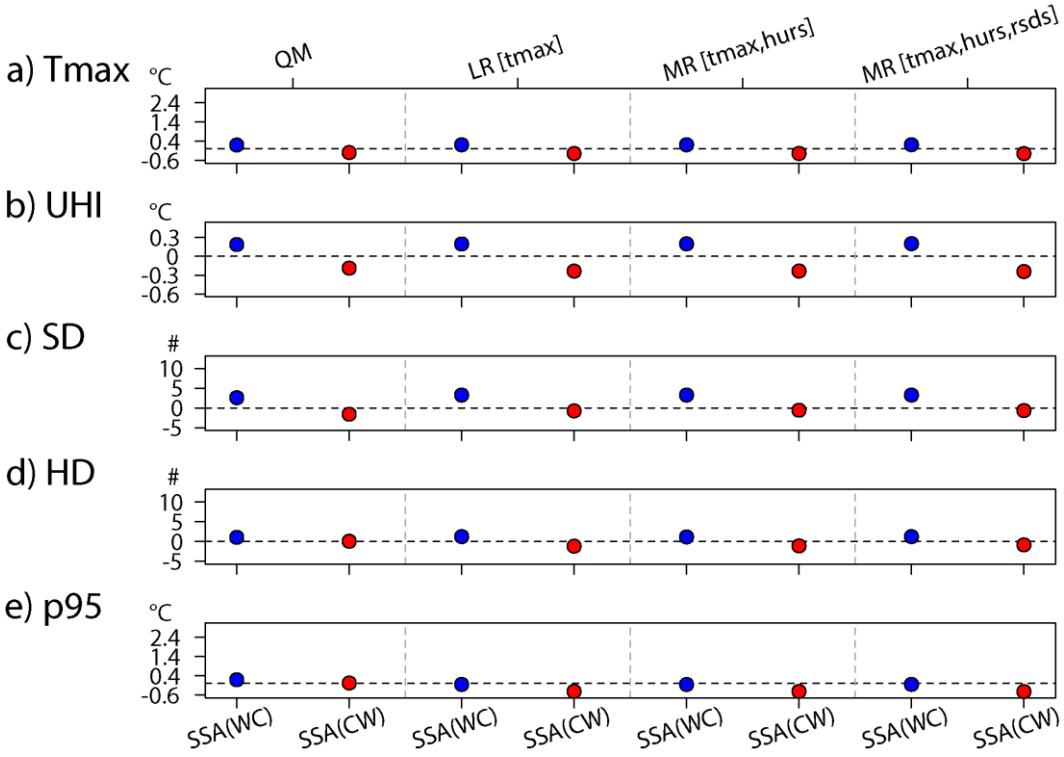

Figure 19: Mean bias for urban daily maximum temperature (tmax) predicted by the different tested approaches shown on the upper x-axis. The evaluation is done for tmax (a), urban heat island (UHI; b), number (#) of summer days (SD; c) and hot days (HD; d) and the 95th percentile of urban tmax (p95; e) shown on the y-axis at the exemplary station couple SMA-NABZUE in the period 1995-2018 (JJA).The bias has been calculated based on the split sample approach warm-cold -SSA(WC)- (blue dot) and cold-warm -SSA(CW)- (red dot). The horizontal dashed line indicates a bias of zero; the vertical dashed lines split the results of the different approaches.

While tmax is generally captured well by QM and the regression-based models, both approaches indicate larger biases for the UHI (Figure 19b): the positive biases for tmax when trained in warmer summers and tested in colder - SSA (WC) - and the slightly negative biases when training is in colder summers and

testing in warmer - SSA(CW) - are somewhat intensified in terms of urban-rural temperature differences. Both QM and the (multiple) linear regressions are able to approximately model the frequency of the heat indices SD and HD. Yet, for the former index, biases are higher than for the latter. Note that SD (on average 46 per year at the urban site based on observations from 1995-2018) occur much more frequent than HD (on average 15 per year), which is associated with a reduced probability of modeling the exact number of SD compared to a higher probability of accurately predicting the less frequent HD. As already shown for the number of TN, biases are reduced when considering the 95th percentile instead of threshold-based heat indices like SD and HD since no absolute boundary levels are present. For all validation metrics (Figure 19a-e) and approaches, the SSA(WC) validation technique reveals a systematic overestimation, while the SSA(CW) indicates a systematic underestimation. Varying conditions in the training and testing periods are responsible for these pattern (see Section 6.1). Overall, the evaluation of the QM and the regression-based models used for transferring scenarios from rural to urban sites reveal satisfactory performances in the present-day climate for all validation metrics (tmin, tmax, UHI, TN, SD, HD, p95 of tmin and tmax). Nonetheless, some biases remain: especially in terms of values that lie outside the calibration period, as tested in the SSA(CW) cross-validation, and in terms of threshold-based indices, like the number of TN. The diagnostic equation, in turn, reveals large biases throughout the whole validation exercise. Especially in terms of the heat index TN, the distinct overestimation suggests pronounced limitations (see further Chapter 7). The equation might not be applicable in climate impact research.

6.5 Climate Scenarios for Urban Sites

Raising temperatures associated with climate change will have an effect on the frequency of temperature-based heat indices like TN, SD and HD. In the following, we present an overview of the projected evolution of the employed heat indices for both rural and urban sites over the course of the 21st century in terms of the absolute number of days averaged over three 30-year scenario periods. The exercise focuses on the emission scenario RCP8.5 and considers all

three methods (Chapter 5) tested for transferring climate scenarios of the rural site into urban settings. Note that the following results are exemplary for the station couple SMA-NABZUE. Scenarios for the remaining station couples (see Table 1) are provided in Appendix 2-22.

As observations reveal, TN are basically absent at the rural site SMA under current conditions (Figure 20a). Yet, scenario data suggest an increase of TN in the future for all scenario periods with up to 18 days by the end of the century (multi-model ensemble median). These results are based on the first-step QM, as applied in CH2018 (2018). Results for the urban site NABZUE (Figure 20b) during present climate agree well with results shown in Section 6.4, revealing a slight underestimation of TN by QM and the regression models and an overestimation by the Theeuwes equation (compare grey bars with red x and plus sign; however consider the limitations[5]). Consistent with what is known from numerous studies about the UHI (see Chapter 3), the number of TN is substantially higher in urban areas than in the rural counterpart for all considered periods and methods. In Zurich (SMA-NABZUE), observations suggest the number of TN to be around seven times larger in the urban than the rural fraction, when focusing on the present climate. In the future, NABZUE is expected to experience about 25 more TN per year than SMA for the late scenario period based on QM. Projections based on the regression-based models and the diagnostic equation of Theeuwes et al. (2017) reveal more conservative results and propose less TN compared to QM for the late scenario period at the urban site.

[5] Note that urban observational data cannot be provided for the full 30-year reference period (1981-2010), as suggested by WMO, since urban data (NABZUE) are available only from 1995. The red x and plus signs in Figures 20-22 are thus just indications for the approaches' performances and cannot be directly compared with the corresponding modeled data, which are always based on the period 1981-2010.

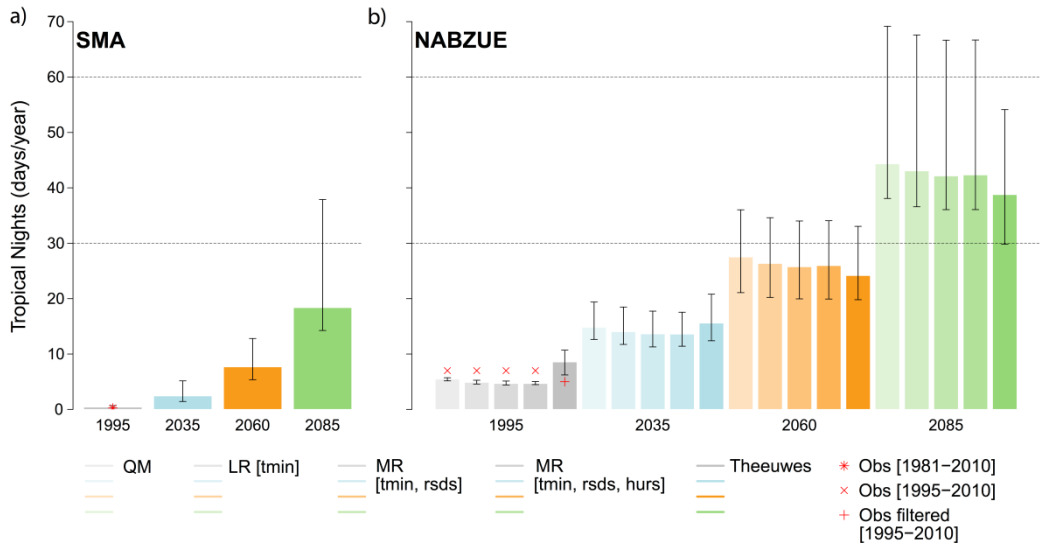

Figure 20: Frequency of tropical nights (TN) per year averaged over the 30-yrs reference period (1995) and the three 30-yrs scenario periods (2035, 2060, 2085; multi-model combination) for RCP8.5 at the exemplary station couple SMA (rural site; a) and NABZUE (urban site; b). Bars indicate the ensemble median value; whiskers the 5-95% model range. In (a), scenarios are based on the first-step quantile mapping (CH2018 2018). The different shadings of the bars in (b) refer to the employed methods tested within the present thesis: second-step quantile mapping (QM), simple linear regression using rural tmin as predictor (LR tmin), multiple linear regression using rural tmin and solar shortwave incoming radiation as predictors (MR tmin, rsds) and additionally using humidity as predictor (MR tmin, rsds, hurs) and the diagnostic equation (Theeuwes). The red asterisk in (a) shows the mean number at the rural site SMA during the observational period 1981-2010. The red x in (b) corresponds to the mean number at the urban site NABZUE during the observational period 1995-2010. The red plus sign in (b) indicates the same as x but with filtered observations based on the exclusion criteria for which the diagnostic equation holds (Theeuwes et al. 2017).

SD occur regularly at both the urban and the rural site under current conditions (Figure 21). As expected, urban-rural temperature differences for indices based on tmax, like SD, are not as noticeable as they are for indices that are built upon tmin, like TN (Figure 20a,b). Some station couples even show (approximately) equal numbers of SD (see e.g. BAS-BKLI; Appendix 6). SMA (Figure 21a) reveals almost 40 SD per year and NABZUE almost 55 days per year (Figure 21b), considering observations[5] and/or modeled data during the reference period. The frequency of SD is projected to increase at both sites. By the end of the century,

the frequency is projected to increase up to 87 days per year at the rural site and up to 100 days per year and more at the urban site, independent of the considered approaches. When taking into account model uncertainty, scenario data of all tested approaches suggest about 110 SD per year at the rural site and over 120 SD per year at the urban site. Throughout all scenario periods, the employed approaches offer highly consistent results both in terms of the median number of SD and the uncertainty model ranges (whiskers).

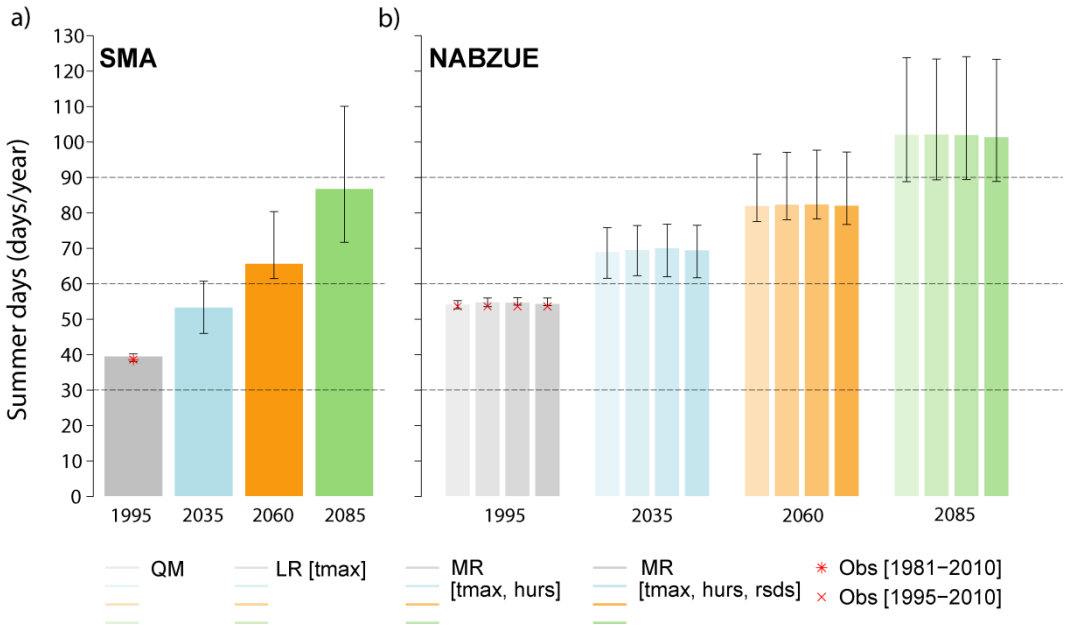

Figure 21: Same as Figure 20 but for the frequency of summer days (SD) per year and without the diagnostic equation of Theeuwes et al. (2017). The regressions use as predictors rural tmax (LR tmax), rural tmax and humidity (MR tmax, hurs) and solar shortwave incoming radiation (MR tmax, hurs, rsds).

HD rarely occur at the rural site SMA under current climate (about five HD per year in the observations and the modeled data; Figure 22a). At the urban site, there are approximately 13 HD per year in the present period (observations[5] and modeled data; Figure 22b). In the future, however, both sites will be affected by considerable increases in the number of HD. At SMA, almost 30 HD per year are expected for the period 2085. In the urban counterpart, almost 50 days per year will be possible. These numbers are lower for earlier scenario periods. Yet, the projected frequency of HD at the urban site will already surpass the number of HD at the rural site for the period of 2085 one period earlier (2060). Thus, the

urban-rural temperature difference in terms of the frequency of HD is quite pronounced in Zurich. Yet, for most of the analyzed station couples distinct urban-rural temperature differences are restricted to the number of TN, as one expects (see Appendix 2-22).

As for the projections of SD, the employed approaches offer very consistent results both in terms of the median number of HD and the model uncertainty ranges (whiskers) with just slightly fewer HD projected by the regression-based models.

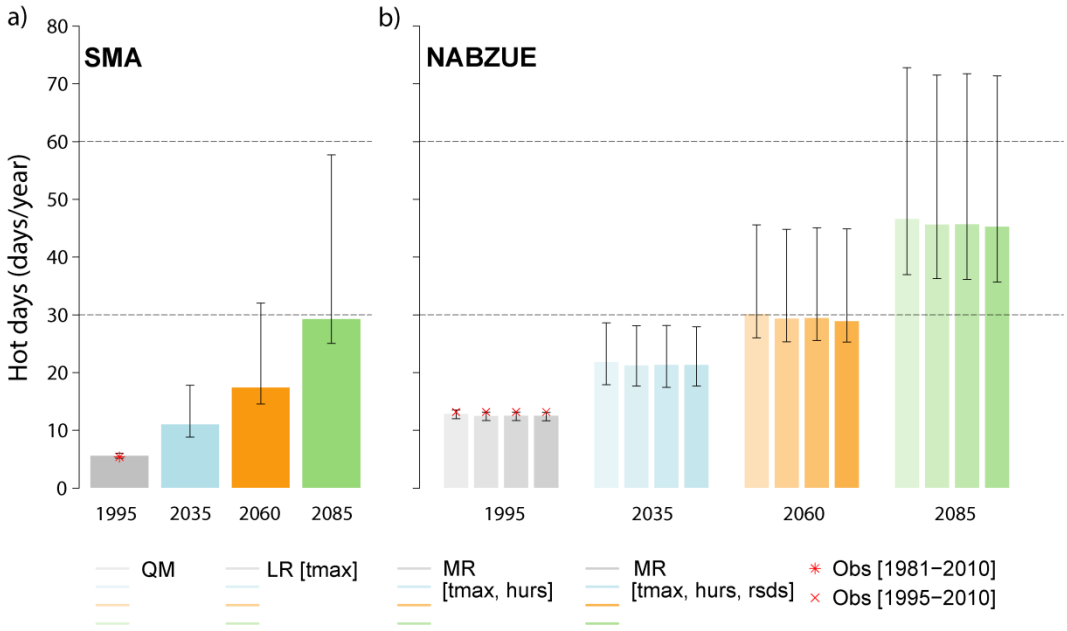

Figure 22: Same as Figure 20 but for the frequency of hot days (HD) per year and without the diagnostic equation of Theeuwes et al. (2017). The regressions use as predictors rural tmax (LR tmax), rural tmax and humidity (MR tmax, hurs) and solar shortwave incoming radiation (MR tmax, hurs, rsds).

7 Limitations and Discussion

Based on the evaluation results during present climate, QM and the regression-based statistical learning methods are considered as attractive and versatile approaches for the generation of transient scenarios for sites with short and (or) sparse data coverage. The diagnostic equation of Theeuwes et al. (2017), in turn, seems to be no reasonable alternative as suggested by large biases and strongly overestimated predictions (Figure 16-18). In the following, we provide an overview on the limitations of all tested approaches and give potential reasons for the differing scenario results as shown in Figure 20-22. The focus, though, mainly lies on QM and the diagnostic equation, as these offer the largest differences in terms of skill.

While the diagnostic equation incorporates physically-based knowledge and has been derived from observational data of European weather stations, QM and the regression-based models are purely statistical and data-driven methods. The underlying concepts of the latter two require a model that needs to be calibrated in a common historical period based on urban and rural data before it is applied to the entire simulated time series of 1981-2099 of the rural site. Hence, both approaches implicitly assume the calibrated correction function (for QM) and regression coefficients (for LR and MR) to be stationary in time. More precisely, they consider a stationary relation between rural and urban site (UHI). Note that especially under climate change conditions and for multiple further reasons, this assumption is linked to considerable uncertainties (e.g. Hoffmann et al. 2012). The physically-derived equation of Theeuwes et al. (2017), in turn, neither requires a calibration before it is applied to the full scenario time series nor does it make assumptions about the urban-rural relation. Instead, the future maximum UHI is directly derived by entering rural scenario data (1981-2099) of meteorological input parameters to the formula. For the urban site, no meteorological variables are taken into consideration but the parameters SVF and fveg, which are assumed to be stationary in time.

Bearing this in mind and comparing the median numbers of predicted TN for the three scenario periods in Figure 20b based on the diagnostic equation and QM,

for instance, we encounter highly differing results: the number of TN based on the equation indicates a much flatter increase compared to QM (and the regression-based models). To better explain these varying results, we compare the urban-rural relationship assumed by QM (UHI QM) and the diagnostic equation (UHI Theeuwes) over the entire historical and scenario period 1981-2099, considering only summer months. This analysis is motivated by the fact that both (the urban-rural relationship assumed by QM and the UHI calculated with the diagnostic equation) are factors that are added to the rural time series to generate the urban time series. As the rural time series is equal for both approaches (CH2018), urban scenarios can only differ in terms of the increment which is added to the rural scenario data. Note that the diagnostic equation approximates daily maximum UHI whereas UHI QM is derived as the difference of urban and rural tmin, which might not be the daily maximum difference. Figure 23 reveals a positive trend of the UHI based on QM (UHI QM) over the 21st century for most of the GCM-RCM simulations considered (see Appendix 23 for the remaining GCM-RCM simulations). This agrees with the larger number of TN with time, based on QM (first colored bars in Figure 20b).

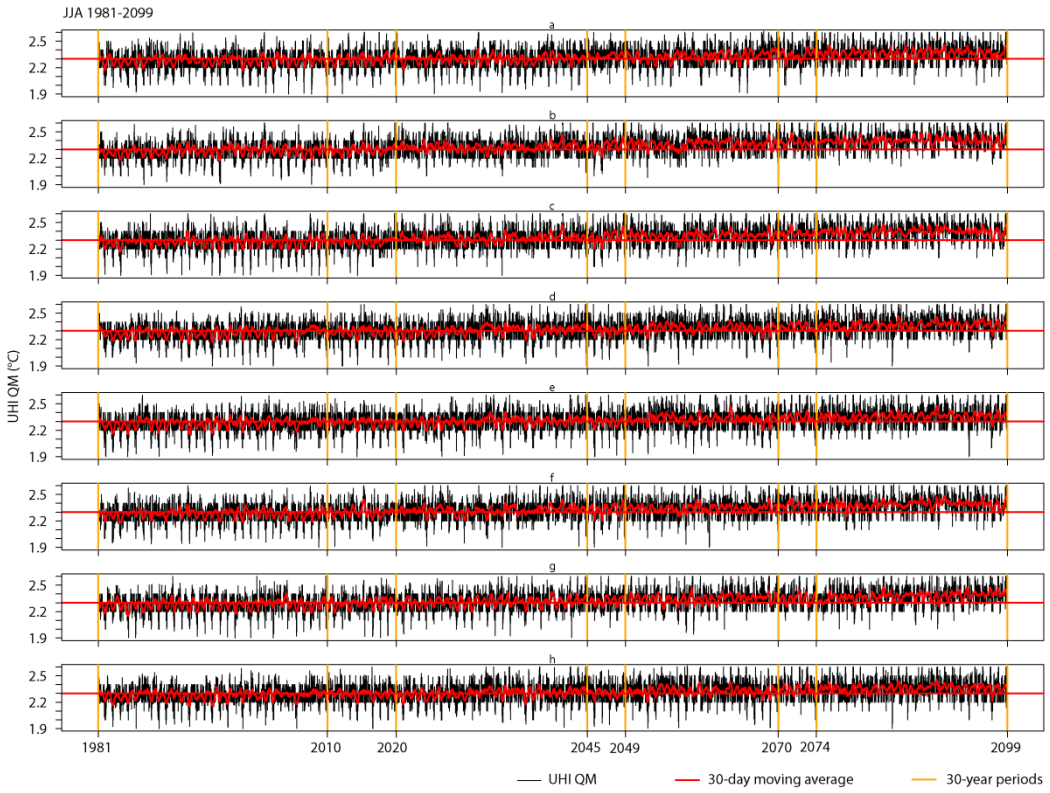

Figure 23: Time series of daily UHI based on QM (UHI QM) at the exemplary station couple SMA-NABZUE for the period 1981-2099 for eight different GCM-RCM simulations (a-h; see Table 3). The red line marks the 30-day moving average, plotted over a straight reference line (red). The vertical orange lines indicate the reference period (1981-2010) and the three scenario periods.

The diagnostic equation of Theeuwes et al. (2017), in turn, predicts no overall trend of the UHI in future climates, as indicated in Figure 24. See Appendix 24 for the remaining GCM-RCM simulations.

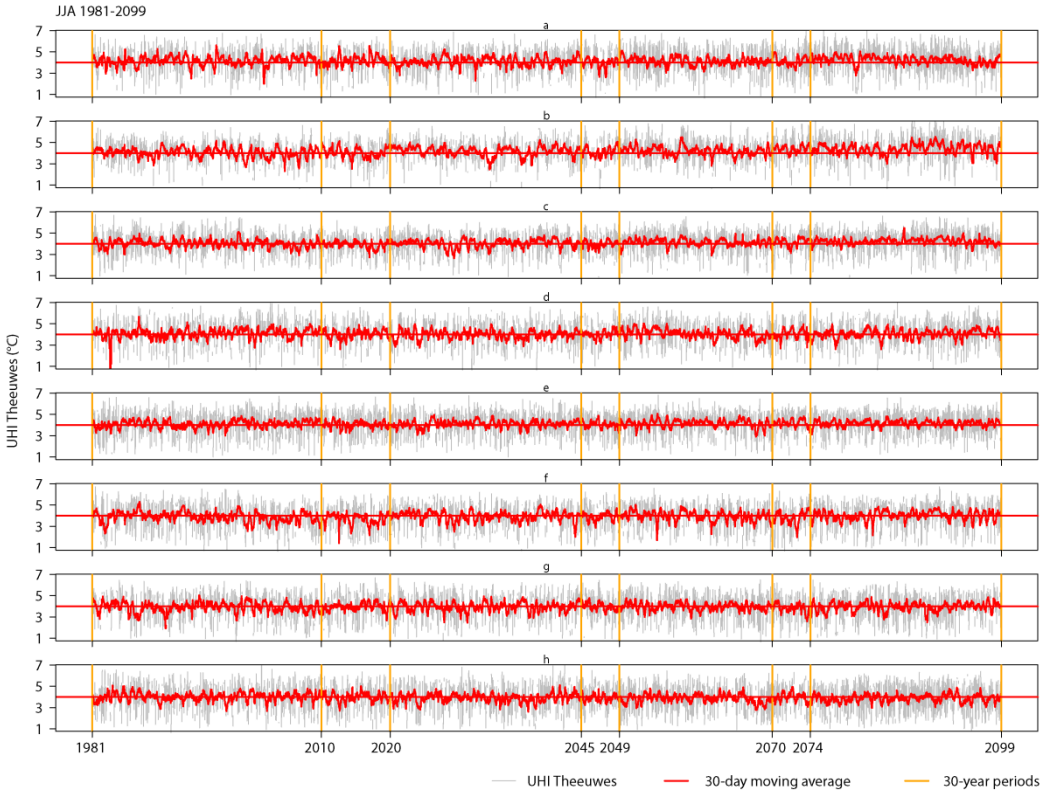

Figure 24: Same as Figure 23 but for UHI based on the diagnostic equation of Theeuwes et al. (2017) (UHI Theeuwes).

The more or less time-invariant UHI in the Theeuwes approach is partly based on the assumption of constant non-meteorological input parameters (SVF, fveg) in the equation. As Figure 25 indicates, the equation is very sensitive to the urban input parameters SVF and fveg. Thus, the first factor in Equation 8, given by the term 2-SVF-fveg, can largely modify the overall result (UHI Theeuwes) already with little changes. Hence, we assume that the assumption of keeping the non-meteorological input variables constant throughout the scenario period is too strong to be maintained until the end of the century, i.e. the method is more valid when the assumed conditions for SVF and fveg still hold, which is probably a few decades only.

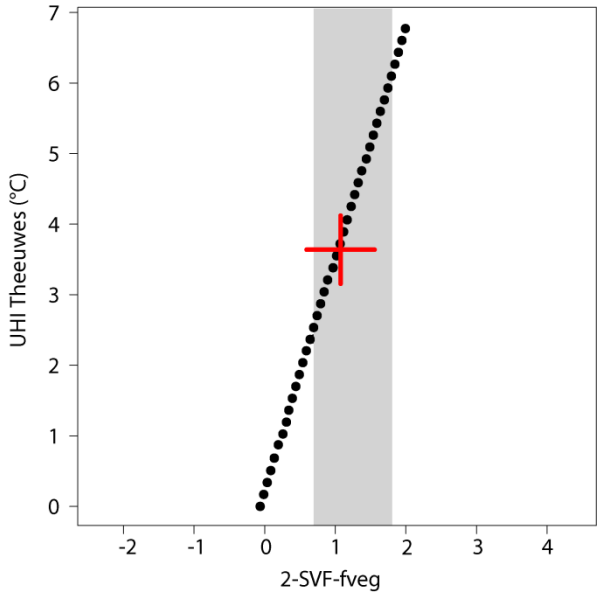

Figure 25: Influence of non-meteorological input variables 2-SVF-fveg to the equation result (UHI Theeuwes; y-axis) if only changing the first factor of Equation 8 (2-SVF-fveg; x-axis) and keeping the second factor (meteorological input variables of rural site) constant. The grey area marks the valid range of 2-SVF-fveg (0.7-1.8), limited by 0.2 < SVF < 0.9 and 0 < fveg < 0.4 (Theeuwes et al. 2017). The red plus sign indicates the value of 2-SVF-fveg valid for NABZUE (1.075), which corresponds to an UHI Theeuwes of 3.64°C.

No positive trend of the UHI based on Theeuwes et al. (2017; Figure 24) likewise indicates that there is no strong climate change signal inherent in the meteorological input variables either. Although temperature data are part of the equation, for which a strong positive trend has been confirmed by numerous studies (e.g. CH2018 2018), its implementation as diurnal temperature range (DTR) with tmax-tmin prevents a climate change trend, as Figure 26a indicates for one exemplary GCM-RCM simulation (see further simulations in Appendix 25-26). Also for rsds and wind, no overall positive trends are to be expected until the end of the century, as shown in Figure 26b and c for the same GCM-RCM simulation (see further simulations in Appendix 27-30). This implies that for the whole period (approximately) the same increment (see Figure 24) is added to the modeled tmin values of the rural site in order to receive urban scenarios. Thus, the still visible increase of TN over time (Figure 20b) must stem from the climate change trend of rural tmin data exclusively.

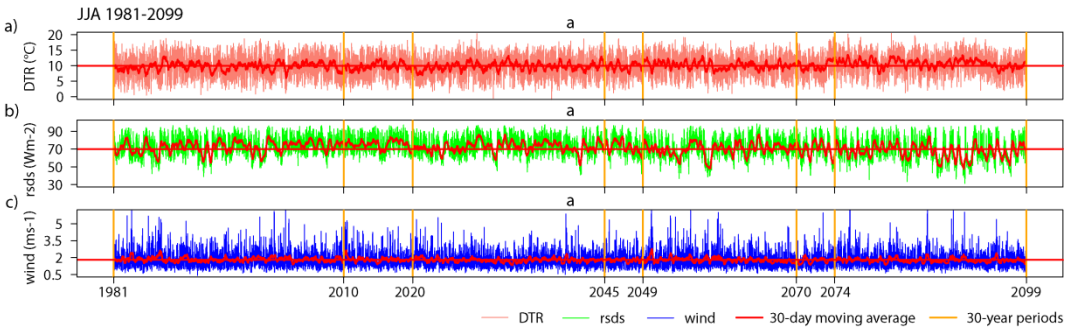

Figure 26: Scenarios for meteorological input variables to the diagnostic equation (Theeuwes et al. 2017), namely diurnal temperature range (DTR; a), incoming shortwave radiation (rsds; b) and wind speed (wind; c) for one GCM-RCM simulation (a in Table 3) at the rural site SMA for the period 1981-2099. The red line marks the 30-day moving average, plotted over a straight reference line (red). The vertical orange lines indicate the reference period (1981-2010) and the three scenario periods.

When comparing the assumed UHIs of the diagnostic equation and QM not in terms of an overall trend, but in terms of absolute levels, the 30-day moving averages of UHI QM (about 2.3°C) in Figure 23 and UHI Theeuwes (about 4°C) in Figure 24 reveal large differences as well. For the whole scenario period, the equation offers substantially higher UHI values compared to QM (comparing Figure 23 with Figure 24). The large differences in the predictions compared to QM are likewise visible when focusing on the modeled numbers of TN in the reference period 1981-2010, shown in Figure 20 (indicated with *1995*). The number of TN based on the equation is predicted much higher compared to QM and the observations. What is surprising, though, is that for the far future (2060 and 2085), the number of TN is predicted lower compared to QM, despite the larger UHI increment of the diagnostic equation throughout the whole scenario period. We assume the data exclusion, necessary before applying the equation, to play an important role. The exclusion criteria are based on modeled data of pr, hurs, tas and wind (all at the rural site; see Section 5.3; CH2018 2018). The equation thus relies on variables whose bias correction is not as explored and validated as temperature data (CH2018 2018). Any remaining bias in those variables or their intervariable dependencies (all exclusion criteria simultaneously) can therefore have a high influence: although they (pr, hurs, tas, wind) do not enter in the equation they affect the data which are excluded. Since

we apply absolute thresholds to exclude one day or not, data with even small biases might be excluded.

Considering the median sum of TN over the period 1981-2099 and all model simulations, around 45% of TN are not counted in the scenarios because of data exclusion. This is mainly due to the exclusion criteria based on precipitation (excludes 29% of TN), meaning TN that occur on days when precipitation exceeds 0.3mm are excluded. When focusing on the rate of excluded TN for each 30-year period, the numbers slightly increase over time, meaning that by the end of the century slightly less TN are included. Considering the number of excluded TN per year averaged over the 30-year periods shows that 8 TN are excluded in the historical period (1981-2010), 13 TN in the period 2020-49, 19 TN in the period 2045-2074 and even 24 TN in the late scenario period 2070-2099, when taking the respective multi-model median. To make visible the number of modeled TN if no data were excluded, Figure 27b reveals scenarios for the number of TN with all data considered. Not surprisingly, the number of predicted TN is overestimated even more throughout all considered periods, resulting in substantially larger projected TN than QM and the linear regression models (Figure 20).

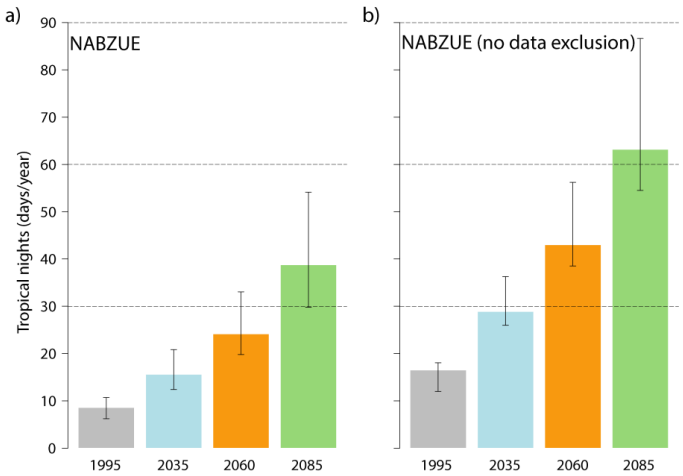

Figure 27: Frequency of tropical nights (TN) per year averaged over the 30-yrs reference period (1995) and the three 30-yrs scenario periods (2035, 2060, 2085; multi-model combination) for RCP8.5 at the urban site NABZUE. Bars indicate the ensemble median value; whiskers the 5-95% model range. In (a), scenarios are based on the diagnostic equation of Theeuwes et al. (2017) with data exclusion and in (b) without data exclusion.

Compared to the diagnostic equation, QM and the regression-based statistical learning methods have a number of advantages (no data exclusion, considering meteorological data of the urban site, etc.). However, they also involve certain limitations, which are briefly discussed below. More detailed information on the QM limitations (especially for the first-step QM) can be found in the CH2018 Technical Report (CH2018 2018) and in the referenced literature (e.g. Feigenwinter et al. 2018).

It is important to notice that the QM correction function as well as the regression models for high and low values can be subject to large uncertainties that arise partly from sampling issues due to the limited number of years considered for the calibration (e.g. 1995-2018 for SMA-NABZUE). It especially raises particular concerns for values that lie outside the range of observed values in the historical period (e.g. new temperature extremes). QM, as employed in the present thesis, uses a constant extrapolation of the correction function for the 1st and the 99th percentiles (CH2018 2018; Feigenwinter et al. 2018; Themeßl et al. 2012), therefore the shape of the correction function in the last percentiles might include statistical artifacts in the future signals (Casanueva et al. 2018). The statistical learning approaches apply the regression model, calculated in a common reference period, to the whole data set of 1981-2099 without considering potential changes in the assumed urban-rural relation. Thus, urban new extremes will highly depend on the magnitude of the regression coefficients (slope) of the fitted model. Moreover, the shorter the overlapping calibration period of urban and rural sites is, the higher are the uncertainties (see e.g. Figure 11a,b for QM), which limits the application of the two approaches (QM and regression-based models) to station couples with long overlapping datasets. The LDA, as tested for QM and the station couple SMA-NABZUE (see Section 6.1), suggests systematically lower biases for a calibration length of at least seven years, yet it depends on the considered variable/index and can vary among station couples.

When employed in a spatial transfer context, QM can misrepresent small scale climate variability on short time scales, e.g. at daily scales. This is due to its deterministic nature when spatially-transferring data from the rural site to the urban site based on a fixed urban-rural temperature relation, i.e. a certain rural

temperature always refers to a fixed temperature value at the urban site. In the observations, however, the urban-rural relation varies with time, e.g. due to different weather conditions, so that a certain rural temperature of x°C can refer to an urban temperature of y°C and another day to z°C, etc. The distribution of the observed UHI thus shows a larger variability than the UHI based on quantile-mapped urban data, as Figure 28 indicates. For the latter, UHI values lie within a fixed range of 2-(almost) 3°C, whereas observations reveal a much larger spread of UHI values ranging between 1-4°C.

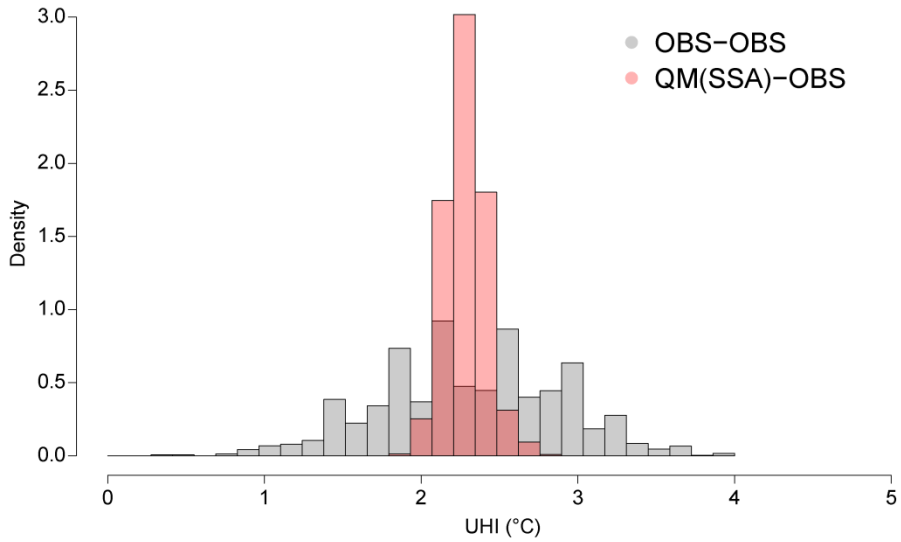

Figure 28: Distribution of daily observed UHI (OBS-OBS; grey) and modeled UHI based on the split sample approach (QM(SSA)-OBS; red) for the exemplary station couple SMA-NABZUE and the summer months of 1995-2018. The y-axis reveals the density of the respective distribution, the x-axis shows the UHI.

With urban climate models it is possible to overcome to some extent the limitations related to a fixed urban-rural temperature relation assumed by QM and the regression-based models for future climates, namely by explicitly modeling the UHI and how it is affected by climate change. There are two modes of urban climate model applications that need to be distinguished: (i) an inline mode and (ii) an offline mode. In the former implementation, the urban climate model is directly represented in GCMs or RCMs and can thus simulate the interactions of urban surfaces and large-scale atmospheric phenomena. For the latter mode, the urban climate model is decoupled from the large-scale host

model. Thus, atmospheric feedback processes are not taken into account. One example is the urban climate model *Town Energy Balance* (*TEB*; Masson 2000) scheme, which is used within a land-surface model (*SURFEX*) and coupled inline or offline to an RCM to simulate the present (Hamdi et al. 2012) and future UHI intensity (Hamdi et al. 2014, Hamdi et al. 2015). The extensive urban climate model *MUKLIMO_3*, i.e. in German *Mikroskaliges Urbanes KLImaMOdell* (Sievers 1990; Sievers 1995; Sievers 2012; Sievers 2016; Sievers, Zdunkowski 1986) developed at the German Meteorological Service (DWD), provides another example for an offline-coupled implementation. The model allows for analyzing the climate of entire cities, including future projections at the urban and suburban scale. For this purpose, the so-called cuboid method is used for downscaling ensembles of projected regional climates to finer scales. Accordingly, *MUKLIMO_3* is able to simulate atmospheric flow fields in presence of buildings, and in the thermodynamical version of the model (Sievers 2016) provides in addition three-dimensional fields of air temperature and humidity in high (horizontal) resolution between 20 x 20 m² and 100 x 100 m², including their diurnal variation.

8 Summary and Conclusions

The current thesis presents three different approaches that allow for the generation of climate scenarios for daily minimum (tmin) and maximum temperature (tmax) at urban sites, in order to account for the urban heat island (UHI) effect in future climates. All tested approaches focus on the greenhouse gas emission scenario RCP8.5 and use model simulations (16 GCM-RCM simulations; see Table 3) available for rural sites through CH2018 (2018), where a first-step QM approach was used to bias correct and downscale modeled data to the site scale. The approaches employed within the present thesis are the following:

a) a second-step QM (QM) procedure based on climate model simulations (tmin, tmax) being spatially transferred to the urban target site to gain urban climate scenarios for tmin and tmax. The approach originates from the work of Rajczak et al. (2016).
b) regression-based statistical learning methods using an increasing number of meteorological predictor variables (one to three variables) at the rural site in order to model urban temperatures (tmin, tmax). Predictor variables are selected based on physical relevance and correlation with the urban target variable. For urban tmin and tmax, the highest correlation coefficients are given for rural tmin and tmax, respectively, radiation (rsds) and humidity (hurs).
c) a physically-based method, namely the diagnostic equation designed by Theeuwes et al. (2017), using basic meteorological parameters at the rural site and morphology data at the urban site in order to parametrize daily maximum UHI for days that meet certain atmospheric conditions. To be consistent with the former two approaches, the resulting UHI values are added as increment to rural tmin scenarios in order to generate urban scenarios for tmin. Note that the diagnostic equation is valid for creating urban scenarios for tmin only, since daily maximum UHI and tmax do not show a clear temporal correspondence.

The resulting products of the tested methods provide transient time series (except for the Theeuwes approach, where values are available only for days

with certain synoptic conditions) at daily resolution for several urban stations in Switzerland and Southern Germany. By analyzing the temperature differences of the observed climate at urban and rural sites, we can represent the UHI in future climates, which is quantified in terms of widely-used heat indices, namely the frequency of tropical nights (TN), summer days (SD) and hot days (HD).

The different approaches are validated in a dedicated evaluation framework using long-term measurements from an operationally-run station couple in Zurich, i.e. the rural site SMA and the corresponding urban site NABZUE. Validation results reveal satisfactory performances in the present-day climate for QM and the regression-based models. Despite certain limitations - e.g. values that lie outside the calibration period (e.g. higher temperatures in future climates that do not occur in the observations used for calibrating the model) are not explicitly considered (CH2018 2018; Feigenwinter et al. 2018) and the urban-rural relation is assumed to be stationary in time - both approaches reveal promising results with low biases and uncertainties due to data sampling. In contrast, the diagnostic equation of Theeuwes et al. (2017) cannot be considered as a reasonable alternative to the latter methods as results substantially differ from observations. The exclusion of large amounts of data before applying the equation is assumed to be the main limitation. According to the authors, the exclusion of specific data is relevant as the formula is derived and thus only valid for certain synoptic situations. Moreover, assuming in the present thesis the urban morphology variables (sky view factor, SVF; vegetation ratio, fveg) of the equation to be stationary in time might be too strong to hold until the end of the century. Given the large biases and uncertainties in the evaluation results, the approach is considered less suitable for generating climate scenarios but rather serves as "a tool to make a first-order estimate" (Theeuwes et al. 2017) of the daily maximum UHI.

Results of urban and rural climate scenarios clearly indicate a strong increase in frequency for all heat indices considered until the end of the 21st century. These findings hold for all analyzed station couples, both urban and rural sites (for the latter see also Zubler et al. 2014), and are independent of the employed method. By the end of the century, Zurich, for instance, might experience climatic

conditions as during the hot summers of 2003 or 2015 and even warmer temperatures every other year, meaning about 40 TN, almost 50 HD and over 100 SD per year at the urban site. Consistent with what is known from literature and local observational evidence (e.g. Gehrig et al. 2018; Oke 1982), the scenarios simulate distinct urban-rural temperature differences (urban heat island -UHI-effect) during nighttime, which becomes obvious when considering the frequency of TN based on tmin. In contrast, there are weak differences during the day, which is revealed when focusing on the frequency of SD and HD based on tmax. By the end of the century, climate projections of the urban site in Zurich show over 25 more TN than its rural counterpart, but only about 10 more SD (based on QM). The projected frequency of TN at the urban site will already surpass the number of TN at the rural site for the period of 2085 one period earlier (2060). The urban-rural temperature difference being a nighttime phenomenon (i.e. higher differences considering TN compared to SD or HD) is visible for all scenario periods and applied methods and for all analyzed station couples, making urban areas especially vulnerable to heat stress. This is because high nighttime temperatures hamper human recovery from daytime heat loads and may lead to sleep deprivation and heat-related discomfort (e.g. Grize et al. 2005; Ragettli et al. 2017). As projections suggest not only the frequency of SD and HD to dramatically rise by the end of the century but also the number of TN, especially in urban areas, a strong focus on the unique aspects of urban climate is vital, given the large and continuously growing fraction of people living within cities (Fischer et al. 2012; Wicki et al. 2018). The findings of this thesis add important value by offering a robust quantification of (temperature-based) climatic conditions specifically at urban sites until the end of the century, which enables to represent the UHI in future climates.

9 References

AMS, American Meteorological Society (2019): Glossary of meteorology. http://glossary.ametsoc.org/wiki/Main_Page (15.08.2019).

Arnfield A. (2003). Two decades of urban climate research: A review of turbulence, exchanges of energy and water, and the urban heat island. In: International Journal of Climatology 23(1), 1-26.

Büyükalaca O., Bulut H., Yilmaz T. (2001): Analysis of variable-base heating and cooling degree-days for Turkey. In: Applied Energy 69(4), 269-283.

Casanueva A., Bedia J., Herrera S., Fernández J., Gutiérrez J. M. (2018): Direct and component-wise bias correction of multi-variate climate indices: the percentile adjustment function diagnostic tool. In: Climatic Change 147(3-4), 411-425.

CH2018 (2018). Climate scenarios for Switzerland, technical report. Zurich: National Center for Climate Services.

Chen F., Kusaka H., Bornstein R., Ching J., Grimmond C., Grossman-Clarke S., Loridan T., Manning K. W., Martilli A., Miao S., Sailor D., Salamanca F. P., Taha H., Tewari M., Wang X., Wyszogrodzki A. A., Zhang Ch. (2011): The integrated WRF/urban modelling system: development, evaluation, and applications to urban environmental problems. In: International Journal of Climatology 31(2), 273-288.

Coutts A., Beringer J., Tapper N. (2007): Impact of increasing urban density on local climate: spatial and temporal variations in the surface energy balance in Melbourne, Australia. In: Journal of Applied Meteorology and Climatology 46(4), 477-493.

Dickinson R. E., Errico R. M., Giorgi F., Bates G. T. (1989): A regional climate model for the western United States. In: Climatic Change 15(3), 383-422.

ETCCDI, Expert Team on Climate Change Detection and Indices (2019): Climate change indices. http://etccdi.pacificclimate.org/list_27_indices.shtml (12.06.2019).

Feigenwinter I., Kotlarski S., Casanueva A., Fischer A. M., Schwierz C., Liniger M. A. (2018): Exploring quantile mapping as a tool to produce user-tailored climate scenarios for Switzerland. In: Technical Report MeteoSwiss, 270, 1-43.

Fischer E. M., Schär C. (2010): Consistent geographical patterns of changes in high-impact European heatwaves. In: Nature Geoscience 3(6), 398-403.

Fischer E. M., Oleson K. W., Lawrence D. M. (2012): Contrasting urban and rural heat stress responses to climate change. In: Geophysical Research Letters 39(3), 1-8.

Gabriel K., Endlicher W. (2011): Urban and rural mortality rates during heat waves in Berlin and Brandenburg, Germany. In: Environmental Pollution 159(8-9), 2044-50.

Gehrig R., König N., Scherrer S. (2018): Städtische Wärmeinseln in der Schweiz - Klimatologische Studie mit Messdaten in fünf Städten. In: Technical Report MeteoSwiss, 273, 1-62.

Giorgi F. (1990): Simulation of regional climate using a limited area model nested in a general circulation model. In: Journal of Climate 3(9), 941-964.

Giorgi F. (2006): Regional climate modeling: status and perspectives. In: Journal de Physique IV (Proceedings) 139(1), 101-118.

Giorgi F. (2019): Thirty years of regional climate modeling: where are we and where are we going next? In: Journal of Geophysical Research: Atmospheres 124(11), 5696-5723.

Giorgi F., Bates G. T. (1989): The climatological skill of a regional model over complex terrain. In: Monthly Weather Review 117(11), 2325-2347.

GIS-Browser Canton of Zurich (2019): Klimamodell - Klimaanalysekarte. https://maps.zh.ch/ (22.07.2019).

Grize L., Huss A., Thommen O., Schindler C., Braun-Fahrländer C. (2005): Heat wave 2003 and mortality in Switzerland. In: Swiss Medical Weekly 135(13-14), 200-205.

Gudmundsson L., Bremnes J. B., Haugen J., Engen Skaugen T. (2012): Technical note: downscaling RCM precipitation to the station scale using quantile mapping – a comparison of methods. In: Hydrology and Earth System Sciences Discussions 9(5), 6185-6201.

Gutiérrez J. M., Maraun D., Widmann M., Huth R., Hertig E., Benestad R., Roessler O., Wibig J., Wilcke R., Kotlarski S., San Martín D., Herrera S., Bedia J., Casanueva A., Manzanas R., Iturbide M., Vrac M., Dubrovsky M., Ribalaygua J., Pórtoles J., Räty O., Räisänen J., Hingray B., Raynaud D., Casado M. J., Ramos P., Zerenner T., Turco M., Bosshard T., Štěpánek P., Bartholy J., Pongracz R., Keller D. E., Fischer A. M., Cardoso R. M., Soares P. M. M., Czernecki B., Pagé C. (2018): An intercomparison of a large ensemble of statistical downscaling methods over Europe - Results from the VALUE perfect predictor cross-validation experiment. In: International Journal of Climatology 39(9), 1-36.

Hamdi R., Degrauwe D., Termonia P. (2012): Coupling the Town Energy Balance (TEB) scheme to an operational limited-area NWP model: evaluation for a highly urbanized area in Belgium. In: Weather and Forecasting 27(2), 323-344.

Hamdi R., Van de Vyver H., De Troch R., Termonia P. (2014): Assessment of three dynamical urban climate downscaling methods: Brussels's future urban heat island under an A1B emission scenario. In: International Journal of Climatology 34(4), 978-999.

Hamdi R., Giot O., De Troch R., Deckmyn A., Termonia P. (2015): Future climate of Brussels and Paris for the 2050s under the A1B scenario. In: Urban Climate 12, 160-182.

Hessami M., Gachon P., Ouarda T., St-Hilaire A. (2008): Automated regression-based statistical downscaling tool. In: Environmental Modelling and Software 23(6), 813-834.

Hoffmann P., Krueger O., Schlünzen H. (2012): A statistical model for the urban heat island and its application to a climate change scenario. In: International Journal of Climatology 32(8), 1238–1248.

IPCC (2013): Climate change 2013: the physical science basis. Contribution of Working Group I to the Fifth Assessment Report of the Intergovernmental Panel on Climate Change. Cambridge, United Kingdom and New York, NY, USA: Cambridge University Press.

Ivanov M. A., Kotlarski S. (2017): Assessing distribution-based climate model bias correction methods over an alpine domain: added value and limitations. In: International Journal of Climatology 37(5), 2633-2653.

Jacob D., Petersen J., Eggert B., Alias A., Christensen O., Bouwer L. M., Braun A., Colette A., Déqué M., Georgievski G., Georgopoulou E., Gobiet A., Menut L., Nikulin G., Haensler A., Hempelmann N., Jones C., Keuler K., Kovats S., Kröner N., Kotlarski S., Kriegsmann A., Martin E., van Meijgaard E., Moseley C., Pfeifer S., Preuschmann S., Radermacher C., Radtke K., Rechid D., Rounsevell M., Samuelsson P., Somot S., Soussana J.-F., Teichmann C., Valentini R., Vautard R., Weber B., Yiou P. (2014): EURO-CORDEX: new high-resolution climate change projections for European impact research. In: Regional Environmental Change 14(2), 563-578.

Kidder S. Q., Essenwanger O. M. (1995): The effect of clouds and wind on the difference in nocturnal cooling rates between urban and rural areas. In: Journal of Applied Meteorology and Climatology 34, 2440-2448.

Kjellstrom T., Weaver H. (2009): Climate change and health: impacts, vulnerability, adaptation and mitigation. In: New South Wales Public Health Bulletin 20(1-2), 5-9.

Koomen E., Diogo V. (2015): Assessing potential future urban heat island patterns following climate scenarios, socio-economic developments and spatial planning strategies. In: Mitigation and Adaptation Strategies for Global Change 22(2), 287-306.

Kotlarski S., Keuler K., Christensen O. B., Colette A., Déqué M., Gobiet A., Goergen K., Jacob D., Lüthi D., van Meijgaard E., Nikulin G., Teichmann C., Vautard R., Warrach-Sagi K., Wulfmeyer V. (2014): Regional climate modelling on European scales: a joint standard evaluation of the EURO-CORDEX RCM ensemble. In: Geoscientific Model Development 7(4), 1297-1333.

Kovats R. S., Hajat S. (2008): Heat stress and public health: a critical review. In: Annual Review of Public Health 29(1), 41-55.

Kusaka H., Chen F., Tewari M., Dudhia J., Gil D. O., Duda M. G., Wang W., Yukako M. (2012): Numerical simulation of urban heat island effect by the WRF model with 4-km grid increment: an inter-comparison study between the Urban Canopy Model and Slab Model. In: Journal of the Meteorological Society of Japan 90B, 33-45.

Lauwaet D., De Ridder K., Saeed S., Brisson E., Chatterjee F., van Lipzig N. P. M., Maiheu B., Hooyberghs H. (2016): Assessing the current and future urban heat island of Brussels. In: Urban Climate 15, 1-15.

Masson V. (2000): A physically-based scheme for the urban energy budget in atmospheric models. In: Boundary-Layer Meteorology 94, 357-397.

McGregor J. L. (1997): Regional climate modelling. In: Meteorology and Atmospheric Physics 63(1-2), 105-117.

MeteoSwiss, Federal Office of Meteorology and Climatology (2019): Hitzetage, Frosttage und andere Indikatoren. https://www.meteoschweiz.admin.ch/home/klima/klimawandel-schweiz/hitzetage-frosttage-und-andere-indikatoren.html (01.06.2019).

Monhart S., Spirig C., Bhend J., Bogner K., Schär C., Liniger M. A. (2018): Skill of subseasonal forecasts in Europe: effect of bias correction and downscaling using surface observations. In: Journal of Geophysical Research: Atmospheres 123(15), 7999-8016.

Morris C. J. G., Simmonds I., Plummer N. (2001): Quantification of the influences of wind and cloud on the nocturnal urban heat island of a large city. In: Journal of Applied Meteorology and Climatology 40(2), 169-182.

Moss R. H., Edmonds J. A., Hibbard K. A., Manning M. R., Rose S. K., van Vuuren D. P., Carter T. R., Emori S., Kainuma M., Kram T., Meehl G. A., Mitchell J. F. B., Nakicenovic N., Riahi K., Smith S. J., Stouffer R. J., Thomson A. M., Weyant J. P., Wilbanks T. J. (2010): The next generation of scenarios for climate change research and assessment. In: Nature 463(7282), 747-56.

Oke T. R. (1973): City size and the urban heat island. In: Atmospheric Environment 7(8), 769-779.

Oke T. R. (1982): The energetic basis of the urban heat island. In: Quarterly Journal of the Royal Meteorological Society 108(455), 1-23.

Oke T. R., Johnson G. T., Steyn D. G., Watson I., D. (1991): Simulation of surface urban heat islands under "ideal" condistions at night. Part 2. Diagnosis of causation. In: Boundary-Layer Meteorology 56(4), 339-358.

Oleson K., Bonan G. B., Feddema J. J., Jackson T. (2011): An examination of urban heat island characteristics in a global climate model. In: International Journal of Climatology 31(12), 1848-1865.

Parlow E. (2011): Besonderheiten des Stadtklimas. In: Gebhardt H., Glaser R., Radtke U., Reuber P. (eds.): Geographie: Physische Geographie und Humangeographie. 2nd ed., München: Spektrum Akademischer Verlag, 287-294.

Parlow E., Vogt R., Feigenwinter C. (2014): The urban heat island of Basel - Seen from different perspectives. In: Die Erde; Zeitschrift der Gesellschaft für Erdkunde zu Berlin 145(1-2), 96-110.

Ragettli M. S., Vicedo-Cabrera A. M., Schindler C., Röösli M. (2017): Exploring the association between heat and mortality in Switzerland between 1995 and 2013. In: Environmental Research 158, 703-709.

Rajczak J., Kotlarski S., Salzmann N., Schär C. (2016): Robust climate scenarios for sites with sparse observations: A two-step bias correction approach. In: International Journal of Climatology 36(3), 1226-1243.

Roth M. (2013): Urban heat islands. In: Fernando H. J. S. (ed.): Handbook of Environmental Fluid Dynamics, Volume Two. 1st ed., Boca Raton, FL, USA: CRC Press, 143-159.

Salamanca F., Martilli A., Tewari M., Chen F. (2011): A study of the urban boundary layer using different urban parameterizations and high-resolution urban canopy parameters with WRF. In: Journal of Applied Meteorology and Climatology 50(5), 1107-1128.

Schär C., Vidale P. L., Lüthi D., Frei C., Häberli C., Liniger M. A., Appenzeller C. (2004): 2004: The role of increasing temperature variability in European summer heatwaves. In: Nature 427(6972), 332-336.

Scherer D., Fehrenbach U., Lakes T., Lauf S., Meier F., Schuster C. (2013): Quantification of heat-stress related mortality hazard, vulnerability and risk in Berlin, Germany. In: Die Erde 144(3-4), 238-259.

Sievers U. (1990): Dreidimensionale Simulationen in Stadtgebieten. In: Umweltmeteorologie, Schriftenreihe Band 15: Sitzung des Hauptausschusses II am 7. und 8. Juni in Lahnstein. Kommission Reinhaltung der Luft im VDI und DIN, Düsseldorf, 92-105.

Sievers U. (1995): Verallgemeinerung der Stromfunktionsmethode auf drei Dimensionen. In: Meteorologische Zeitschrift 4, 3-15.

Sievers U. (2012): Das kleinskalige Strömungsmodell MUKLIMO_3, Teil 1: Theoretische Grundlagen, PC-Basisversion und Validierung. In: Deutscher Wetterdienst (ed.): Berichte des Deutschen Wetterdienstes (240). Offenbach am Main: Selbstverlag des Deutschen Wetterdienstes, 1-142.

Sievers U. (2016): Das kleinskalige Strömungsmodell MUKLIMO_3, Teil 2: Thermodynamische Erweiterungen. In: Deutscher Wetterdienst (ed.): Berichte des Deutschen Wetterdienstes (248). Offenbach am Main: Selbstverlag des Deutschen Wetterdienstes, 1-155.

Sievers U., Zdunkowski W. (1986): A microscale urban climate model. In: Beiträge zur Physik der Atmosphäre 59, 13-40.

Sippel S., Meinshausen N., Merrifield A., Lehner F., Pendergrass A. G., Fischer E. M., Knutti R. (2019): Uncovering the forced climate response from a single ensemble member using statistical learning. In: Journal of Climate 32, 5677-5699.

Steeneveld G.-J., Koopmans S., Heusinkveld B., van Hove B., Holtslag B. (2011): Quantifying urban heat island effects and human comfort for cities of variable size and urban morphology in The Netherlands. In: Journal of Geophysical Research: Atmospheres 116(D20), 1-14.

Stewart I. D., Oke T. R. (2012): Local climate zones for urban temperature studies. In: Bulletin of the American Meteorological Society 93(12), 1879-1900.

Theeuwes N., Steeneveld G.-J., Ronda R. J., Rotach M. W., Holtslag B. (2015): Cool city mornings by urban heat. In: Environmental Research Letters 10(11), 1-9.

Theeuwes N., Steeneveld G.-J., Ronda R. J., Holtslag B. (2017): A diagnostic equation for the daily maximum urban heat island effect for cities in northwestern Europe. In: International Journal of Climatology 37(1), 443–454.

Themeßl M., Gobiet A., Heinrich G. (2012): Empirical-statistical downscaling and error correction of regional climate models and its impact on the climate change signal. In: Climatic Change 112(2), 449-468.

Vogt R., Parlow E. (2011): Die städtische Wärmeinsel von Basel - tages- und jahreszeitliche Charakterisierung. In: Regio Basiliensis 52(1), 7-15.

Voogt J. A., Oke T. R. (2003): Thermal remote sensing of urban climates. In: Remote Sensing of Environment 86(3), 370-384.

Wicki A., Parlow E., Feigenwinter C. (2018): Evaluation and modeling of urban heat island intensity in Basel, Switzerland. In: Climate 6(3), 1-25.

Wilby R. (2006): Past and projected trends in London's Urban heat island. In: Weather 58(7), 251-260.

Wilby R. (2008): Constructing climate change scenarios of urban heat island intensity and air quality. In: Environment and Planning B: Planning and Design 35(5), 902-919.

Wilcke R. A. I., Mendlik T., Gobiet A. (2013): Multi-variable error correction of regional climate models. In: Climatic Change 120(4), 871-887.

Zhang X., Steeneveld G.-J., Zhou D., Duan C., Holtslag A. A. M. (2019): A diagnostic equation for the maximum urban heat island effect of a typical Chinese city: a case study for Xi'an. In: Building and Environment 158, 39-50.

Zhou B., Rybski D., Kropp J. (2017): The role of city size and urban form in the surface urban heat island. In: Scientific Reports 7(1), 1-9.

Zubler E. M., Scherrer S. C., Croci-Maspoli M., Liniger M. A., Appenzeller C. (2014): Key climate indices in Switzerland; expected changes in a future climate. In: Climatic Change 123(2), 255-271.

10 Appendix

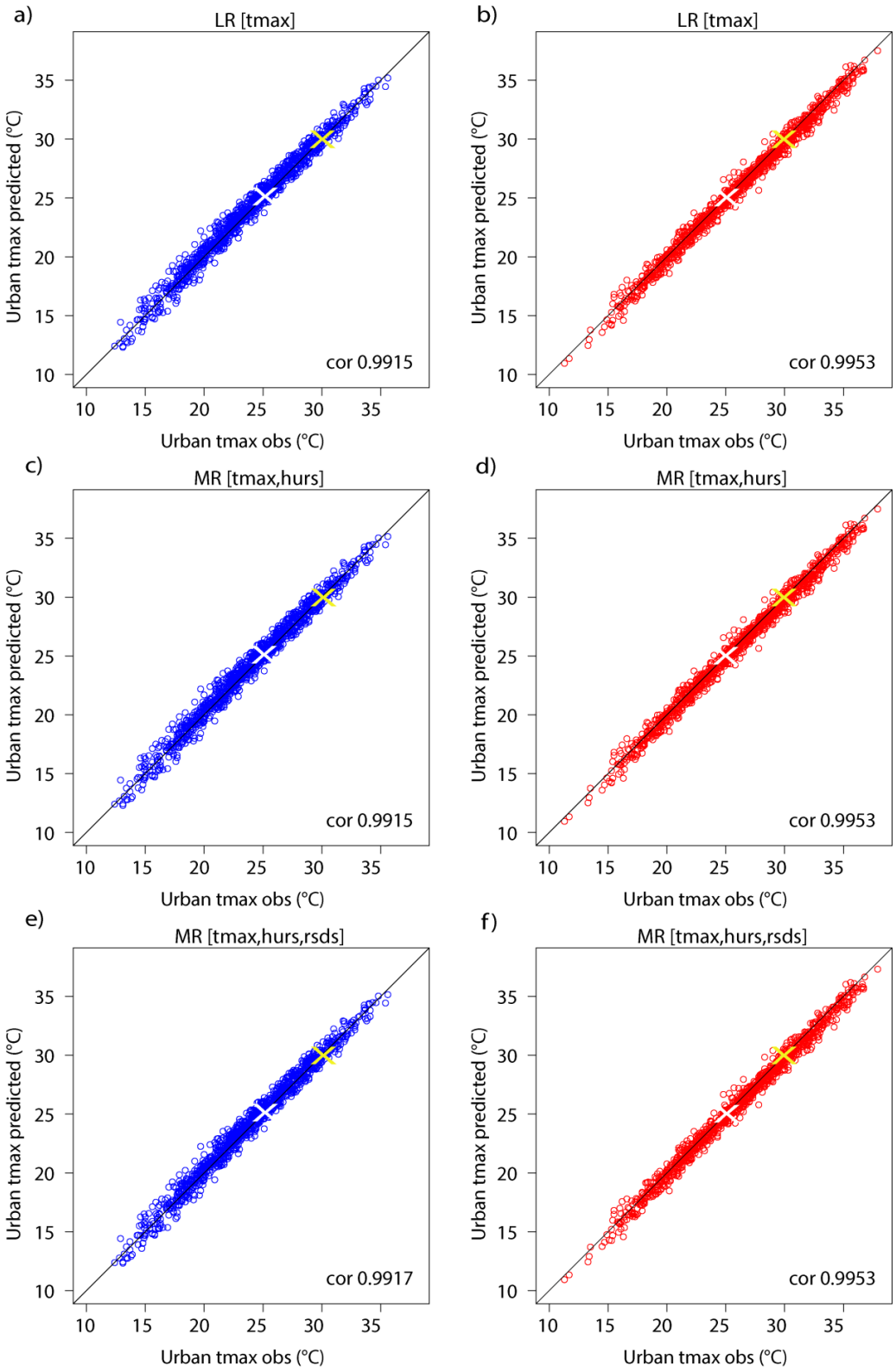

Appendix 1: Same as Figure 15 but for tmax.

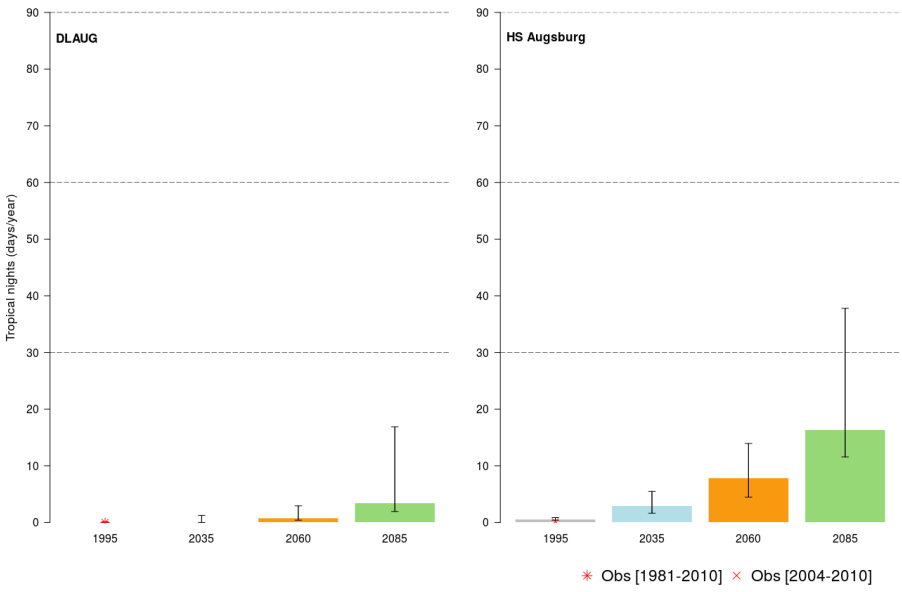

Appendix 2: Frequency of tropical nights (TN) per year averaged over the 30-yrs reference period (1995) and the three 30-yrs scenario periods (2035, 2060, 2085; multi-model combination) for RCP8.5 at the station couple DLAUG (left)-HS Augsburg (right). Bars indicate the ensemble median value; whiskers the 5-95% model range. In (a), scenarios are based on the first-step QM (CH2018 2018) and in (b) on the second-step QM. The red asterisk in (a) shows the mean number at the rural site during the observational period 1981-2010. The red x in (b) corresponds to the mean number at the urban site during the observational period 2004-2010.

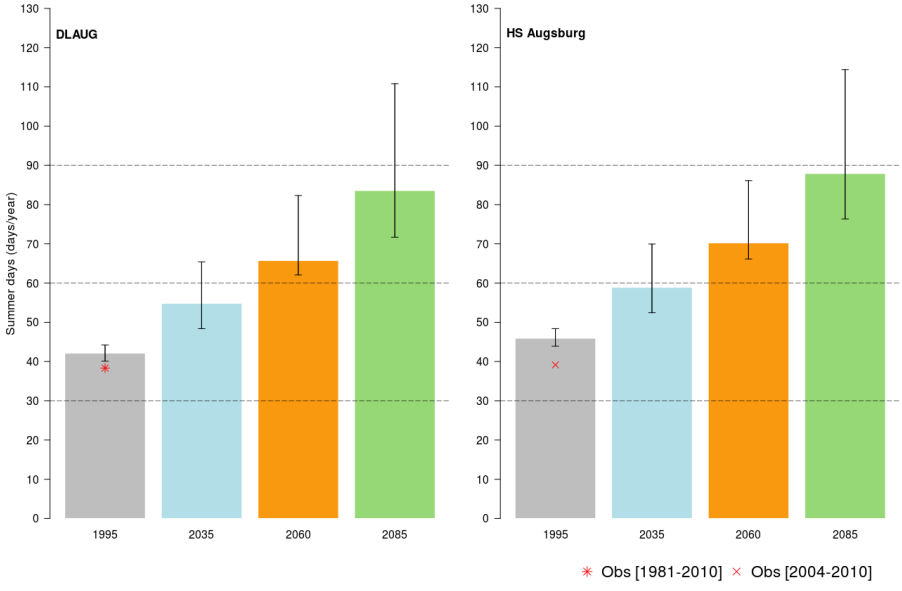

Appendix 3: Frequency of summer days (SD) per year averaged over the 30-yrs reference period (1995) and the three 30-yrs scenario periods (2035, 2060, 2085; multi-model combination) for RCP8.5 at the station couple DLAUG (left)-HS Augsburg (right). Bars indicate the ensemble median value; whiskers the 5-95% model range. In (a), scenarios are based on the first-step QM (CH2018 2018) and in (b) on the second-step QM. The red asterisk in (a) shows the mean number at the rural site during the observational period 1981-2010. The red x in (b) corresponds to the mean number at the urban site during the observational period 2004-2010.

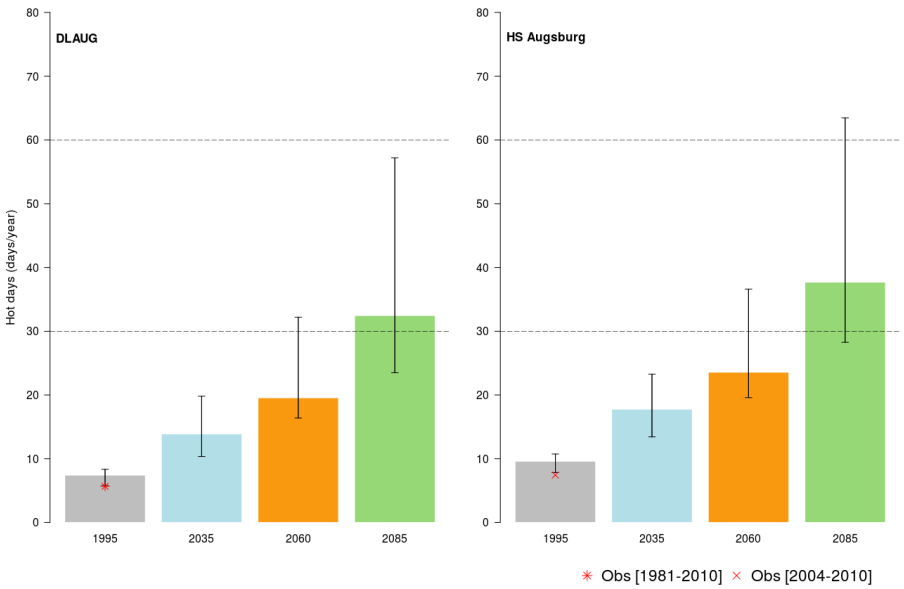

Appendix 4: Frequency of hot days (HD) per year averaged over the 30-yrs reference period (1995) and the three 30-yrs scenario periods (2035, 2060, 2085; multi-model combination) for RCP8.5 at the station couple DLAUG (left)-HS Augsburg (right). Bars indicate the ensemble median value; whiskers the 5-95% model range. In (a), scenarios are based on the first-step QM (CH2018 2018) and in (b) on the second-step QM. The red asterisk in (a) shows the mean number at the rural site during the observational period 1981-2010. The red x in (b) corresponds to the mean number at the urban site during the observational period 2004-2010.

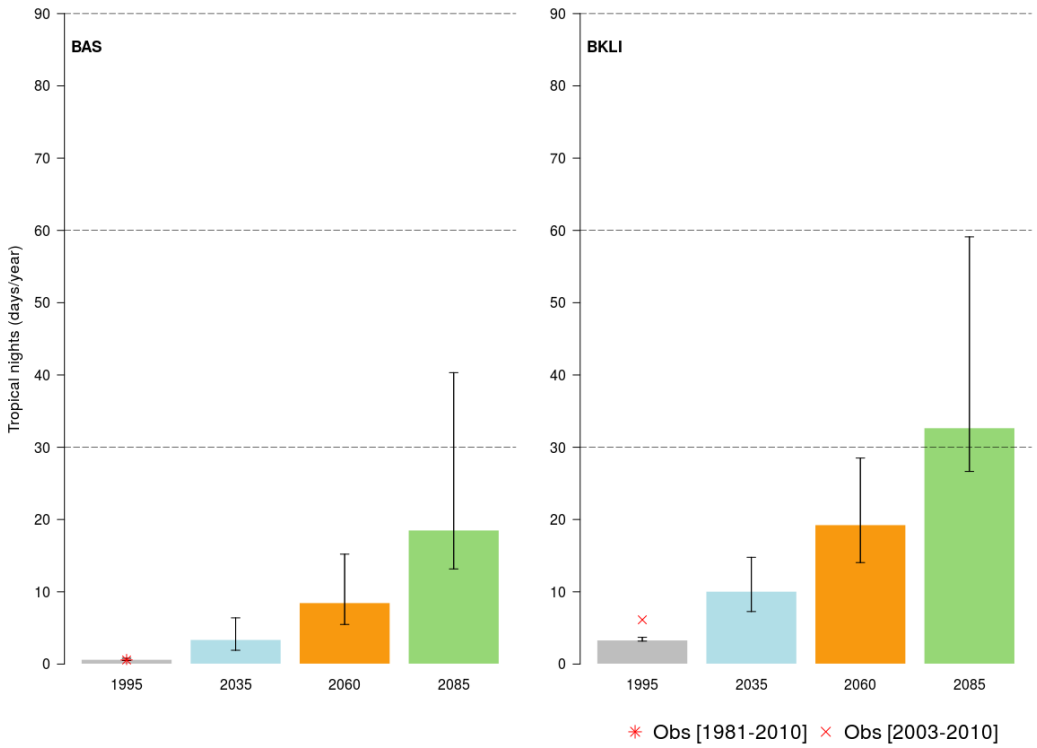

Appendix 5: Same as Appendix 2 but for the station couple BAS (left)-BKLI (right).

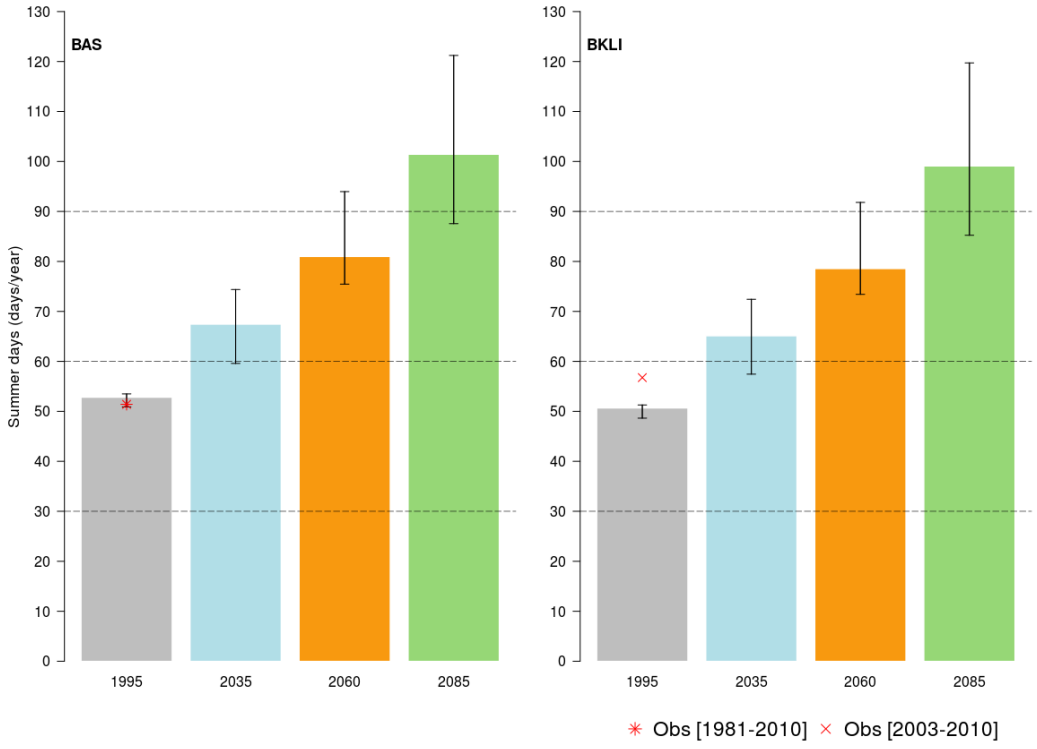

Appendix 6: Same as Appendix 3 but for the station couple BAS (left)-BKLI (right).

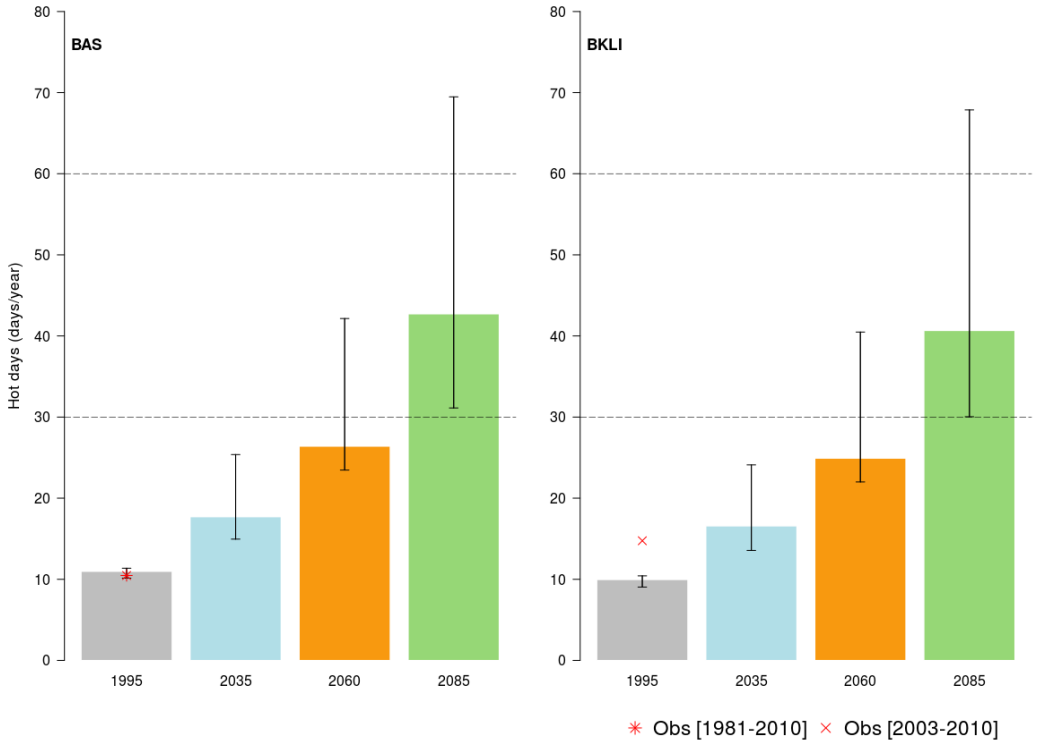

Appendix 7: Same as Appendix 4 but for the station couple BAS (left)-BKLI (right).

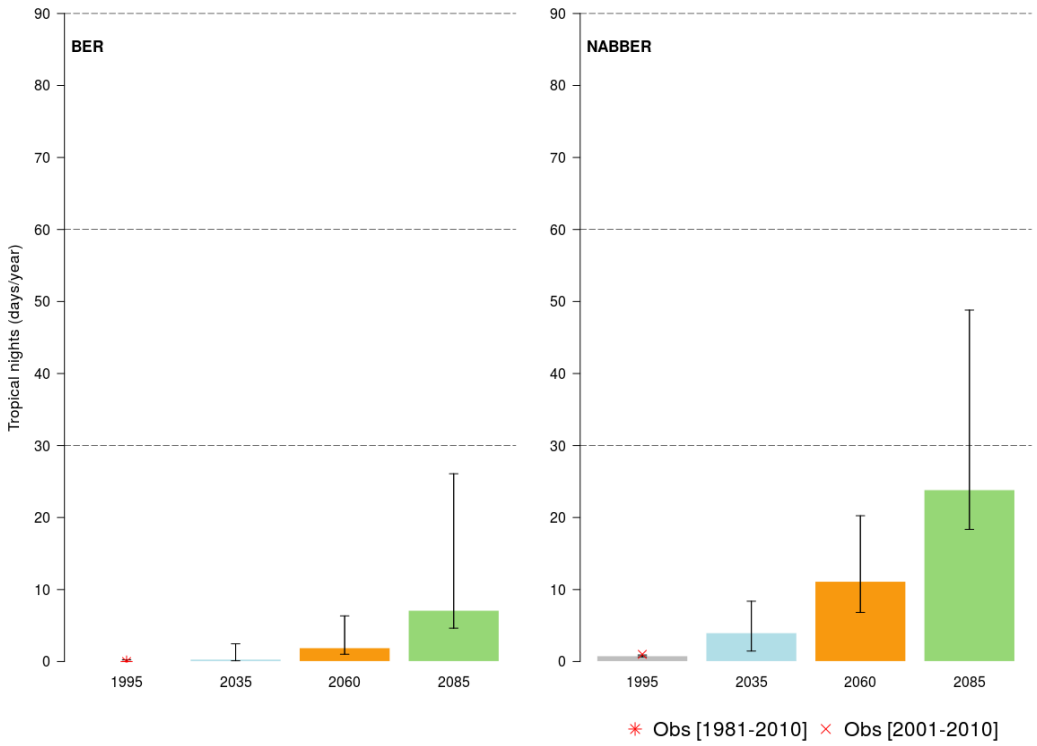

Appendix 8: Same as Appendix 2 but for the station couple BER (left)-NABBER (right).

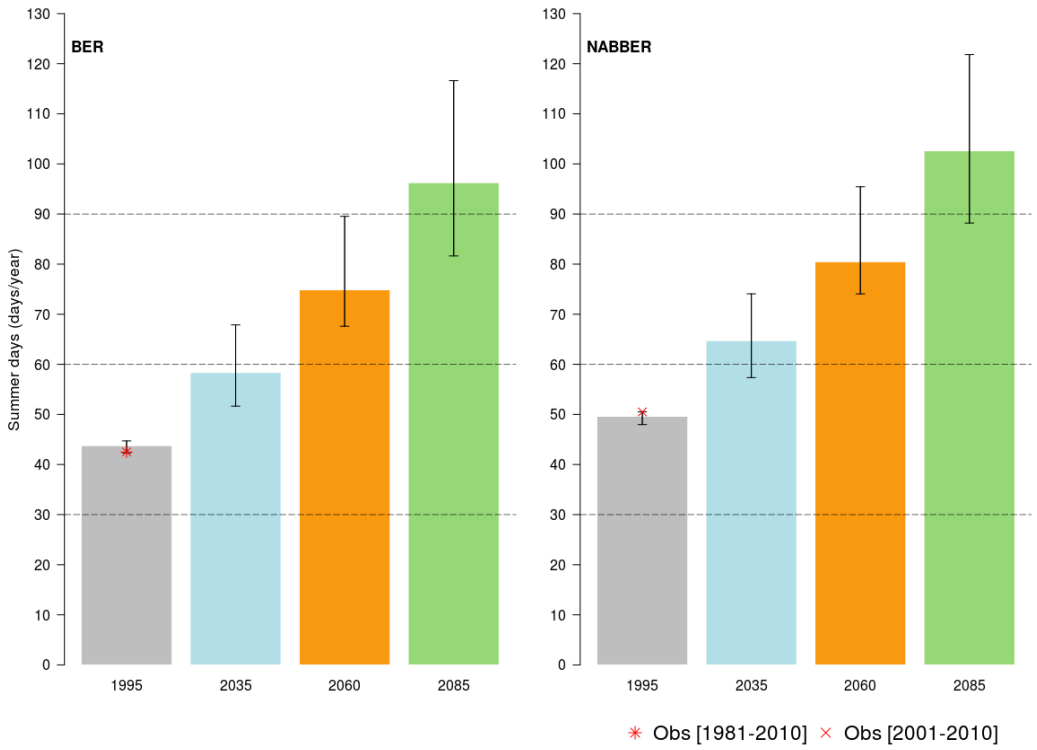

Appendix 9: Same as Appendix 3 but for the station couple BER (left)-NABBER (right).

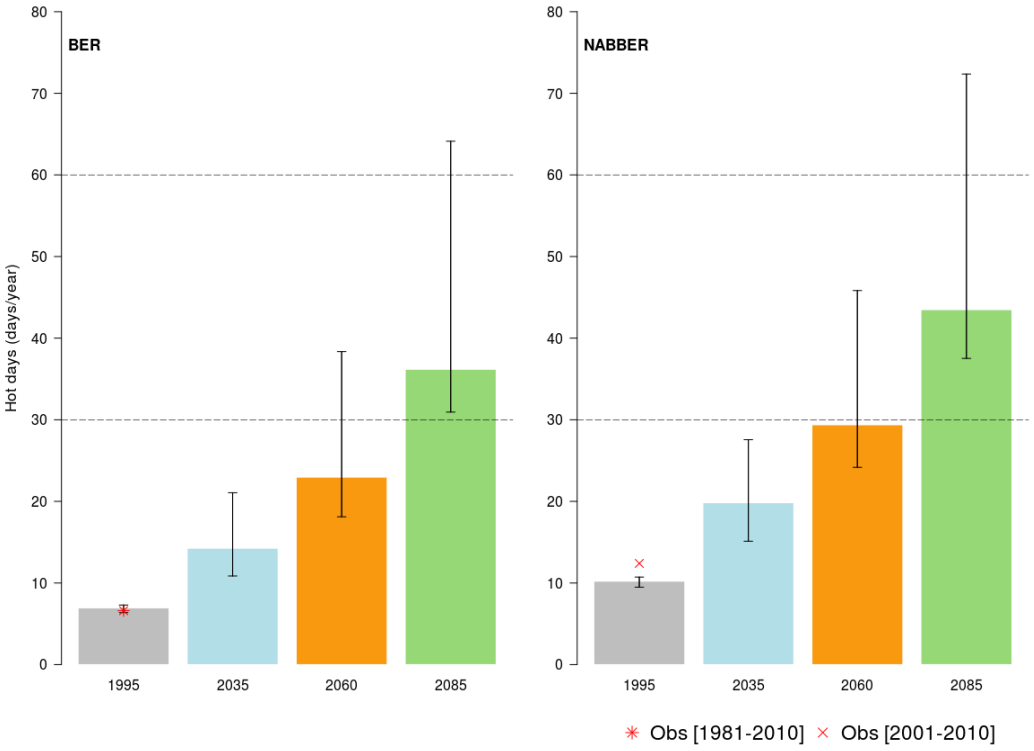

Appendix 10: Same as Appendix 4 but for the station couple BER (left)-NABBER (right).

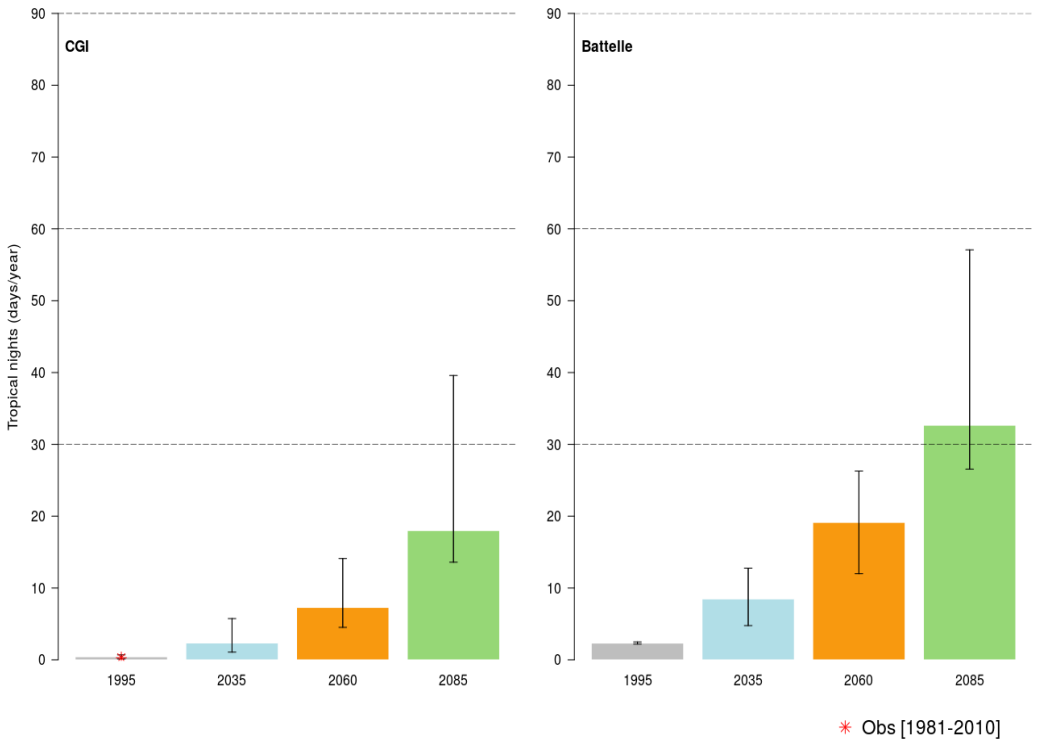

Appendix 11: Same as Appendix 2 but for the station couple CGI (left)-Batelle (right).

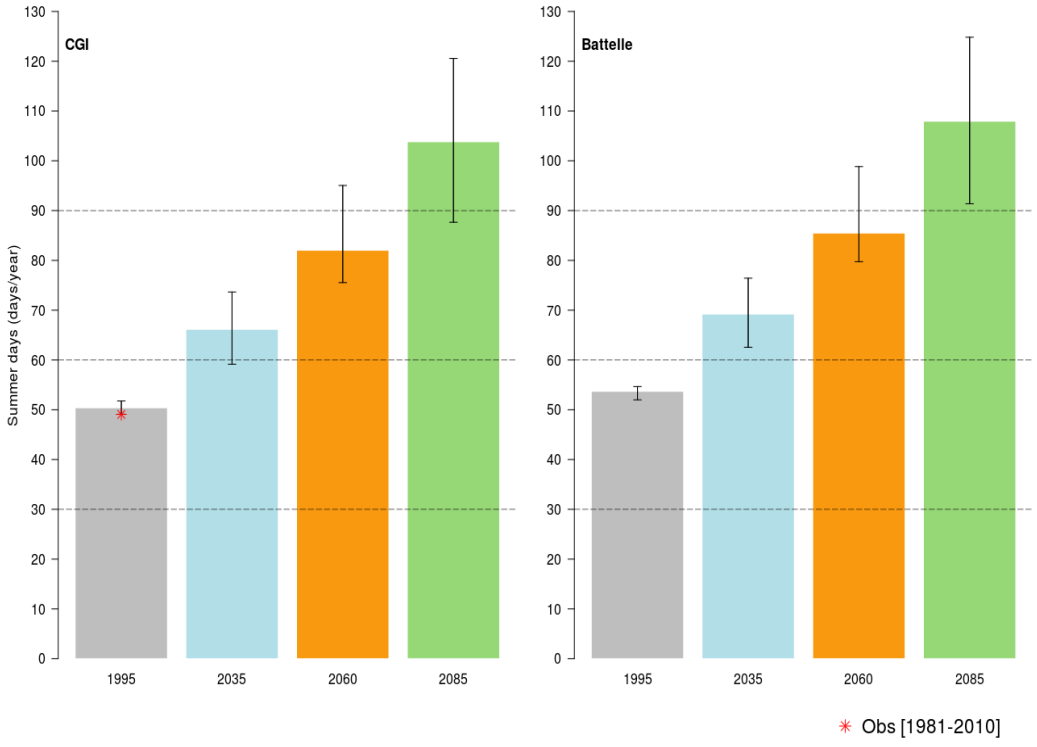

Appendix 12: Same as Appendix 3 but for the station couple CGI (left)-Batelle (right).

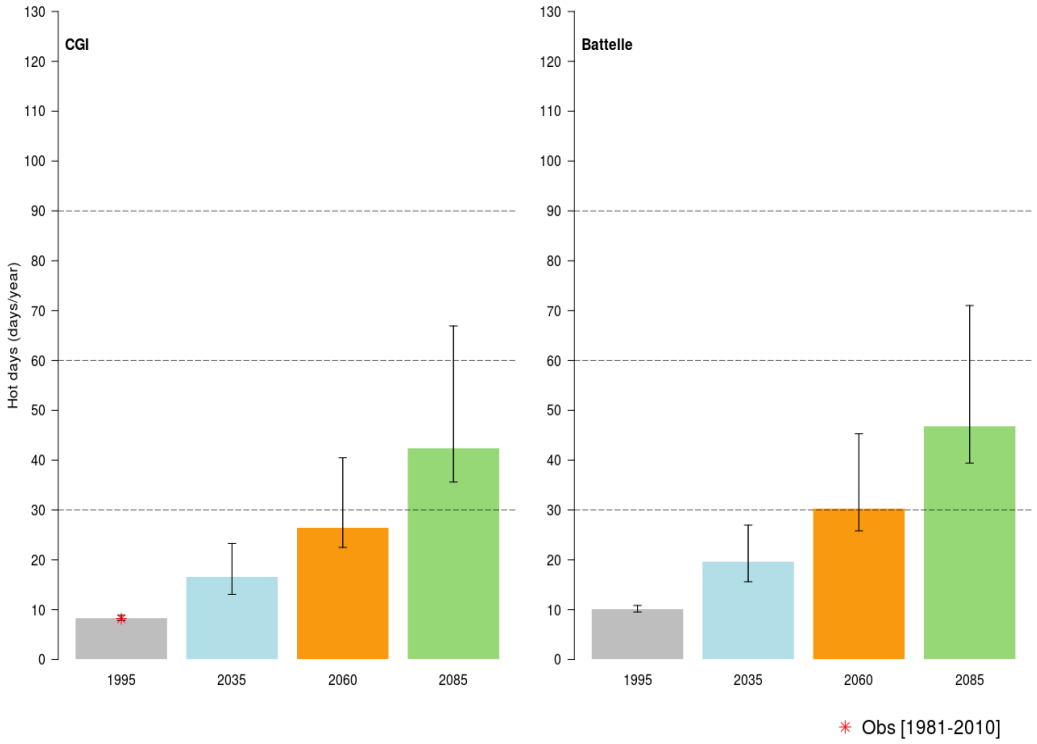

Appendix 13: Same as Appendix 4 but for the station couple CGI (left)-Batelle (right).

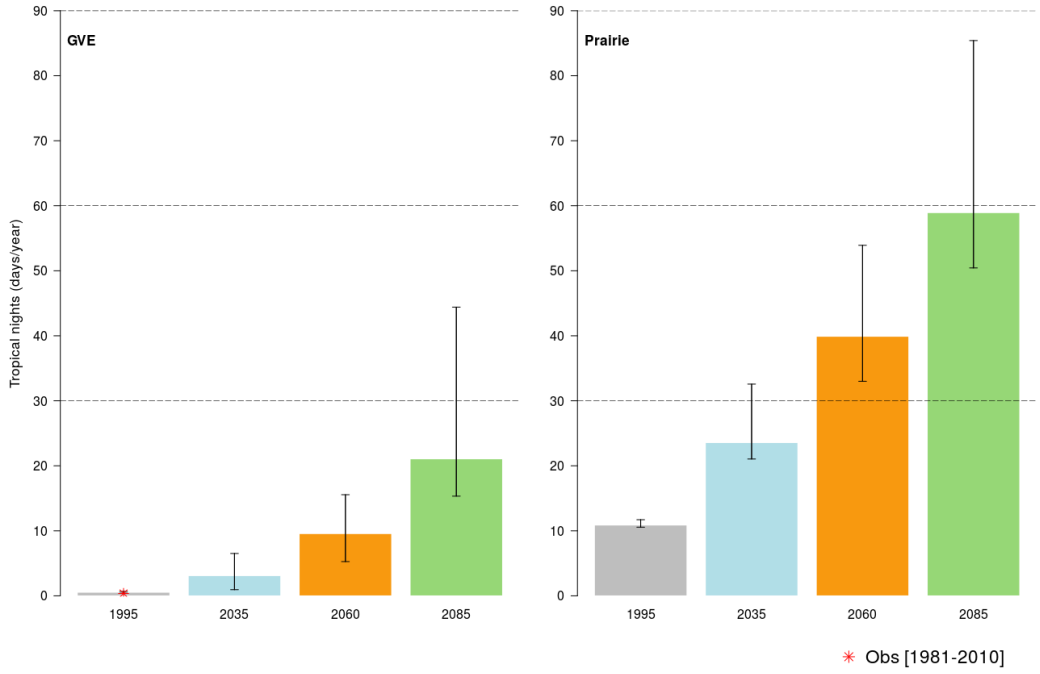

Appendix 14: Same as Appendix 2 but for the station couple GVE (left)-Prairie (right).

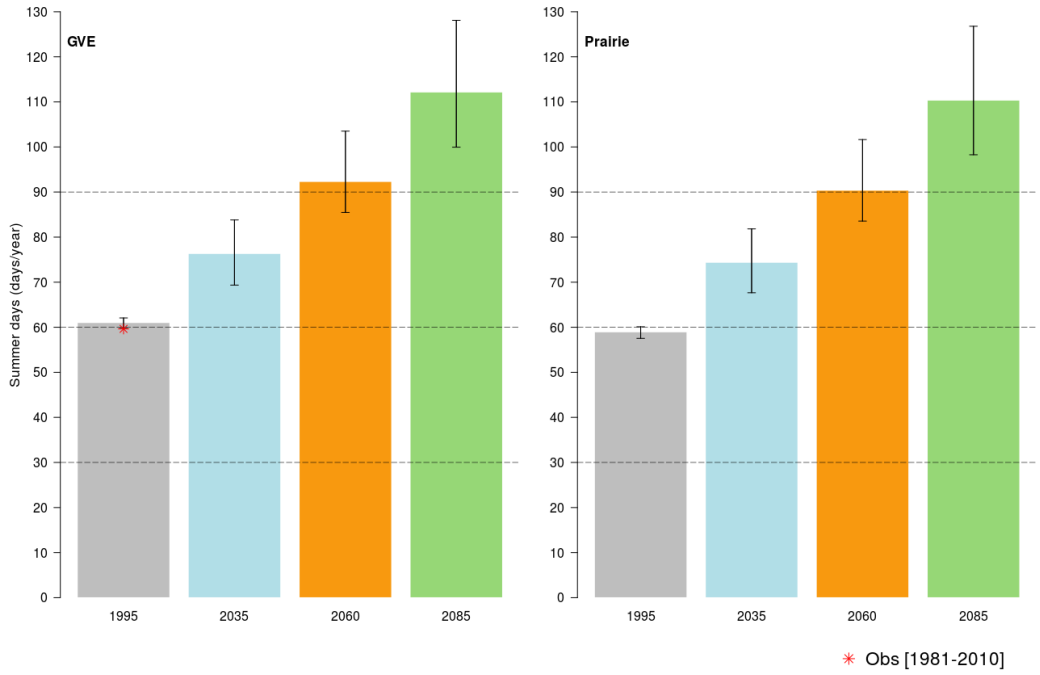

Appendix 15: Same as Appendix 3 but for the station couple GVI (left)-Prairie (right).

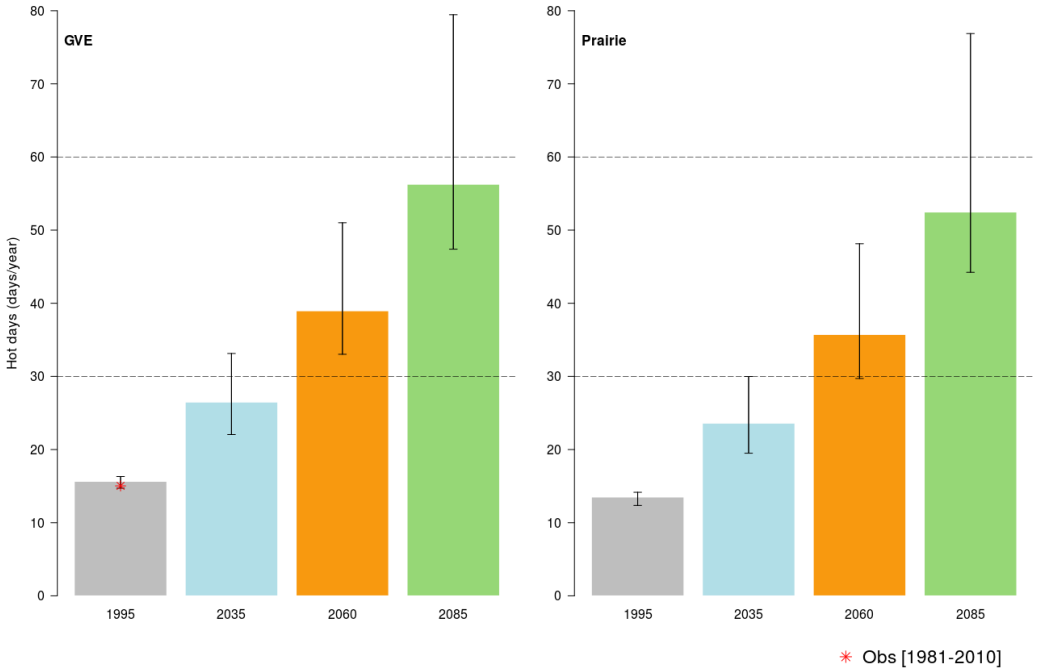

Appendix 16: Same as Appendix 4 but for the station couple GVE (left)-Prairie (right).

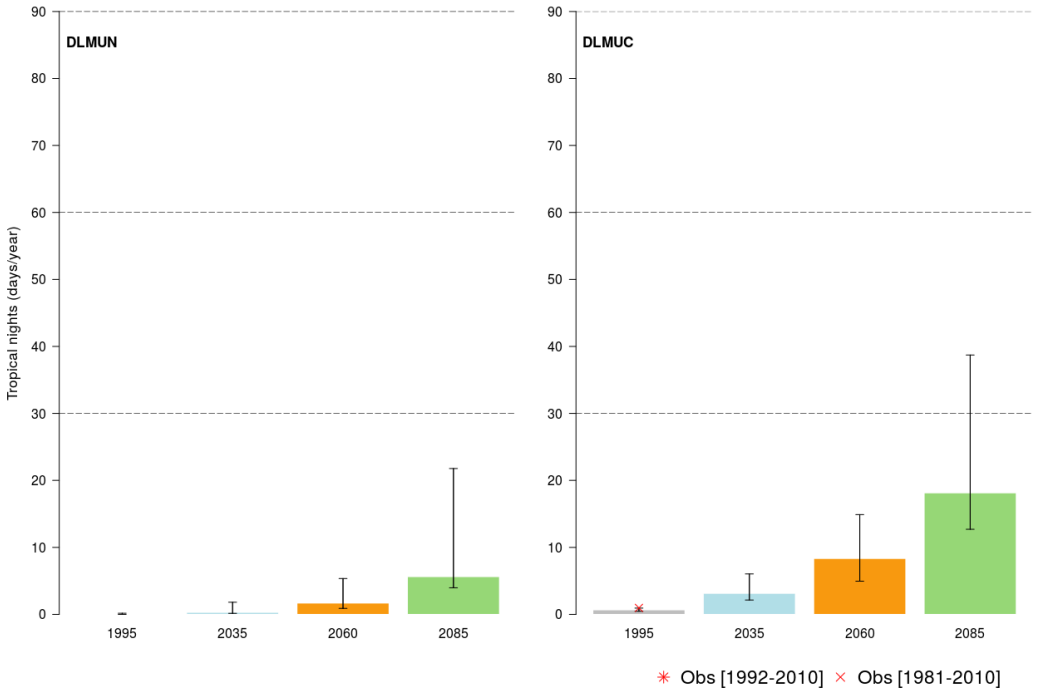

Appendix 17: Same as Appendix 2 but for the station couple DLMUN (left)-DLMUC (right).

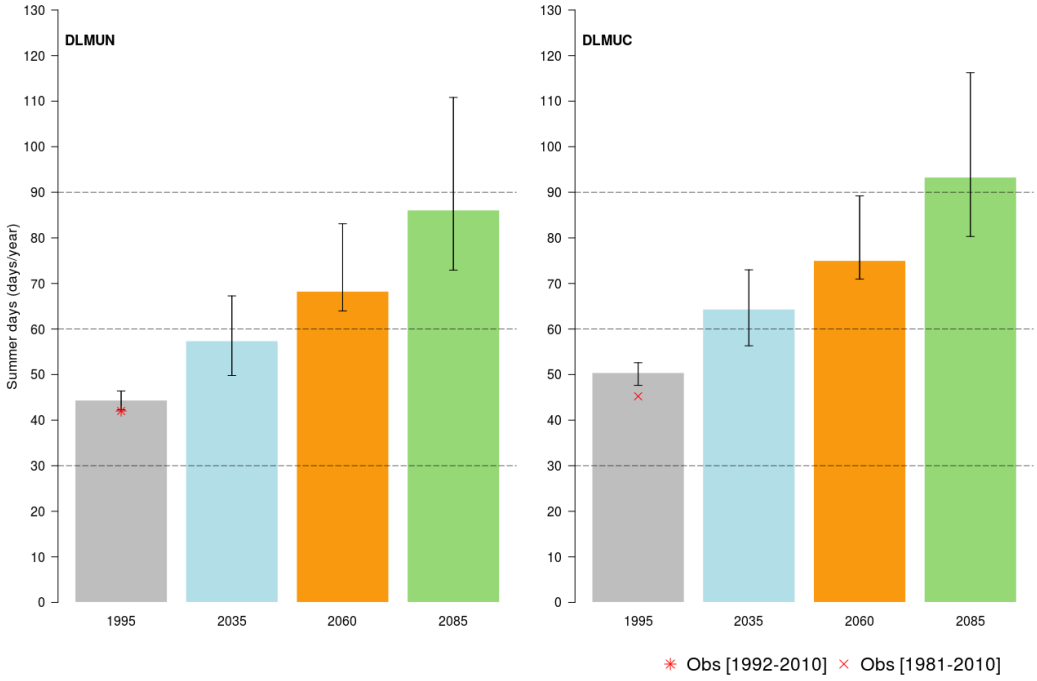

Appendix 18: Same as Appendix 3 but for the station couple DLMUN (left)-DLMUC (right)

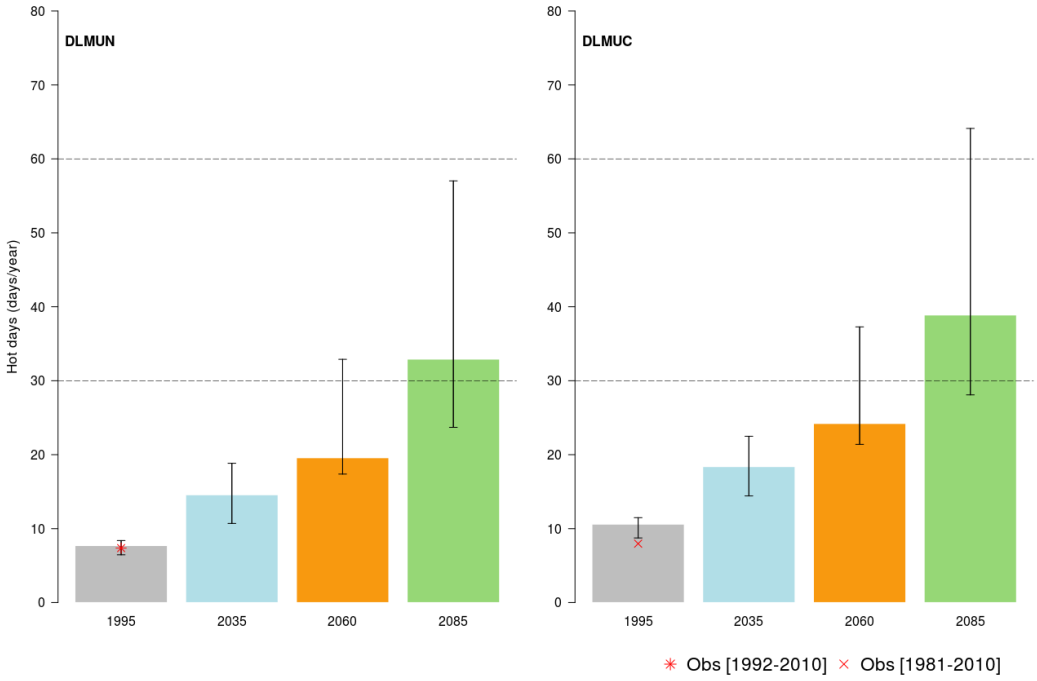

Appendix 19: Same as Appendix 4 but for the station couple DLMUN (left)-DLMUC (right).

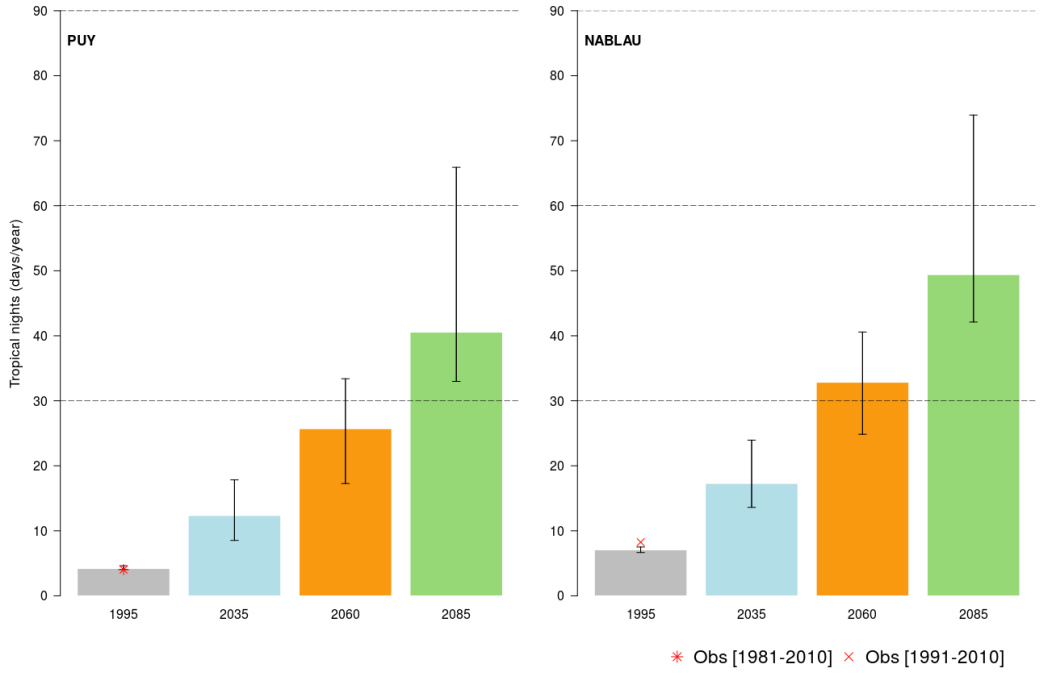

Appendix 20: Same as Appendix 2 but for the station couple PUY (left)-NABLAU (right).

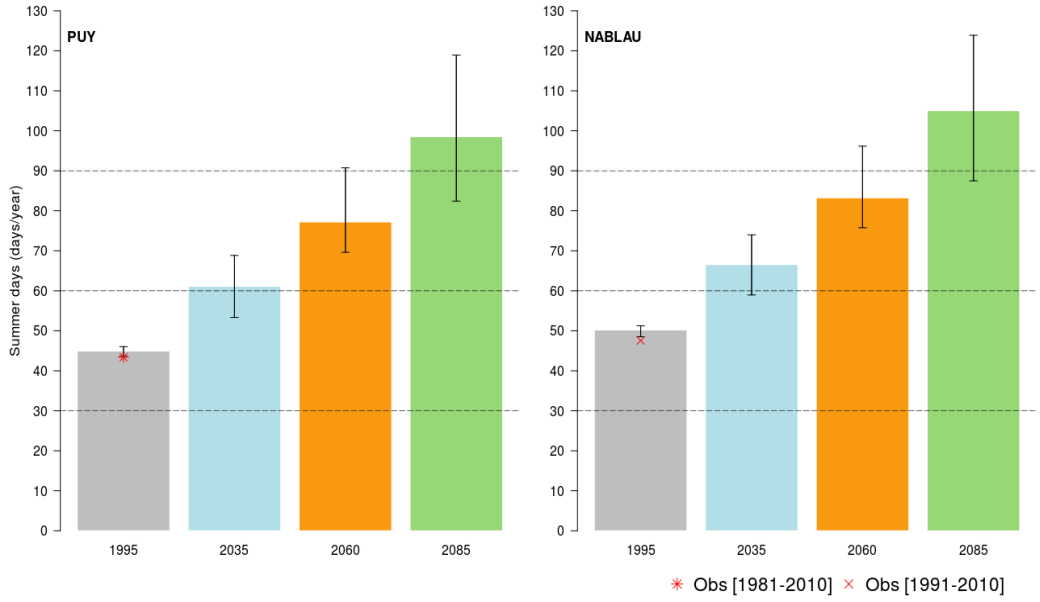

Appendix 21: Same as Appendix 3 but for the station couple PUY (left)-NABLAU (right)

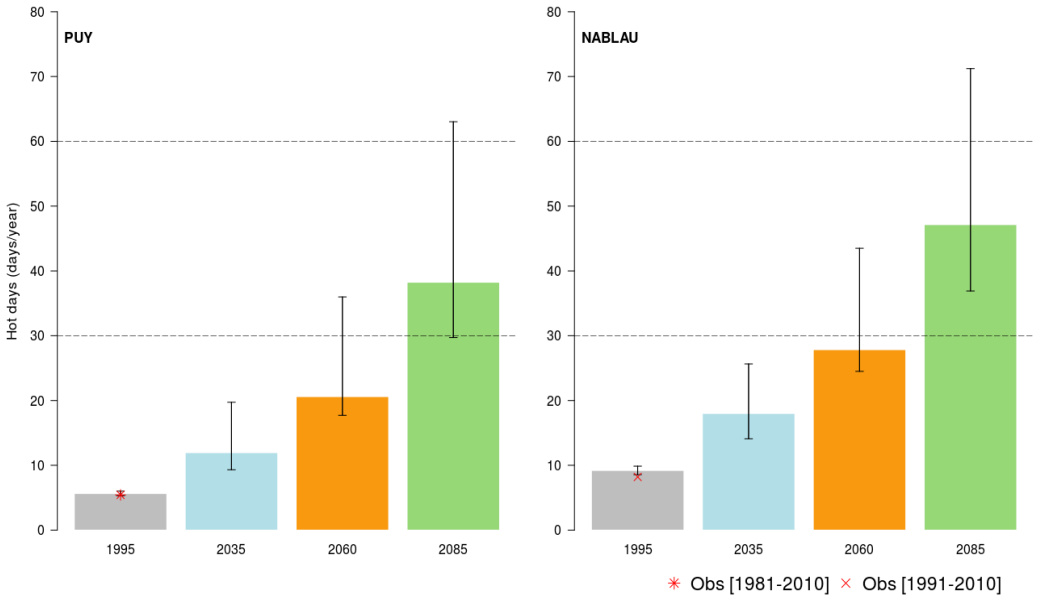

Appendix 22: Same as Appendix 4 but for the station couple PUY (left)-NABLAU (right).

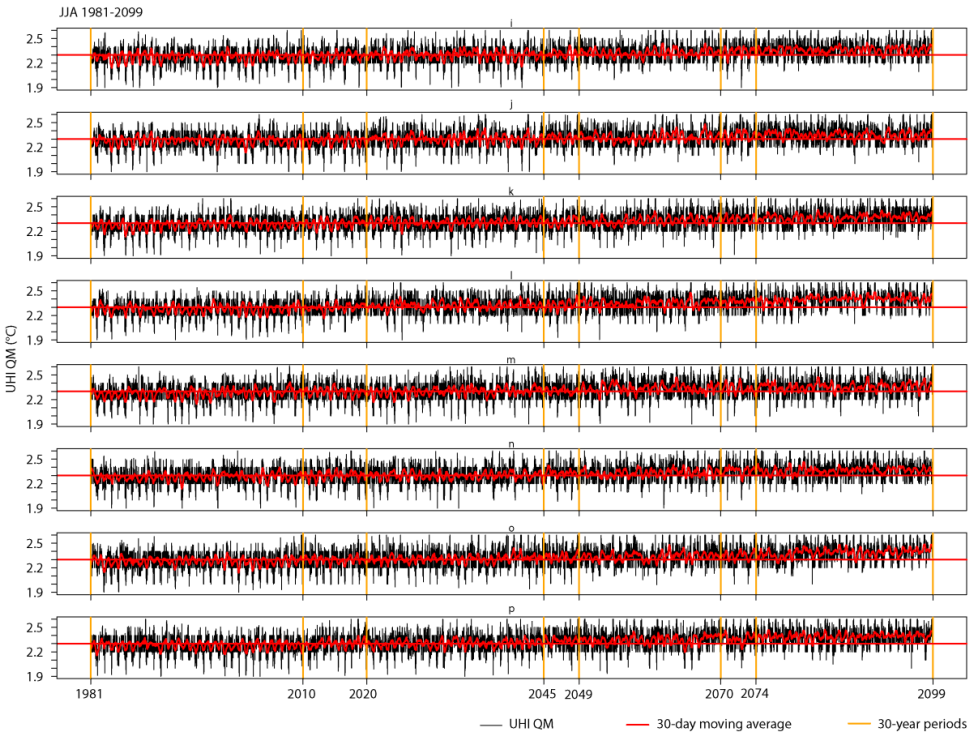

Appendix 23: Time series of daily UHI based on QM (UHI QM) at the exemplary station couple SMA-NABZUE for the period 1981-2099 for eight different GCM-RCM simulations (i-p; see Table 3). The red line marks the 30-day moving average, plotted over a straight reference line (red). The vertical orange lines indicate the reference period (1981-2010) and the three scenario periods.

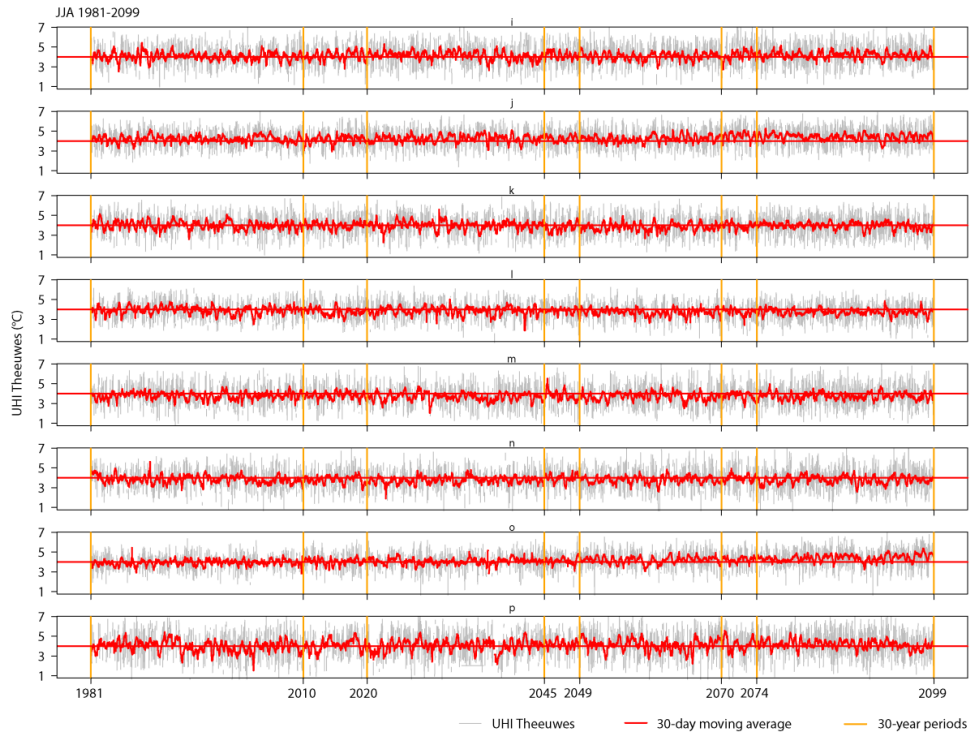

Appendix 24: Same as Appendix 23 but for UHI based on the diagnostic equation of Theeuwes et al. (2017) (UHI Theeuwes).

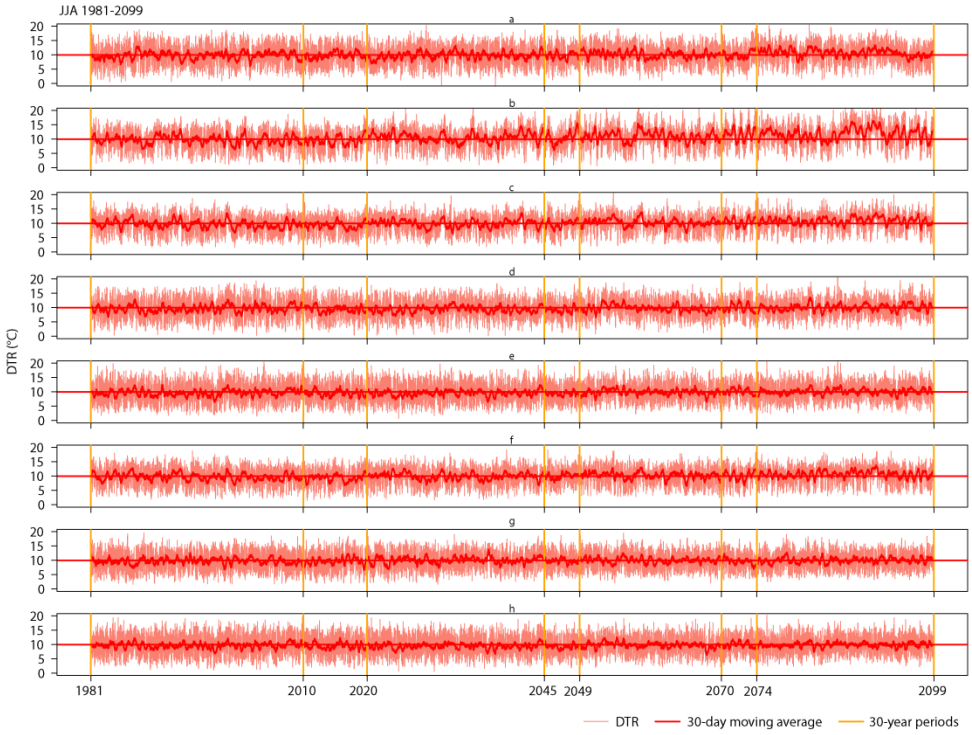

Appendix 25: Scenarios for the diurnal temperature range (DTR) at the rural site SMA for the period 1981-2099 for eight different GCM-RCM simulations (a-h; see Table 3). The red line marks the 30-day moving average, plotted over a straight reference line (red). The vertical orange lines indicate the reference period (1981-2010) and the three scenario periods.

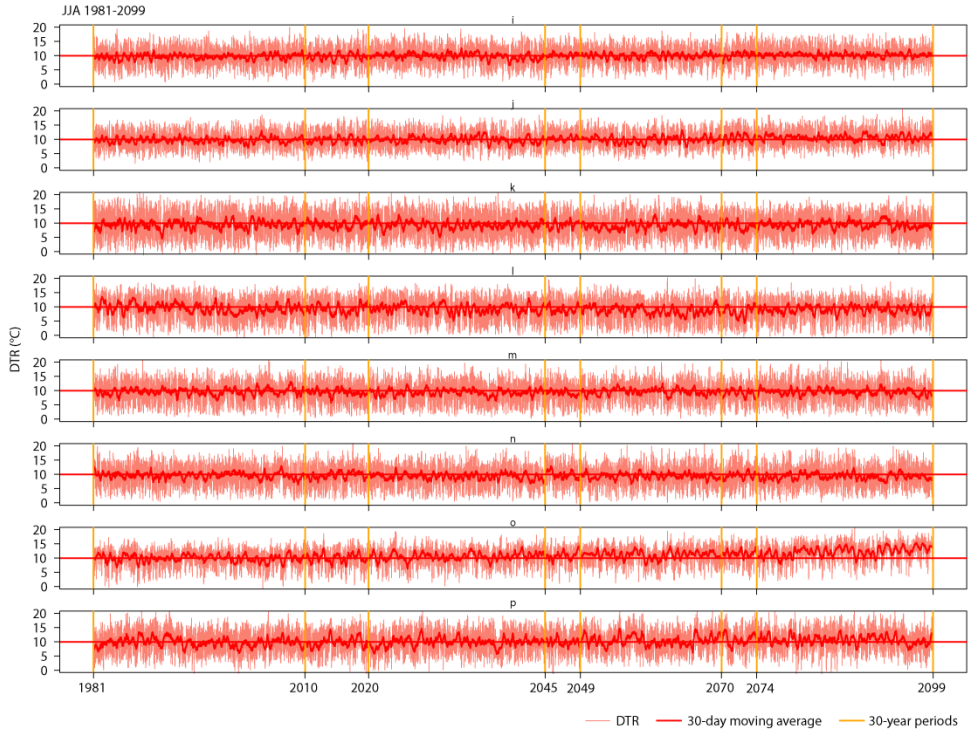

Appendix 26: Scenarios for the diurnal temperature range (DTR) at the rural site SMA for the period 1981-2099 for eight different GCM-RCM simulations (i-p; see Table 3). The red line marks the 30-day moving average, plotted over a straight reference line (red). The vertical orange lines indicate the reference period (1981-2010) and the three scenario periods.

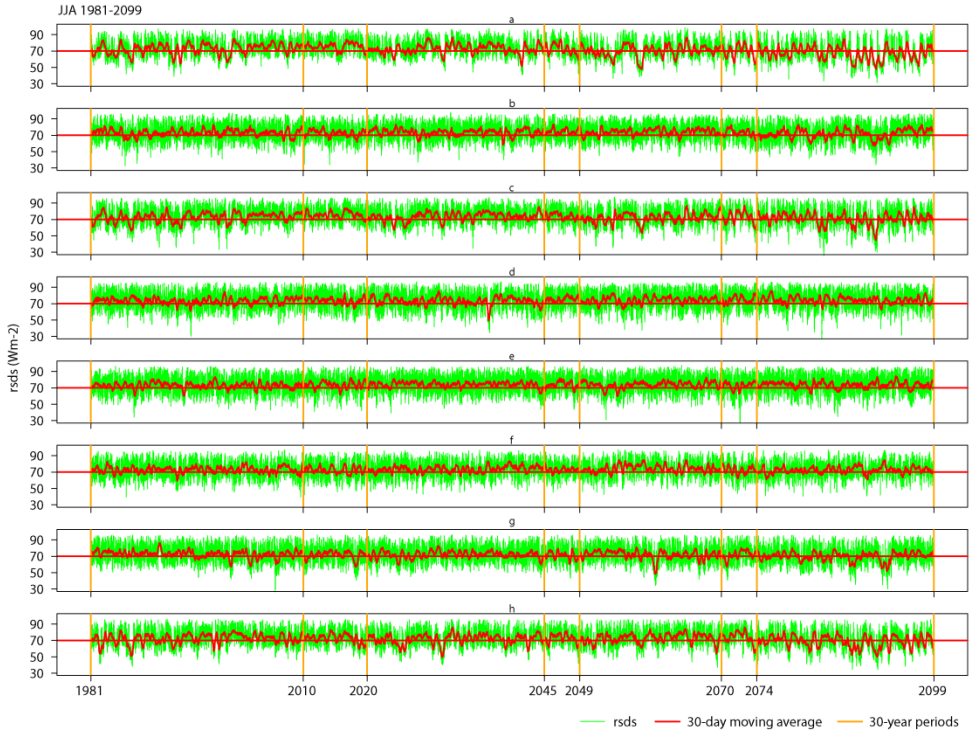

Appendix 27: Same as Appendix 25 but for daily mean solar shortwave incoming radiation (rsds), based on eight different GCM-RCM simulations (a-h; see Table 3).

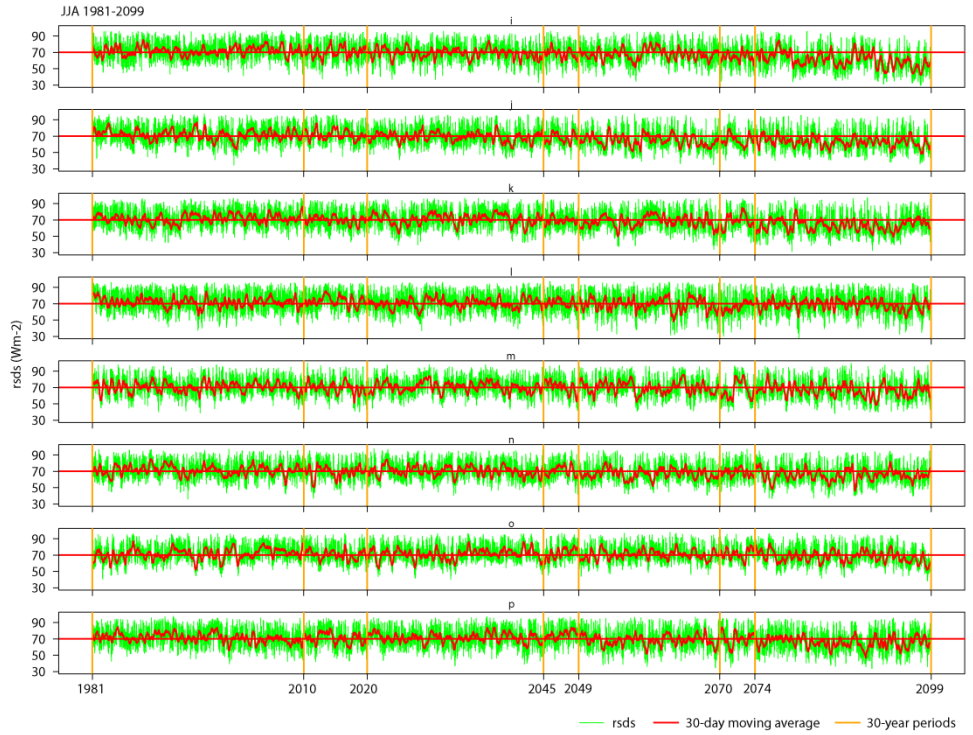

Appendix 28: Same as Appendix 26 but for daily mean solar shortwave incoming radiation (rsds), based on eight different GCM-RCM simulations (i-p; see Table 3).

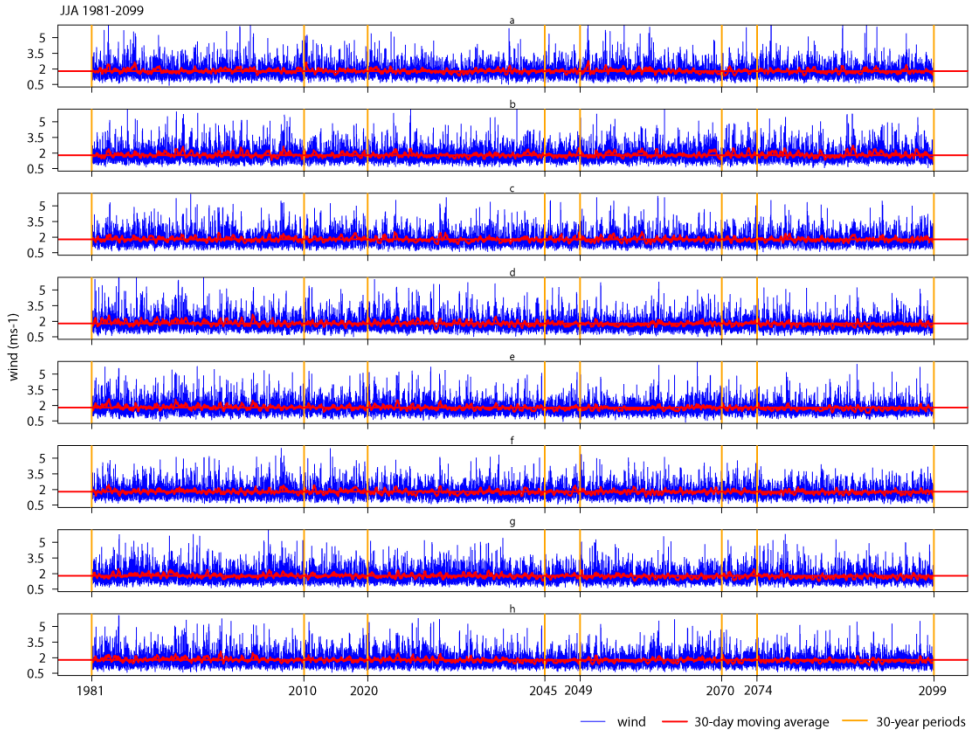

Appendix 29: Same as Appendix 25 but for daily mean 10m wind speed (wind), based on eight different GCM-RCM simulations (a-h; see Table 3).

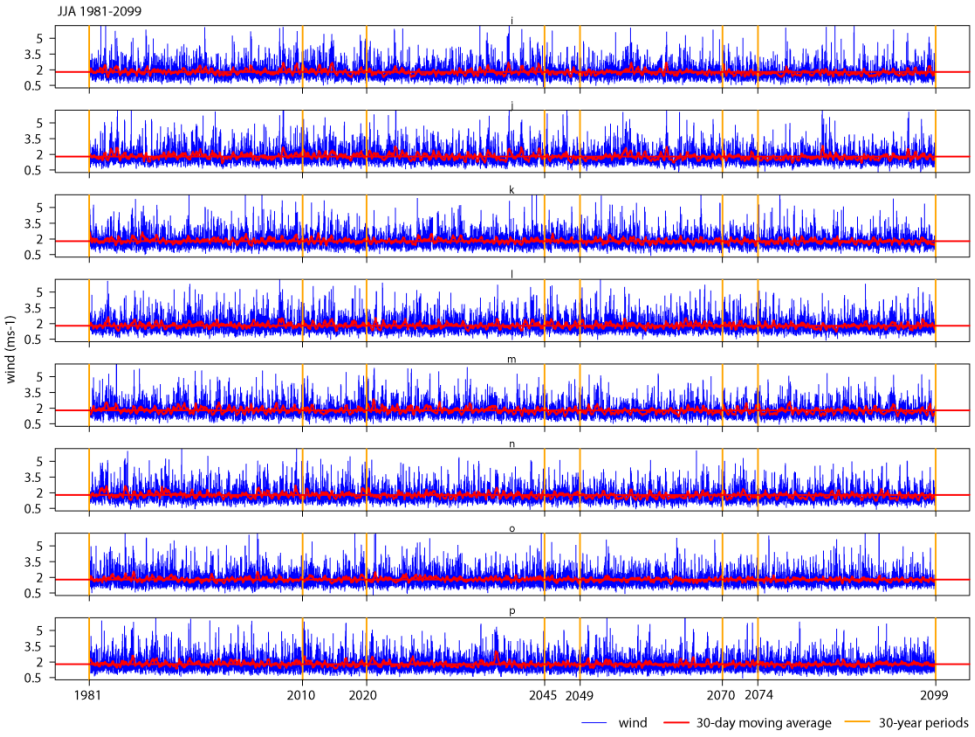

Appendix 30: Same as Appendix 26 but for daily mean 10m wind speed (wind), based on eight different GCM-RCM simulations (i-p; see Table 3).

Eidesstattliche Erklärung

Ich versichere, dass ich die vorliegende Arbeit ohne fremde Hilfe und ohne Benutzung anderer als der angegebenen Quellen angefertigt habe, und dass die Arbeit in gleicher oder ähnlicher Form noch keiner anderen Prüfungsbehörde vorgelegen hat. Alle Ausführungen der Arbeit, die wörtlich oder sinngemäß übernommen wurden, sind als solche gekennzeichnet.

_____

Annkatrin Burgstall

Augsburg, 30. August 2019

MeteoSchweiz
Operation Center 1
CH-8044 Zürich-Flughafen
T +41 58 460 99 99
www.meteoschweiz.ch

MeteoSvizzera
Via ai Monti 146
CH-6605 Locarno Monti
T +41 58 460 97 77
www.meteosvizzera.ch

MétéoSuisse
7bis, av. de la Paix
CH-1211 Genève 2
T +41 58 460 98 88
www.meteosuisse.ch

MétéoSuisse
Chemin de l'Aérologie
CH-1530 Payerne
T +41 58 460 94 44
www.meteosuisse.ch